NASA TECHNICAL NOTE

NASA TN D-2071

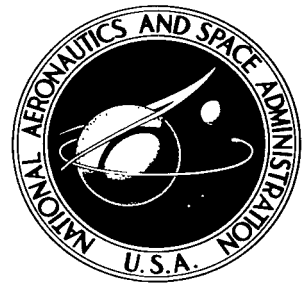

NASA TN D-2071

ELECTROMAGNETIC WAVE PROPAGATION IN A COLD, COLLISIONLESS ATOMIC HYDROGEN PLASMA

by Richard R. Woollett

Lewis Research Center
Cleveland, Ohio

NATIONAL AERONAUTICS AND SPACE ADMINISTRATION • WASHINGTON, D. C. • APRIL 1964

ELECTROMAGNETIC WAVE PROPAGATION IN A COLD, COLLISIONLESS ATOMIC HYDROGEN PLASMA

By Richard R. Woollett

Lewis Research Center
Cleveland, Ohio

NATIONAL AERONAUTICS AND SPACE ADMINISTRATION

For sale by the Office of Technical Services, Department of Commerce,
Washington, D.C. 20230 -- Price $2.75

ELECTROMAGNETIC WAVE PROPAGATION IN A COLD, COLLISIONLESS ATOMIC HYDROGEN PLASMA

by Richard R. Woollett

Lewis Research Center

SUMMARY

The characteristics of electromagnetic wave propagation in a cold, collisionless plasma immersed in a steady, uniform magnetic field are presented in dimensional units. Data for the "principal" waves are presented as curves of wave number, wavelength, phase velocity, and group velocity as functions of frequency. Wave numbers for oblique propagation are presented for angles of 0.1°, 1°, 10°, 45°, 80°, 89°, and 89.9° relative to the magnetic-field direction. The range of magnetic-field strengths covered by the plots is 10^{2} to 10^{5} gauss, and the range of electron densities is 10^{10} to 10^{15} ions per cubic centimeter. Cutoff and resonance frequencies are also plotted as functions of density and magnetic-field strength.

INTRODUCTION

The intense interest shown in plasma waves has led to several independent, though similar, theoretical treatments of the problem. Results have appeared in a variety of forms. The case of wave propagation in a cold, collisionless plasma is typical in this regard. Although the analysis of the cold plasma has been quite exhaustive, the wave characteristics have been presented either as sketches showing the limiting cases in detail or as detailed plots covering restricted ranges of the propagation frequency. These presentations used nondimensional expressions over a restricted frequency region in order to correlate the data from many conditions on a single plot. The experimentalist, however, usually prefers dimensional data that cover a broad range of application. In this report the more common wave propagation parameters are presented as dimensional quantities and are plotted over an extended frequency range. These curves are intended to complement the nondimensional plots that have been presented over various frequency ranges (refs. 1 and 2).

Characteristics of the plasma wave commonly used in microwave diagnostics to measure electron density (termed the ordinary wave) are independent of magnetic field. Therefore, its wave properties can be presented conveniently in either nondimensional or dimensional form, because the only parameter is electron density. It is possible, however, to devise diagnostic techniques based on characteristics of other types of waves. Since the plasma densities that can be determined from these other waves generally depend on magnetic field, care is required in selecting the propagation frequency. This detailed selection of test

conditions is made more convenient by the use of comprehensive plots that cover a large range of experimental frequencies.

The curves presented in this report apply for small-amplitude electromagnetic waves (since a perturbation technique is employed) propagating through an atomic hydrogen plasma immersed in a uniform steady magnetic field. Calculations made from Astrom's equations (ref. 2) predict, for a cold, collisionless plasma, all the important electromagnetic wave modes and their resonances. Included in the results are curves of wave number, wavelength, phase velocity, and group velocity of waves propagating parallel and normal to the magnetic field over a spectrum of excitation from low-frequency radio waves (1.6×10^5 cps) to submillimeter microwaves (1.6×10^{12} cps). In addition, wave-number plots for propagation at angles other than 0° and 90° are presented. Ranges of magnetic-field intensity and particle density covered by the graphs are, respectively, 10^2 to 10^5 gauss and 10^{10} to 10^{15} ions per cubic centimeter.

THEORY

The basic equations for the propagation of an electromagnetic wave in a cold plasma with overall charge neutrality have been derived from various mathematical models. The contribution that is usually accepted as the original major work is that by Astrom (ref. 2). He assumed an infinite, homogeneous medium of ions and electrons that were motionless in the unperturbed state and were immersed in a uniform static magnetic field. The plasma was considered collision-free. Therefore, the only forces to act on the charged particles were those originating from the macroscopic electric and magnetic fields. Since there were assumed to be no collisions between particles, the presence of neutral constituents would not alter the results obtained from this theory. The ion and electron velocities were obtained by solving the equation of motion for a charged particle acted on by the Lorentz force. The plasma currents obtained from these particle velocities were substituted into Maxwell's equations to obtain a self-consistent solution in terms of the dielectric constants of the medium. Although Astrom assumed a plane wave in his development of the dielectric coefficients, Epstein (ref. 3) obtained the same dispersion relation for cylindrical waves.

Dispersion Relation

There are various forms in which the resulting equations may be presented, and each form is more convenient under certain circumstances than the others. The equations considered in this report involve the various components of a modified dielectric tensor K; the modified dielectric coefficients used herein are obtained by multiplying Astrom's dielectric coefficients by $(\omega/c)^2$. Components of the tensor are K_l, K_r, K_p, and K_s, where the subscripts l, r, p, and s refer to left rotation, right rotation, axial, and transverse electric-field polarizations. (Symbols are defined in appendix A.) The equations used in this report can be derived from the dispersion relation (ref. 4)

$$\mathcal{A}k^4 - \mathcal{B}k^2 + \mathcal{C} = 0 \qquad (1)$$

where

$$\mathscr{A} = K_s \sin^2\theta + K_p \cos^2\theta$$

$$\mathscr{B} = K_r K_l \sin^2\theta + K_p K_s (1 + \cos^2\theta)$$

$$\mathscr{C} = K_p K_r K_l$$

$$K_l = \frac{\omega_p^2}{c^2}\left[1 - \frac{\omega_p^2}{(\omega - \omega_{ci})(\omega + \omega_{ce})}\right] \tag{2a}$$

$$K_r = \frac{\omega^2}{c^2}\left[1 - \frac{\omega_p^2}{(\omega + \omega_{ci})(\omega - \omega_{ce})}\right] \tag{2b}$$

$$K_p = \frac{\omega^2}{c^2}\left(1 - \frac{\omega_p^2}{\omega^2}\right) \tag{3}$$

$$K_s = \frac{\omega^2}{c^2}\left[1 - \frac{\omega_p^2(\omega^2 - \omega_{ce}\omega_{ci})}{(\omega^2 - \omega_{ci}^2)(\omega^2 - \omega_{ce}^2)}\right] \tag{4}$$

It should be noted that K_p is independent of magnetic-field strength.

Waves propagating at 0° and 90° with respect to the magnetic field are referred to as principal waves or modes. Waves propagating at angles between 0° and 90° are referred to as oblique waves. If a rectangular coordinate system is selected so that the positive directions of x and z are parallel to $(\bar{B}\times\bar{k})\times\bar{B}$ and $\bar{B}$, respectively, the coordinate components of $\bar{k}$ become

$$\left.\begin{aligned} k_{x1}^2 &= \frac{\mathscr{B} + \sqrt{\mathscr{B}^2 - 4\mathscr{A}\mathscr{C}}}{2\mathscr{A}} \sin^2\theta \\ k_{x2}^2 &= \frac{\mathscr{B} - \sqrt{\mathscr{B}^2 - 4\mathscr{A}\mathscr{C}}}{2\mathscr{A}} \sin^2\theta \\ k_{z1}^2 &= \frac{\mathscr{B} + \sqrt{\mathscr{B}^2 - 4\mathscr{A}\mathscr{C}}}{2\mathscr{A}} \cos^2\theta \\ k_{z2}^2 &= \frac{\mathscr{B} - \sqrt{\mathscr{B}^2 - 4\mathscr{A}\mathscr{C}}}{2\mathscr{A}} \cos^2\theta \end{aligned}\right\} \tag{5}$$

where the numbers in the subscript identify the two roots obtained from equation (1). The components k_x and k_z, which are most commonly used in bound plasma problems, are the quantities that are generally measured experimentally.

Another convenient form in which the propagation vector may be presented is

$$\tan^2\theta = \frac{-K_p(k^2 - K_r)(k^2 - K_l)}{(k^2 - K_p)(K_s k^2 - K_r K_l)} \tag{6}$$

This form immediately yields the wave numbers of the principal plasma modes by setting $\theta = 0^\circ$ and 90°. Hence,

$$\left.\begin{aligned} K_p &= 0 \\ k_l^2 &= K_l \\ k_r^2 &= K_r \end{aligned}\right\} \quad \text{for } k_x = 0,\ \theta = 0^\circ$$

$$\left.\begin{aligned} k_p^2 &= K_p \\ k_s^2 &= \frac{K_r K_l}{K_s} \end{aligned}\right\} \quad \text{for } k_z = 0,\ \theta = 90^\circ \tag{7}$$

where k_l and k_r are the wave numbers of the left and right circularly polarized plane waves propagating in the direction of the magnetic field, k_p is the wave number of the P mode (ordinary wave) in which the electric vector is parallel to the field direction, and k_s is the wave number of the S mode (extraordinary wave) in which the electric vector is transverse to the magnetic-field direction. The only dispersion relation of the principal modes that is not directly represented in equation (7) is the one for the S mode, which can be written separately as

$$k_s^2 = \frac{\omega^2}{c^2} \frac{(\omega^2 + \omega_{ci}\omega - \omega_{ce}\omega - \omega_{ci}\omega_{ce} - \omega_p^2)(\omega^2 - \omega_{ci}\omega + \omega_{ce}\omega - \omega_{ci}\omega_{ce} - \omega_p^2)}{(\omega^4 - \omega_{ci}^2\omega^2 - \omega_{ce}^2\omega^2 + \omega_{ci}^2\omega_{ce}^2 - \omega_p^2\omega^2 + \omega_p^2\omega_{ce}\omega_{ci})} \tag{8}$$

Cutoff and Resonant Frequencies

Explicit expressions for the resonant and cutoff frequencies may be readily obtained by setting k^2 equal to infinity and zero, respectively, in equation (1). Cutoff frequencies are designated by subscripts beginning with o. Resonant frequencies are designated by the superscript ∞. For each propagation angle there are usually three cutoffs and three resonances that are designated in the order of increasing frequency by the subscripts 1, 2, and 3.

Cutoff. - For propagation at all angles except 0°,

$$\omega_{o1} = \frac{(\omega_{ci} - \omega_{ce}) + \sqrt{(\omega_{ci} - \omega_{ce})^2 + 4(\omega_{ce}\omega_{ci} + \omega_p^2)}}{2} \tag{9a}$$

$$\omega_{o3} = \frac{-(\omega_{ci} - \omega_{ce}) + \sqrt{(\omega_{ci} - \omega_{ce})^2 + 4(\omega_{ce}\omega_{ci} + \omega_p^2)}}{2} \tag{9b}$$

and

$$\omega_{o2} = \omega_p \tag{10}$$

At 0°, ω_{o2} does not exist. The numerical order of the subscripts in equations (9) and (10) prevails whenever $\omega_p > \omega_{ci}$ or $n > 0.03\ B^2$. If $\omega_p < \omega_{ci}$, equations (9) represent ω_{o3} and ω_{o2} and equation (10) represents ω_{ol}.

Resonance. - At $\theta = 0^\circ$,

$$\left.\begin{aligned} \omega_r^\infty &= \omega_{ci} \\ \omega_l^\infty &= \omega_{ci} \end{aligned}\right\} \tag{11}$$

while at $\theta = 90^\circ$,

$$\omega_{s1}^\infty = \left[\frac{(\omega_{ce}^2 + \omega_{ci}^2 + \omega_p^2) - \sqrt{(\omega_{ce}^2 + \omega_{ci}^2 + \omega_p^2)^2 - 4\omega_{ce}\omega_{ci}(\omega_{ce}\omega_{ci} + \omega_p^2)}}{2}\right]^{1/2} \tag{12a}$$

$$\omega_{s2}^\infty = \left[\frac{(\omega_{ce}^2 + \omega_{ci}^2 + \omega_p^2) + \sqrt{(\omega_{ce}^2 + \omega_{ci}^2 + \omega_p^2)^2 - 4\omega_{ce}\omega_{ci}(\omega_{ce}\omega_{ci} + \omega_p^2)}}{2}\right]^{1/2} \tag{12b}$$

where ω_{s1}^∞ and ω_{s2}^∞ are referred to as the lower and upper hybrid frequencies, respectively.

Resonant frequencies at an arbitrary propagation angle are determined by solving for the roots of the expression $\mathscr{A} = 0$ that was obtained by setting $k^2 = \infty$ in equation (1). Hence,

$$(1 + \tan^2\theta)(\omega^2)^3 - (1 + \tan^2\theta)(\omega_{ce}^2 + \omega_{ci}^2 + \omega_p^2)(\omega^2)^2 + \Big[(1 + \tan^2\theta)\omega_{ci}^2\omega_{ce}^2 + (\omega_p^2\omega_{ci}\omega_{ce})\tan^2\theta + \omega_p^2(\omega_{ci}^2 + \omega_{ce}^2)\Big](\omega^2) - \omega_p^2\omega_{ci}^2\omega_{ce}^2 = 0 \tag{13}$$

This expression is also considered in reference 5.

Phase and Group Velocities

The phase and group velocities for the various modes are given by the expressions

$$U = \frac{\omega}{k}$$

and

$$V = \frac{d\omega}{dk}$$

These are derived from equations (2), (3), (7), and (8). Only the expressions for group velocity are presented here. For the principal modes they are

$$V_l = \left\{\frac{k_l}{2}\left[\frac{2}{\omega} - \left(\frac{1}{\omega - \omega_{ci}} + \frac{1}{\omega + \omega_{ce}}\right)\right] + \frac{1}{2k_l}\frac{\omega^2}{c^2}\left(\frac{1}{\omega - \omega_{ci}} + \frac{1}{\omega + \omega_{ce}}\right)\right\}^{-1}$$

$$V_r = \left\{\frac{k_r}{2}\left[\frac{2}{\omega} - \left(\frac{1}{\omega + \omega_{ci}} + \frac{1}{\omega - \omega_{ce}}\right)\right] + \frac{1}{2k_r}\frac{\omega^2}{c^2}\left(\frac{1}{\omega + \omega_{ci}} + \frac{1}{\omega - \omega_{ce}}\right)\right\}^{-1}$$

$$V_p = \frac{k_p}{\omega}\, c^2$$

$$V_s = \frac{2}{k_s}\left[\frac{2}{\omega} + \frac{2\omega + \omega_{ci} - \omega_{ce}}{\omega^2 + (\omega_{ci} - \omega_{ce})\omega - \omega_{ci}\omega_{ce} - \omega_p^2} + \frac{2\omega - \omega_{ci} + \omega_{ce}}{\omega^2 - (\omega_{ci} - \omega_{ce})\omega - \omega_{ci}\omega_{ce} - \omega_p^2} - \frac{2\omega(2\omega^2 - \omega_{ci}^2 - \omega_{ce}^2 - \omega_p^2)}{\omega^4 - (\omega_{ci}^2 + \omega_{ce}^2 + \omega_p^2)\omega^2 + \omega_{ci}^2\omega_{ce}^2 + \omega_p^2\omega_{ce}\omega_{ci}}\right]^{-1} \quad (14)$$

For the principal modes, the group velocity is in the direction of wave propagation. For waves propagating at some arbitrary angle to the magnetic-field direction, however, the group velocity is generally not in the direction of wave propagation.

The expressions presented in the sections Dispersion Relation and Cutoff and Resonant Frequencies are sufficient to determine the major characteristics of electromagnetic waves propagating through a cold, collisionless plasma. There are several ways in which these equations may be simplified depending upon the approximations that are made. In appendix B three approximate treatments are discussed and compared to the Astrom model. These are (1) the microwave approximation (ref. 6), (2) the Stix approximation (ref. 7), and (3) the simplified Ohm's law (ref. 8).

RESULTS AND DISCUSSIONS

In the section THEORY, Astrom's dispersion relation was used to derive the characteristic wave equations in a plasma. These equations are valid for both

plane waves and cylindrical waves propagating through a cold, collisionless plasma immersed in a uniform magnetic field. Except for figures 13 to 15, the data for all curves presented in this report were calculated from Astrom's equations. Figures 13 to 15 were obtained from equations presented in appendix B. Calculations were performed for a fully ionized atomic hydrogen gas. Table I provides a summary of all the data covered by the curves of figures 1 to 18.

Wave Number of Principal Modes

Figure 1 consists of curves of the wave number squared as a function of the excitation frequency for the principal modes (P, S, R, and L) for a range of densities from 10^{10} to 10^{15} ions per cubic centimeter and at magnetic fields of 10^2, 10^3, 10^4, and 10^5 gauss. A wavelength scale is also included. The dashed sections of the curves that appear in the figures are extrapolations from the calculated solid sections. Cutoff and resonant frequencies are indicated by triangular symbols at the bottom and top of the figure, respectively. Figures 1(a) and (d) present the data for transverse wave propagation ($\theta = 90^\circ$) where the electric field of the wave is alined with the directions of the magnetic field and perpendicular to it, respectively; figures 1(b) and (c) present the data for longitudinal propagation ($\theta = 0^\circ$) where the electric field is perpendicular to the direction of the magnetic field and is left and right circularly polarized, respectively.

Plots of k^2 as a function of ω, such as those in figure 1, may be used directly to determine the feasibility of transmission experiments in which phase shift is measured. It is interesting to note that it is possible at certain conditions to determine an ion density with the use of the S mode, while it is impossible with the use of the P mode. For example, the maximum density that can be determined by a P mode at a frequency of 10^{11} radians per second is about 3×10^{12} ions per cubic centimeter (fig. 1(a)). If the plasma were immersed in a magnetic field of 10^4 gauss, densities up to 9×10^{12} ions per cubic centimeter could be determined with the use of the S mode (fig. 1(d-3)). Consequently, by rotating the waveguide 90° about its axis, it would be possible to increase the upper density limit of the diagnostic system. Increasing the field strengths extends the upper density limits of the S mode to larger values. Another example of the use of the curves is illustrated in figure 1(d-3). At a frequency of 10^8 radians per second, the validity of an experimental determination of plasma properties with the S mode for a 10-centimeter-diameter plasma would be questionable for densities less than 10^{14} ions per cubic centimeter, because the wavelength of this mode is the same magnitude as the plasma size.

Wave Number of Oblique Waves

Wave numbers that have been presented up to now are for the principal modes in which propagation normal to the magnetic-field direction is uncoupled from the parallel propagation. For oblique waves, however, the components of the propagation vectors k_x and k_z, which are respectively normal to and parallel to B, are related to each other and to k through the relations

$$k^2 = k_x^2 + k_z^2$$

$$k_x = k \sin \theta$$

$$k_z = k \cos \theta$$

These x- and z-components of the propagation vector are related to the transverse and parallel wave numbers that appear in the analysis of bound plasmas (ref. 8). These components of the oblique waves (along with components of wavelengths) are presented in figures 2 to 8 as functions of ω for $\theta = 0.1^\circ$, 1°, 10°, 45°, 80°, 89°, and 89.9° and for representative values of B and n. The magnetic-field strengths covered by these plots are 10^2, 10^3, and 10^4 gauss, and the particle densities are 10^{11} and 10^{13} ions per cubic centimeter.

When the propagation angle is varied, the dispersion relation can be altered markedly in some regions of the frequency spectrum and remain relatively unchanged in other regions. In many experiments the exact propagation angle is difficult to determine, such as when waves are generated by induction coils. It becomes important, therefore, to assess the manner in which the wave number changes with the angle.

Sketches (a) to (d) are presented to assist in the interpretation and use of figures 2 to 8 and to illustrate the effects of varying the propagation angle. In these sketches, the wave numbers of the principal modes are compared with components of the waves propagating at angles near 0° and 90°.

Sketch (a) consists of curves taken from figures 1(b), 1(c), 4(a-2), 4(b-2), and 9(b). This sketch presents k^2 as a function of ω for the R and L modes and k_z^2 for a 10° propagation angle. As might be expected, k_z^2 at 10° is very similar to the wave numbers of the R and L modes over most of the frequency spectrum. There are, however, portions of the 10° dispersion relation, marked by crosshatching, that do not have counterparts in the R and L modes. This modification results in a resonance, which occurs at the plasma frequency, that cannot be predicted by the R and L modes. Near the 90° propagation angle the wave number might be expected to approximate the transverse S or P modes rather than the R and L modes.

In sketch (b), which is taken from the curves of figures 1(b), 1(c), 6(a-2), 6(b-2), and 9(b), k_z^2 for 80° propagation is compared to the R and L modes. Although the general shapes of the 80° curves bear some similarity to the R and L curves, the magnitudes differ appreciably. Obviously, the R and L modes may not be used to approximate the k_z relation for large angles.

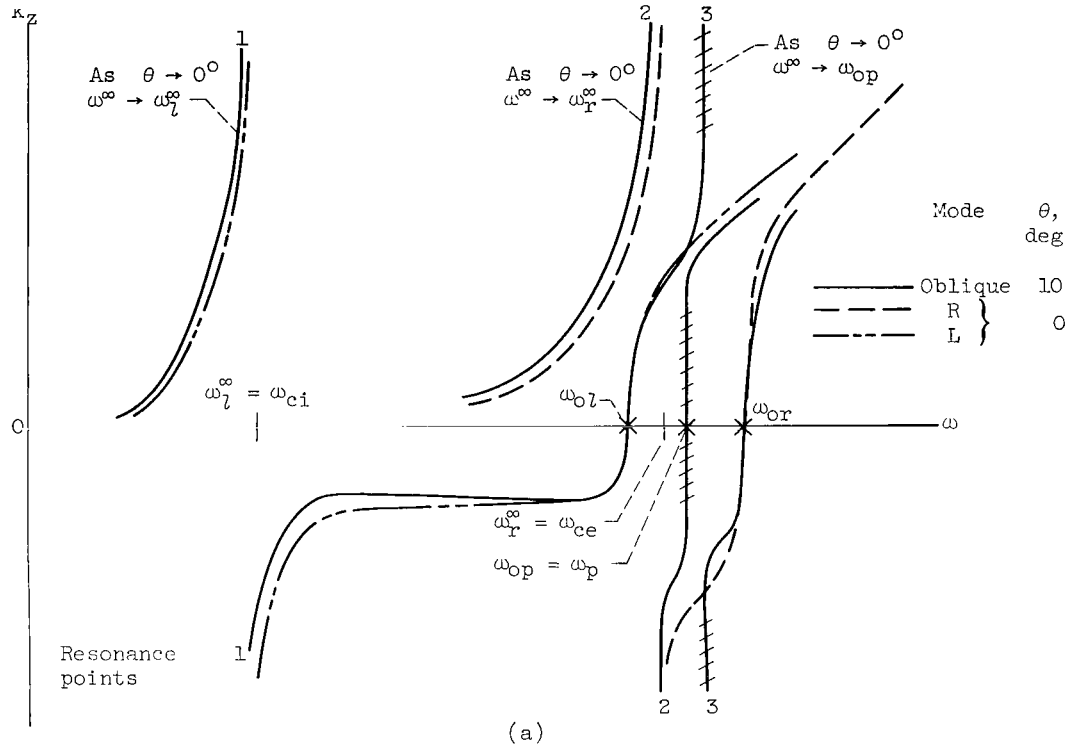
k_z
As $\theta \to 0^\circ$
$\omega^\infty \to \omega_l^\infty$
As $\theta \to 0^\circ$
$\omega^\infty \to \omega_r^\infty$
As $\theta \to 0^\circ$
$\omega^\infty \to \omega_{op}$
Mode
θ, deg
Oblique 10
R } 0
L }
$\omega_l^\infty = \omega_{ci}$
ω_{ol}
ω_{or}
ω
0
$\omega_r^\infty = \omega_{ce}$
$\omega_{op} = \omega_p$
Resonance points
1
2
3

(a)

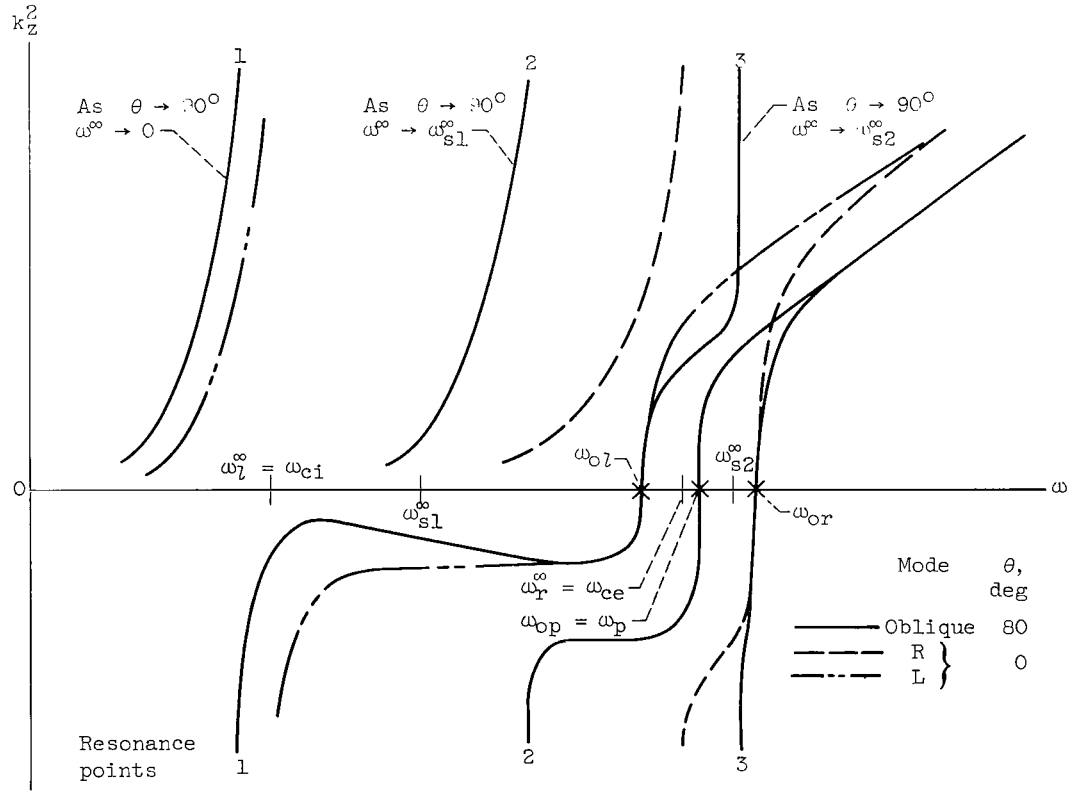
k_z^2
As $\theta \to 90^\circ$
$\omega^\infty \to 0$
As $\theta \to 90^\circ$
$\omega^\infty \to \omega_{s1}^\infty$
As $\theta \to 90^\circ$
$\omega^\infty \to \omega_{s2}^\infty$
$\omega_l^\infty = \omega_{ci}$
ω_{ol}
ω_{s2}^∞
ω_{s1}^∞
ω_{or}
ω
0
$\omega_r^\infty = \omega_{ce}$
$\omega_{op} = \omega_p$
Mode
θ, deg
Oblique 80
R } 0
L }
Resonance points
1
2
3

(b)

Sketch (c) is composed of curves taken from figures 1(a), 1(d), 6(b-1), 7(b-1), 8(a), and 9(a). In this sketch k_x^2 for propagation angles of 80°, 89°, and 89.9° is compared with the S and P wave numbers. Two interesting details should be noted in sketch (c). First, a resonance exists between ω_{ci} and zero frequency for propagation less than 90°; this resonance disappears at 90°.

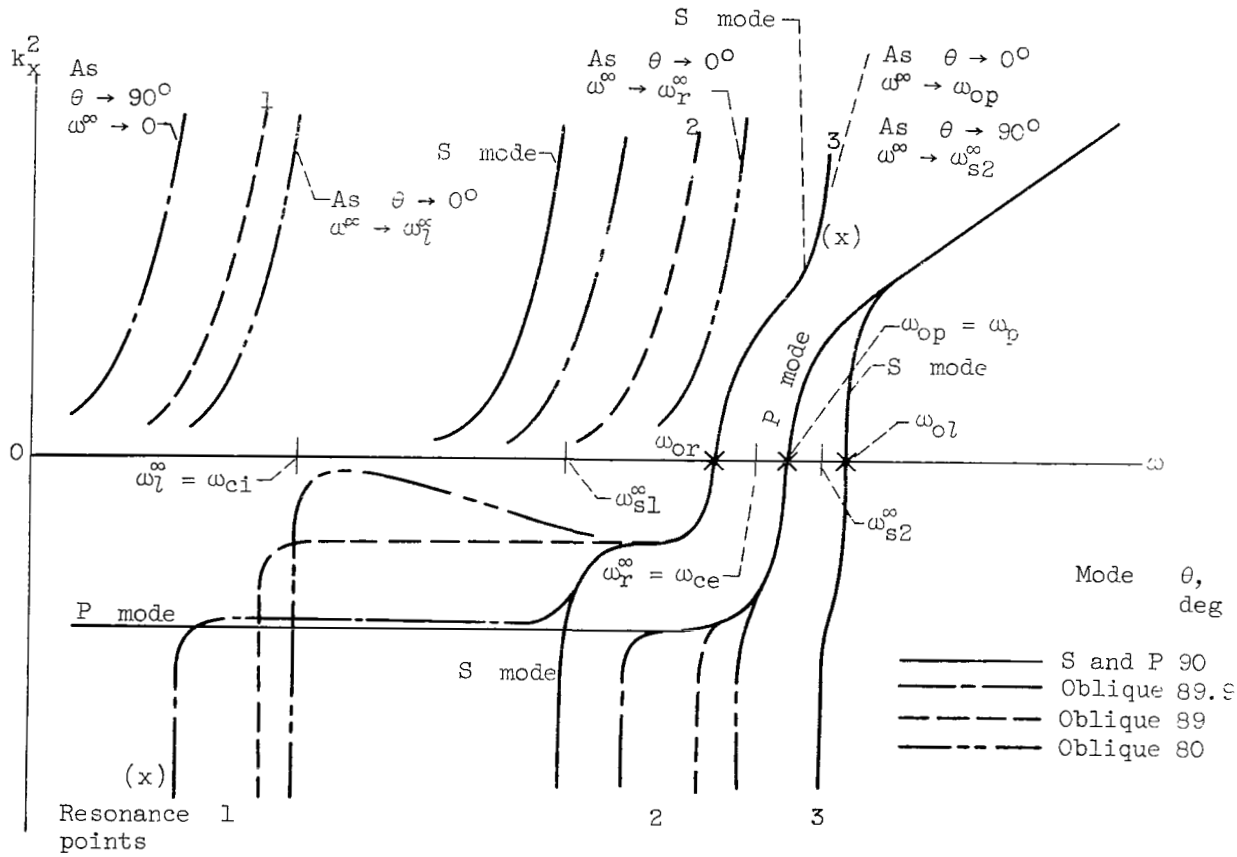

(c)

Second, for frequencies less than ω_p, the wave numbers change very rapidly as the angle is varied near 90°. It follows from sketch (c) that, for θ less than 89.9°, k_x cannot be approximated by the S and P wave numbers. In contrast, in sketch (a) k_z^2 can be approximated by the R and L modes for angular deviations as large as 10°.

Another matter of passing interest is illustrated in sketch (c). For negative values of k^2, a branch of the P curve intersects a branch of the S curve. Their counterparts for angles less than 90° never intersect, however. As illustrated in sketch (d), there appears to be an interchange of branches as θ approaches 90° (see branch marked (x)).

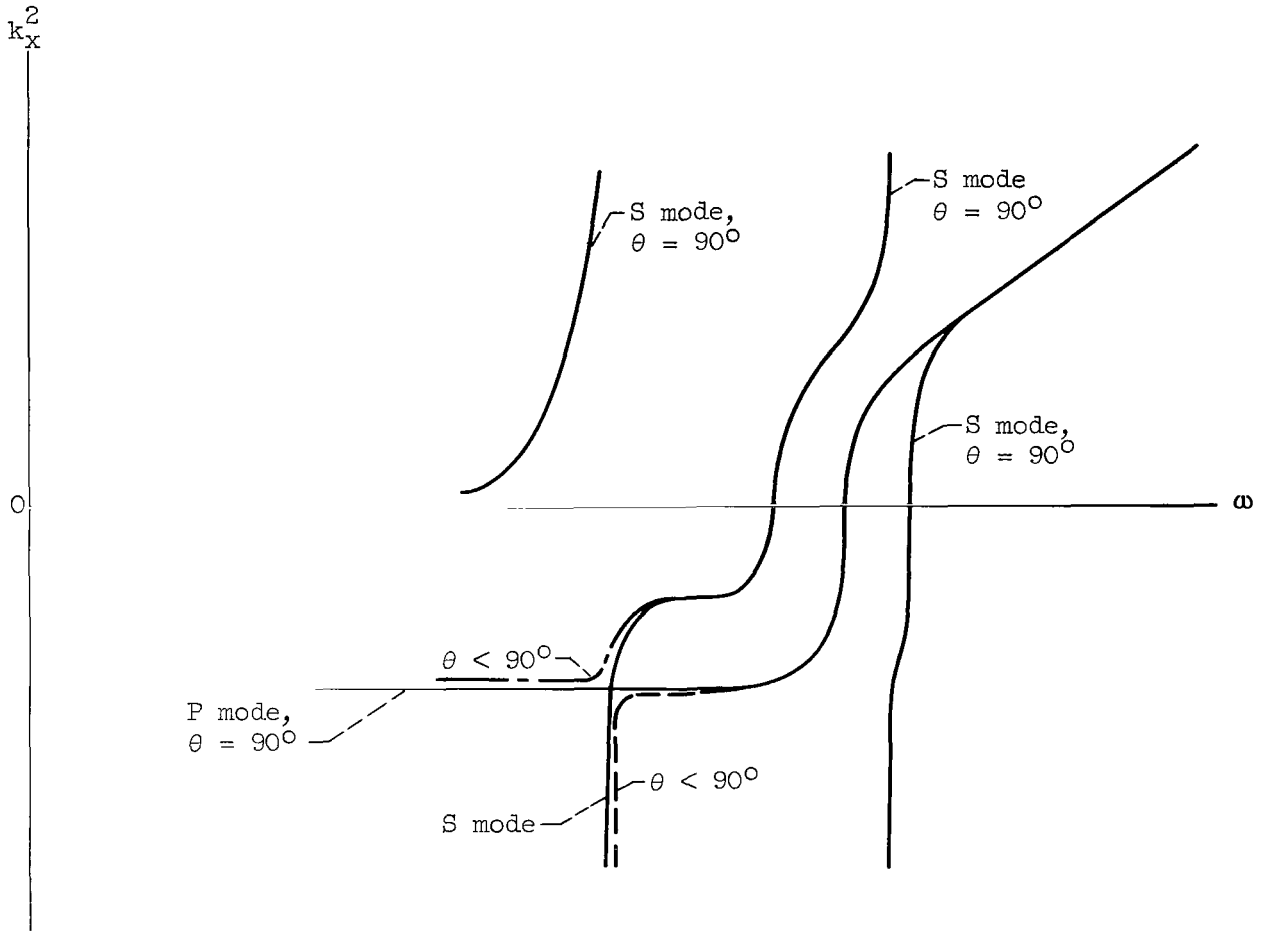

(d)

The trends for imaginary wave numbers are indicated in these sketches. The trends are important since the damping distance associated with wave phenomena can be represented by $d = (k_{im})^{-1}$, where k_{im} signifies the imaginary component of the wave number. In the absence of collisions, k is either purely real or purely imaginary when ω is assumed real as in this report. To give an idea of the magnitude of the numbers involved, the specific case $n = 10^{13}$ ions per cubic centimeter and $B = 10^4$ gauss is plotted in figure 9. The magnitude of k_{im} over most of the various branches readily explains why it is necessary to consider the imaginary region of the dispersion relation in wave propagation problems. As an example, the damping distance for k_p^2 when $\theta = 90^\circ$, $n = 10^{13}$ ions per cubic centimeter, and $B = 10^4$ gauss is roughly 0.17 centimeter (fig. 9(a)). When $\theta = 10^\circ$, however, the average damping distance is of the order of 10 centimeters. If the characteristic length of an experimental plasma were much less than this latter damping distance, the plasma would be transparent over a large part of the imaginary-wave-number region. The plasma would then transmit a disturbance at both higher and lower frequencies than the transmission cutoff frequency, and no sharp and well defined cutoffs would exist.

In summarizing the discussions of sketches (a) to (d), it is worth noting the following for positive values of k^2: Over the range of angles from 0° to 80° the dispersion relations bear some degree of similarity to each other, while over the range 80° to 90° the low-frequency regions of the dispersion relation change in a drastic manner when the angle is slightly varied. This sensitivity to wave propagation direction near 90° is pointed out for the case of resonance in reference 5.

Cutoff and Resonant Frequencies

Cutoff and resonant frequencies are particularly interesting because of their relation to density measurement and power absorption in a plasma. At cutoff k^2 goes through zero and, therefore, is a dividing point between a propagation ($k^2 > 0$) and a nonpropagation ($k^2 < 0$) region. Similarly, at resonance k^2 goes from $+\infty$ to $-\infty$ and thereby again defines a separation between propagating and nonpropagating regions. In a real plasma at cutoff most of the signal is reflected by the plasma, while at resonance most of the signal will either be reflected or absorbed. In either case the signal can be attenuated appreciably as it passes through the plasma. If either the cutoff or resonant frequencies have a detectable variation with density, they may conceivably be applied to measure plasma density.

Cutoff frequency is plotted against density in figure 16. The frequency ω_{0p} of figure 16(a) is the plasma frequency and is independent of magnetic field. The upper and lower hybrid resonant frequencies of the S mode are plotted in figure 17 as a function of ion density with the magnetic field as a parameter. The resonances of the R and L modes, which are the electron and ion-cyclotron frequencies, respectively, are plotted in figure 18 as a function of magnetic-field strength.

The resonant frequencies for oblique waves are plotted in figure 10 as a function of the propagation angle for magnetic-field strengths of 10^2, 10^3, and 10^4 gauss and for densities of 10^{11} and 10^{13} ions per cubic centimeter. These frequencies are the roots of equation (13). Several interesting phenomena are illustrated in these curves. It is observed that the first resonant frequency ω_1^∞ is practically constant between 0° and 80°. Above 80° the resonant frequency drops off very rapidly and goes to zero as θ approaches 90°. This is consistent with the rapid change in the dispersion relation near 90° depicted in sketch (c) for the lowest resonance. The second resonance ω_2^∞ continually decreases as θ goes from 0° to 90°. Therefore, in an experiment, if the propagation angle departs from that expected, the resonant frequency will shift from the expected value according to the presented curves. The third resonant frequency ω_3^∞ is fairly constant with angle, except, perhaps, at high field strengths ($B \geq 10^4$ gauss) and large densities ($n \geq 10^{13}$ ions/cm^3), where it increases with increasing angle.

Another feature of the dispersion equation implied by the sketches and depicted explicity in figure 10 is that the second resonant frequency approaches the smaller of either ω_p or ω_{ce} as θ approaches 0°. The third resonance approaches the larger of the two frequencies.

Phase and Group Velocities of Principal Modes

Phase velocity U is plotted as a function of ω in figure 11 for densities of 10^{11}, 10^{13}, and 10^{15} ions per cubic centimeter and for magnetic fields of 10^2, 10^3, 10^4, and 10^5 gauss. A general property evident from all the plots is that the phase velocity for frequencies below the nonpropagating band (or stop band) is less than the speed of light, while above the highest cutoff frequency it exceeds the speed of light.

To complete the presentation, the group velocity V is plotted as a function of ω in figure 12 for densities of 10^{11}, 10^{13}, and 10^{15} ions per cubic centimeter and for magnetic fields of 10^2, 10^3, 10^4, and 10^5 gauss. It may be noticed from the plots that the magnitude of the group velocity in the frequency region above the highest cutoff frequency is very near the speed of light and, consequently, would be difficult to measure experimentally within the presented frequency range. In the frequency region below the lowest transmission cutoff, however, the group velocity is small enough to be determined experimentally. Although the group velocities in the lower frequency regions of experimental interest are large, plasma densities could be determined by using waves of R or L mode if the propagation path length were sufficiently long to obtain a measurable time delay of the signal. As an example, for the plasma conditions presented in figure 12(b-1) and a propagation length of 100 centimeters, a signal at a frequency of 10^7 radians per second would propagate through the plasma as an R mode with a time delay of the order of 2.5 or 25 microseconds, depending upon whether the density was 10^{13} or 10^{15} ions per cubic centimeter, respectively.

CONCLUDING REMARKS

The characteristics of electromagnetic wave propagation through a cold, collisionless plasma immersed in a magnetic field have been presented in dimensional form so the experimentalist may have quantities in laboratory units. The wave numbers, wavelengths, phase velocity, and group velocity of the principal modes determined from Astrom's equation are presented as functions of frequency. Wave numbers (wavelengths) for oblique waves at various propagation angles are also presented as functions of frequency. These values are of interest in bound plasma experiments. In addition, the cutoff and resonant frequencies for both the principal and oblique waves are presented for a range of plasma conditions. In examining the results for oblique waves, it was noted that, over the range of propagation angles from about 80° to 90° with respect to the magnetic-field direction, the wave characteristics showed a marked sensitivity to propagation direction. This effect must be considered in the design of experiments and in the interpretation of experimental findings.

Lewis Research Center
National Aeronautics and Space Administration
Cleveland, Ohio, August 7, 1963

APPENDIX A

SYMBOLS

$\mathscr{A},\mathscr{B},\mathscr{C}$	dispersion relation coefficients
$\mathscr{A}_1,\mathscr{B}_1,\mathscr{C}_1$	approximate dispersion relation coefficient
B	magnetic-field strength, gauss
$\overline{B}$	magnetic-field vector, gauss
c	velocity of light, cm/sec
d	damping distance
$\overline{E}$	electric field vector, esu
e	electron charge, esu
$\overline{J}$	current vector, abamp
K	modified dielectric coefficient, Astrom's dielectric coefficient multiplied by ω^2/c^2; $K_s = (K_r + K_l)/2$
k	wave number, $2\pi/\lambda$, cm^{-1}
$\overline{k}$	propagation vector
m	mass, g
n	particle density, ions/cm^3
U	phase velocity, ω/k, cm/sec
V	group velocity, $d\omega/dk$, cm/sec
$\overline{v}$	mass velocity, cm/sec
Z	charge number of ions
θ	angle between direction of wave propagation and magnetic-field direction, deg
λ	wavelength, cm
ω	wave frequency, radians/sec
ω_{ce}	electron cyclotron frequency, $Be/m_e c$, radians/sec
ω_{ci}	ion cyclotron frequency, $ZeB/m_i c$, radians/sec

ω^{∞} resonance frequency of oblique waves

ω_l^{∞} resonance frequency of L mode, ω_{ci}, radians/sec

ω_r^{∞} resonance frequency of R mode, ω_{ce}, radians/sec

ω_{ol} cutoff frequency of L mode, ω_{o1} (eq. (9a)) or ω_{o2}, radians/sec

ω_{op} cutoff frequency of P mode, ω_{o2} (eq. (10)) or ω_{o1}, radians/sec

ω_{or} cutoff frequency of R mode, ω_{o3} (eq. (9b)), radians/sec

ω_{os} cutoff frequency of S mode, radians/sec

ω_{osl} lower cutoff frequency of S mode, eq. (9a), radians/sec

ω_{os2} upper cutoff frequency of S mode, eq. (9b), radians/sec

ω_{o1} lower cutoff frequency eq. (9a), radians/sec

ω_{o2} middle cutoff frequency, eq. (10), radians/sec

ω_{o3} upper cutoff frequency, eq. (9b), radians/sec

ω_p plasma frequency, $\left[4\pi n_e e^2\left(\frac{1}{m_e} + \frac{Z}{m_i}\right)\right]^{1/2}$, radians/sec

ω_{pe} electron plasma frequency, $\left(4\pi n_e e^2/m_e\right)^{1/2}$, radians/sec

ω_{pi} ion plasma frequency, $\left(4\pi Z \frac{n_e e^2}{m_i}\right)^{1/2}$, radians/sec

ω_{sl}^{∞} lower hybrid frequency of S mode, eq. (12a), radians/sec

ω_{s2}^{∞} upper hybrid frequency of S mode, eq. (12b), radians/sec

ω_1 approximate resonant frequency for S mode, eq. (B7), radians/sec

ω_2 approximate resonant frequency for S mode, eq. (B5), radians/sec

ω_3 $\omega_{ci}\omega_{ce} + \omega_p^2$, radians/sec

Subscripts:

e electron

i ion

l	L mode, left circular polarization
p	P mode, axial polarization
r	R mode, right circular polarization
s	S mode, transverse polarization
x	rectangular coordinate, perpendicular to $\overline{B}$
z	rectangular coordinate, parallel to $\overline{B}$

APPENDIX B

APPROXIMATE DISPERSION EQUATIONS

The various approximations that are presented herein first appeared in the literature as developments of individual physical models. Because of their common usage, wave numbers as functions of frequency were computed for these approximate dispersion relations and were compared with the results of Astrom's expressions. The results of these comparisons are presented in this appendix.

Microwave Approximation (ref. 6)

When the ions are present only to maintain overall charge neutrality, a condition exists that is referred to as the microwave approximation. In this case the ions do not contribute to the total current, and an electron gas with charge neutrality results. Mower (ref. 6) has shown that the dielectric coefficients can be represented by the following equations (which can also be obtained from Astrom's expressions if it is assumed that $\omega \gg \omega_{ci}$ and if the inequality $m_e \ll m_i$ is used):

$$k_l^2 = K_l = \frac{\omega^2}{c^2}\left[1 - \frac{\omega_{pe}^2}{\omega(\omega + \omega_{ce})}\right] \tag{B1a}$$

$$k_r^2 = K_r = \frac{\omega^2}{c^2}\left[1 - \frac{\omega_{pe}^2}{\omega(\omega - \omega_{ce})}\right] \tag{B1b}$$

$$k_p^2 = K_p = \frac{\omega^2}{c^2}\left(1 - \frac{\omega_{pe}^2}{\omega^2}\right) \tag{B2}$$

$$K_s = \frac{\omega^2}{c^2}\left(1 - \frac{\omega_{pe}^2}{\omega^2 - \omega_{ce}^2}\right) \tag{B3}$$

From equations (B1) and (B3),

$$k_s^2 = \frac{\omega^2}{c^2}\,\frac{\left(\omega^2 - \omega\omega_{ce} - \omega_{pe}^2\right)\left(\omega^2 + \omega\omega_{ce} - \omega_{pe}^2\right)}{\omega^2\left(\omega^2 - \omega_2^2\right)} \tag{B4}$$

where

$$\omega_2^2 = \omega_{ce}^2 + \omega_{pe}^2 \tag{B5}$$

As long as the frequency satisfies the inequality $\omega \gg \omega_{ci}$, the expression

developed for the microwave approximation yields practically the same results as Astrom's expression; however, terms are dropped in this approximation that introduce errors in wave number whenever calculations are made near the cutoff (ω_{op}, ω_{ol}, ω_{os}, and ω_{os2}) or resonant (ω_{s2}^{∞}) frequencies. These errors only become large when the transmission frequency is within a fraction of a percent of the cutoff or resonant conditions.

Stix Approximation (ref. 7)

Another model that is frequently used involves the simultaneous solution of Ohm's law and the equation of motion of a fluid element. If the electron-ion mass ratio is not neglected relative to unity in the generalized Ohm's law for a collisionless plasma, results for K_l, K_r, K_p, K_s, and k_s^2 are obtained that are identical to Astrom's results. In the calculations of reference 7 certain terms that contain the electron-ion mass ratio were neglected, and the wave numbers are practically identical to Astrom's results. Stix, in addition, used approximate factors for a quadratic expression that appears in the equation for the dielectric coefficient. These approximations result in the expression

$$k_s^2 = \frac{\omega^2}{c^2} \frac{\left(\omega^2 - \omega\omega_{ce} - \omega_3^2\right)\left(\omega^2 + \omega\omega_{ce} - \omega_3^2\right)}{\left(\omega^2 - \omega_1^2\right)\left(\omega^2 - \omega_2^2\right)} \tag{B6}$$

where

$$\omega_1^{-2} = \omega_{ce}^{-1}\omega_{ci}^{-1} + \left(\omega_{pi}^2 + \omega_{ci}^2\right)^{-1} \tag{B7}$$

$$\omega_2^2 = \omega_{ce}^2 + \omega_{pe}^2 \tag{B5}$$

In performing this reduction, it was necessary to neglect $\omega_{ce}\omega_{ci}$ as compared to ω_{ce}^2. This approximation is equivalent to that which neglects the electron-ion mass ratio compared to unity.

In a similar fashion it can be shown that

$$k_p^2 = \frac{\omega^2}{c^2}\left(1 - \frac{\omega_{pe}^2}{\omega^2}\right) \tag{B8}$$

$$k_l^2 = \frac{\omega^2}{c^2}\left[1 - \frac{\omega_{pe}^2}{(\omega - \omega_{ci})(\omega + \omega_{ce})}\right] \tag{B9a}$$

$$k_r^2 = \frac{\omega^2}{c^2}\left[1 - \frac{\omega_{pe}^2}{(\omega + \omega_{ci})(\omega - \omega_{ce})}\right] \tag{B9b}$$

Since the only approximation made in the development of these equations was the neglecting of ω_{ci} compared to ω_{ce}, the error is large only in the vicinity of the frequencies that are within a fraction of a percent of the lower and upper hybrid resonances and the cutoff frequencies.

Simplified Ohm's Law (ref. 8)

The previous approximation may be further simplified by neglecting the electron inertia term in Ohm's law, that is, by using the equation

$$\overline{E} + \frac{\overline{v} \times \overline{B}}{c} - \frac{1}{en_e} \overline{J} \times \overline{B} = 0 \tag{B10}$$

in place of the generalized Ohm's law (eq. 2-12, ref. 1). This approximation is essentially equivalent to the condition that $\omega \ll \omega_{ce}$. For this case the dielectric coefficients are

$$k_l = K_l = \frac{\omega^2}{c^2}\left(1 - \frac{\omega_{pe}^2}{\omega_{ce}} \frac{1}{\omega - \omega_{ci}}\right) \tag{B11a}$$

$$k_r = K_r = \frac{\omega^2}{c^2}\left(1 + \frac{\omega_{pe}^2}{\omega_{ce}} \frac{1}{\omega + \omega_{ce}}\right) \tag{B11b}$$

$$K_s = \frac{\omega^2}{c^2}\left(1 - \omega_{pe}^2 \frac{\omega_{ci}}{\omega_{ce}} \frac{1}{\omega^2 - \omega_{ci}^2}\right) \tag{B12}$$

The wave number for the S mode reduces to

$$k_s^2 = \frac{\omega^2}{c^2} \frac{\left[\omega\omega_{ce} + \left(\omega_{ce}\omega_{ci} + \omega_{pe}^2\right)\right]\left[\omega\omega_{ce} - \left(\omega_{ce}\omega_{ci} + \omega_{pe}^2\right)\right]}{\left[\omega_{ce}^2\left(\omega^2 - \omega_{ci}^2\right) - \omega_{pe}^2\omega_{ci}\omega_{ce}\right]} \tag{B13}$$

For oblique waves the general dispersion relation (eq. (6)) becomes

$$\tan^2\theta = \frac{\left(k^2 - K_r\right)\left(k^2 - K_l\right)}{K_s k^2 - K_r K_l} \tag{B14}$$

for this approximation. Note that K_p does not appear in the $\tan^2\theta$ relation. The component wave numbers may be written in the same form as equation (5), namely,

$$
\left.
\begin{aligned}
k_{x1}^2 &= \frac{\mathscr{B}_1 + \sqrt{\mathscr{B}_1^2 - 4\mathscr{A}_1\mathscr{C}_1}}{2\mathscr{A}_1} \sin^2\theta \\
k_{x2}^2 &= \frac{\mathscr{B}_1 - \sqrt{\mathscr{B}_1^2 - 4\mathscr{A}_1\mathscr{C}_1}}{2\mathscr{A}_1} \sin^2\theta \\
k_{z1}^2 &= \frac{\mathscr{B}_1 + \sqrt{\mathscr{B}_1^2 - 4\mathscr{A}_1\mathscr{C}_1}}{2\mathscr{A}_1} \cos^2\theta \\
k_{z2}^2 &= \frac{\mathscr{B}_1 - \sqrt{\mathscr{B}_1^2 - 4\mathscr{A}_1\mathscr{C}_1}}{2\mathscr{A}_1} \cos^2\theta
\end{aligned}
\right\} \qquad \text{(B15)}
$$

The expressions for $\mathscr{A}_1$, $\mathscr{B}_1$, and $\mathscr{C}_1$ have been modified, however, so that in this case

$$
\left.
\begin{aligned}
\mathscr{A}_1 &= \cos^2\theta \\
\mathscr{B}_1 &= K_s(1 + \cos^2\theta) \\
\mathscr{C}_1 &= K_r K_l
\end{aligned}
\right\} \qquad \text{(B16)}
$$

These expressions are identical to the dispersion relation presented in reference 8 if the proper substitutions for k and θ are made.

Figure 13 presents curves calculated from the dispersion relation obtained by this method. When particle currents are negligible compared to displacement currents, Ohm's law does not affect the results, and, consequently, the restriction $\omega \ll \omega_{ce}$ is not required. Therefore, there are regions of the frequency spectrum, other than $\omega \ll \omega_{ce}$, where the approximate and exact expressions agree. The plots of k_r^2 and k_s^2 for large magnetic fields ($B = 10^5$, figs. 13(b-2), 13(c-2), 1(c-4), and 1(d-4)) demonstrate that agreement may exist for nearly the complete frequency range. Discrepancies between the two models for the example occur in narrow frequency bands centered around the upper resonance points (near ω_{ce}), which, incidentally, are not predicted by the approximate relations. As the magnetic field decreases, there is a wider range of frequencies for which the approximate equation is unsatisfactory. The regions of inaccuracy are particularly large for low densities. These latter conclusions are exemplified by comparing figures 1(b-1), 1(c-1), and 1(d-1) with 13(a-1), 13(b-1), and 13(c-1), respectively.

Figures 14 and 15 present the approximate dispersion relation for oblique

waves propagating at angles of 10° and 80°, respectively, as calculated for the simplified Ohm's law approximation. Curves presenting the corresponding Astrom data are also included in the figures to illustrate, by comparison, in what frequency range the results of this approximation can be applied.

REFERENCES

1. Spitzer, Lyman: Physics of Fully Ionized Gases. Second ed., Intersci. Pub., 1962.

2. Aström, Ernst: On Waves in an Ionized Gas. Arkiv Fysik, bd. 2, no. 42, 1950, pp. 443-457.

3. Epstein, Paul S.: Theory of Wave Propagation in a Gyromagnetic Medium. Rev. Modern Phys., vol. 28, no. 1, Jan. 1956, pp. 3-17.

4. Stix, Thomas Howard: The Theory of Plasma Waves. McGraw-Hill Book Co., Inc., 1962.

5. Reshotko, Eli: Resonance in a Cold Multiconstituent Plasma at Arbitrary Orientation to the Magnetic Field. NASA TN D-1875, 1963.

6. Mower, Lyman: Propagation of Plane Waves in an Electrically Anisotropic Medium. Tech. Rep. MPL-1, Sylvania Electric Products, Inc., Nov. 7, 1956.

7. Stix, Thomas H.: Absorption of Plasma Waves. The Phys. of Fluids, vol. 3, no. 1, Jan.-Feb. 1960, pp. 19-32.

8. Stix, Thomas H.: Oscillations of a Cylindrical Plasma. Phys. Rev., vol. 106, no. 6, June 1957, pp. 1146-1150.

TABLE I. - SUMMARY OF DATA PRESENTED IN FIGURES 1 TO 18

Figure	Curve description	Model	Wave propagation angle, θ, deg	Magnetic-field strength, B, gauss	Particle density, n, ions/cm^3
1	k^2 against ω ($k^2 > 0$)	Astrom	0, 90	10^2 to 10^5	10^{10} to 10^{15}
2 to 8	k_x^2, k_z^2 against ω ($k^2 > 0$)	Astrom	0.1, 1, 10, 45, 80, 89, 89.9	10^2 to 10^4	$10^{11}, 10^{13}$
9	k_x^2, k_z^2 against ω ($k^2 < 0$)	Astrom	1, 10, 45, 80, 89, 89.9, 90	10^4	10^{13}
10	ω^∞ against θ	Astrom	0 to 90	10^2 to 10^4	$10^{11}, 10^{13}$
11	U against ω ($k^2 > 0$)	Astrom	0, 90	10^2 to 10^5	10^{11} to 10^{15}
12	V against ω ($k^2 > 0$)	Astrom	0, 90	10^2 to 10^5	10^{11} to 10^{15}
13	k^2 against ω ($k^2 > 0$)	Simplified Ohm's law	0, 90	$10^2, 10^5$	10^{10} to 10^{15}
14, 15	k_x^2, k_z^2 against ω ($k^2 > 0$)	Simplified Ohm's law	10, 80	$10^2, 10^4$	$10^{11}, 10^{13}$
16 to 18	ω_o, ω^∞ against n	Astrom	0, 90	10^2 to 10^5	10^{10} to 10^{15}

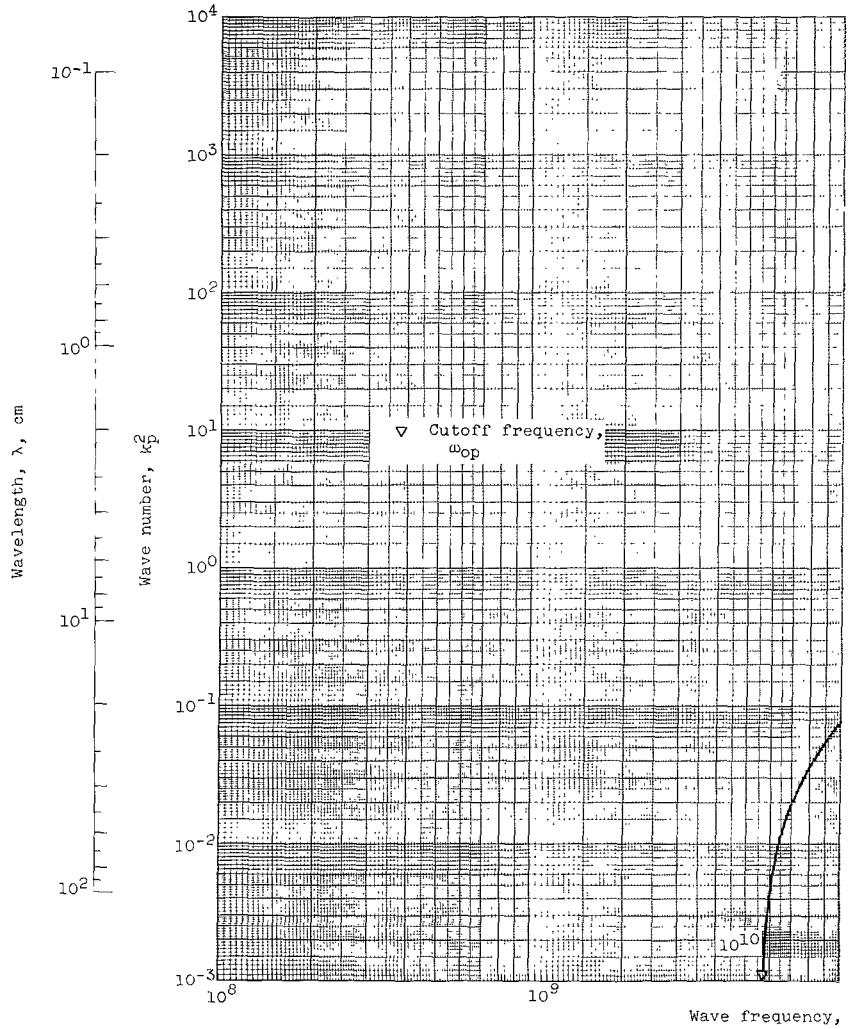

(a) P mode; wave

Figure 1. - Wave number as function of frequency.

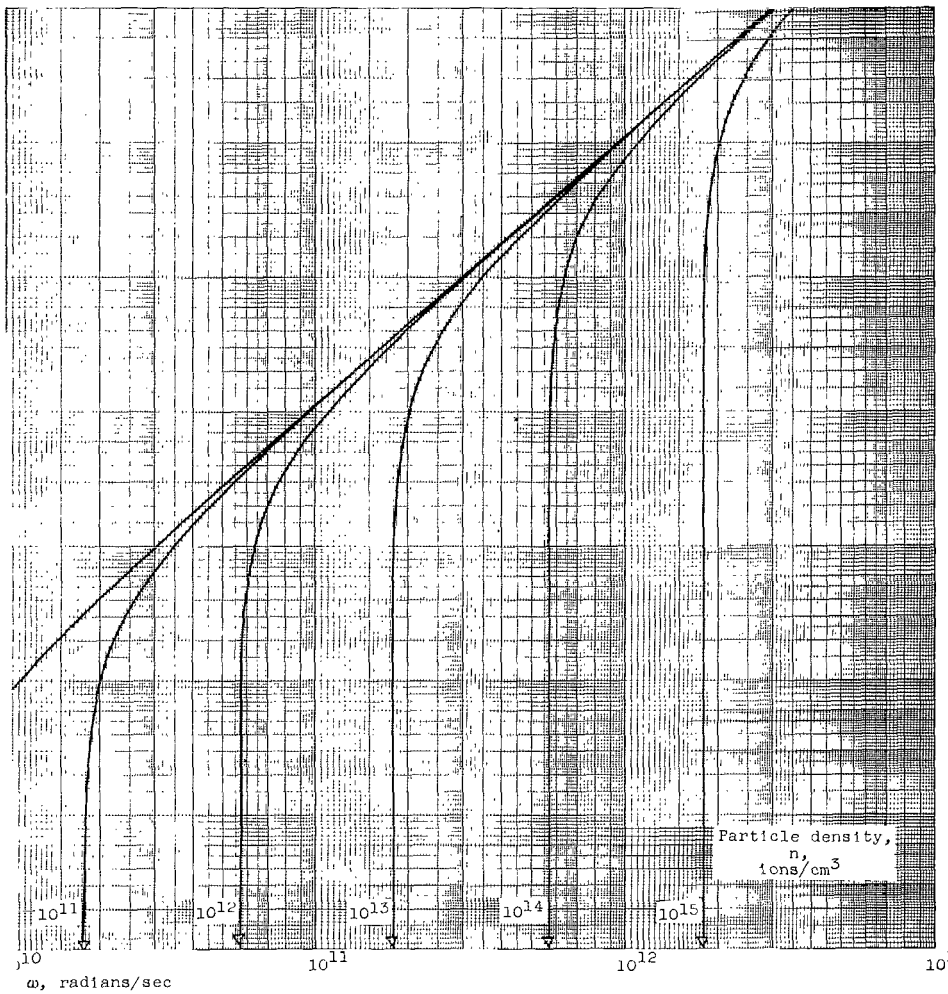

propagation angle, 90°.

Wave propagation angles, 0° and 90°; Astrom's model.

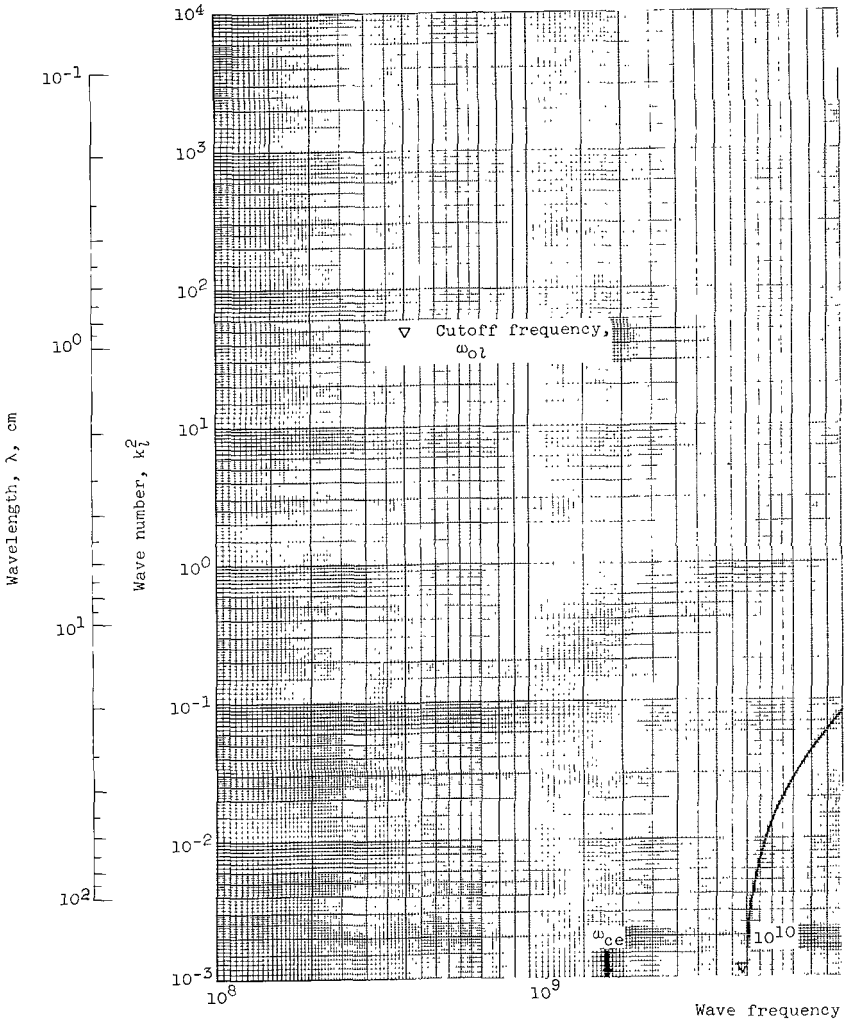

(b-1) Magnetic-fiel

(b) L mode; wav

Figure 1. - Continued. Wave number as function o

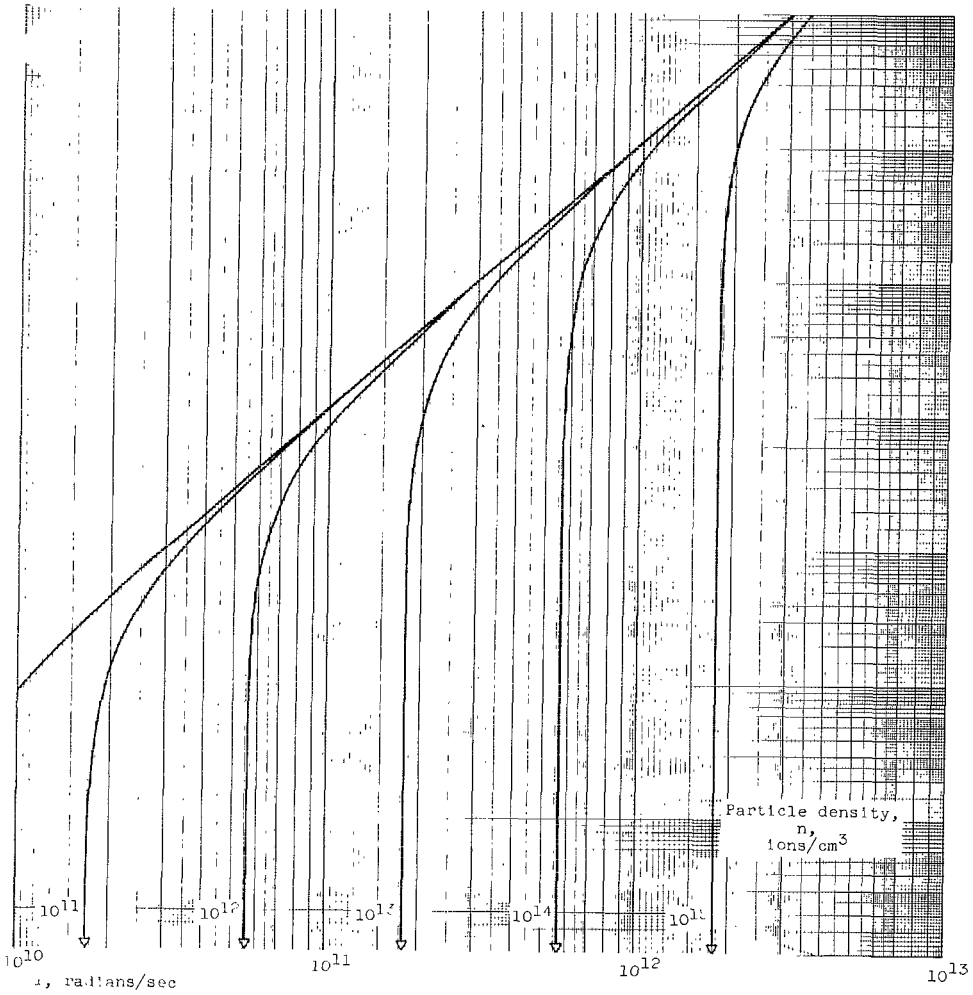

ω, radians/sec

strength, 10^2 gauss.

propagation angle, 0°.

frequency. Wave propagation angles, 0° and 90°; Astrom's model.

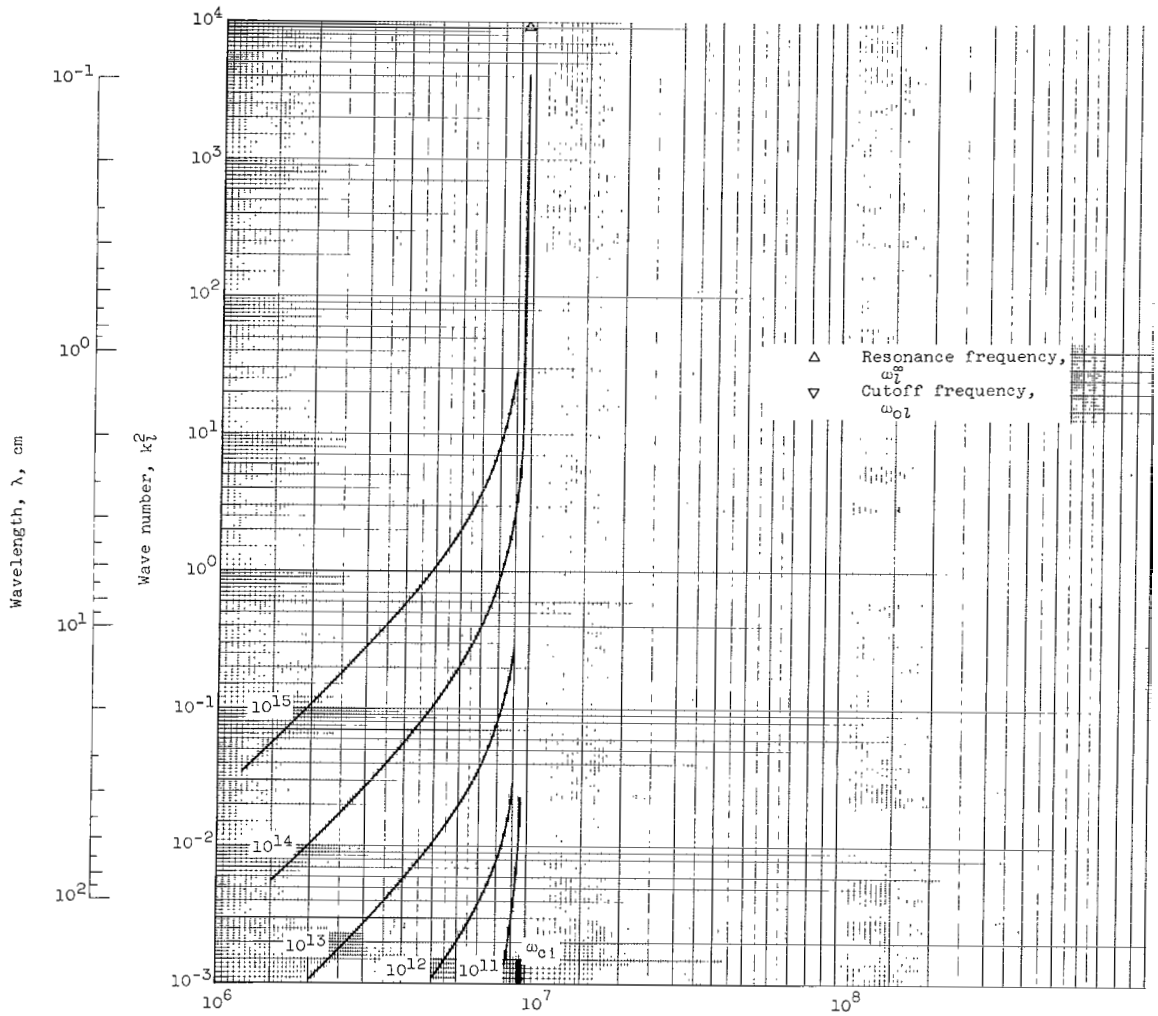

(b-2) Magnetic field

(b) Continued. L mode;

Figure 1. - Continued. Wave number as function of

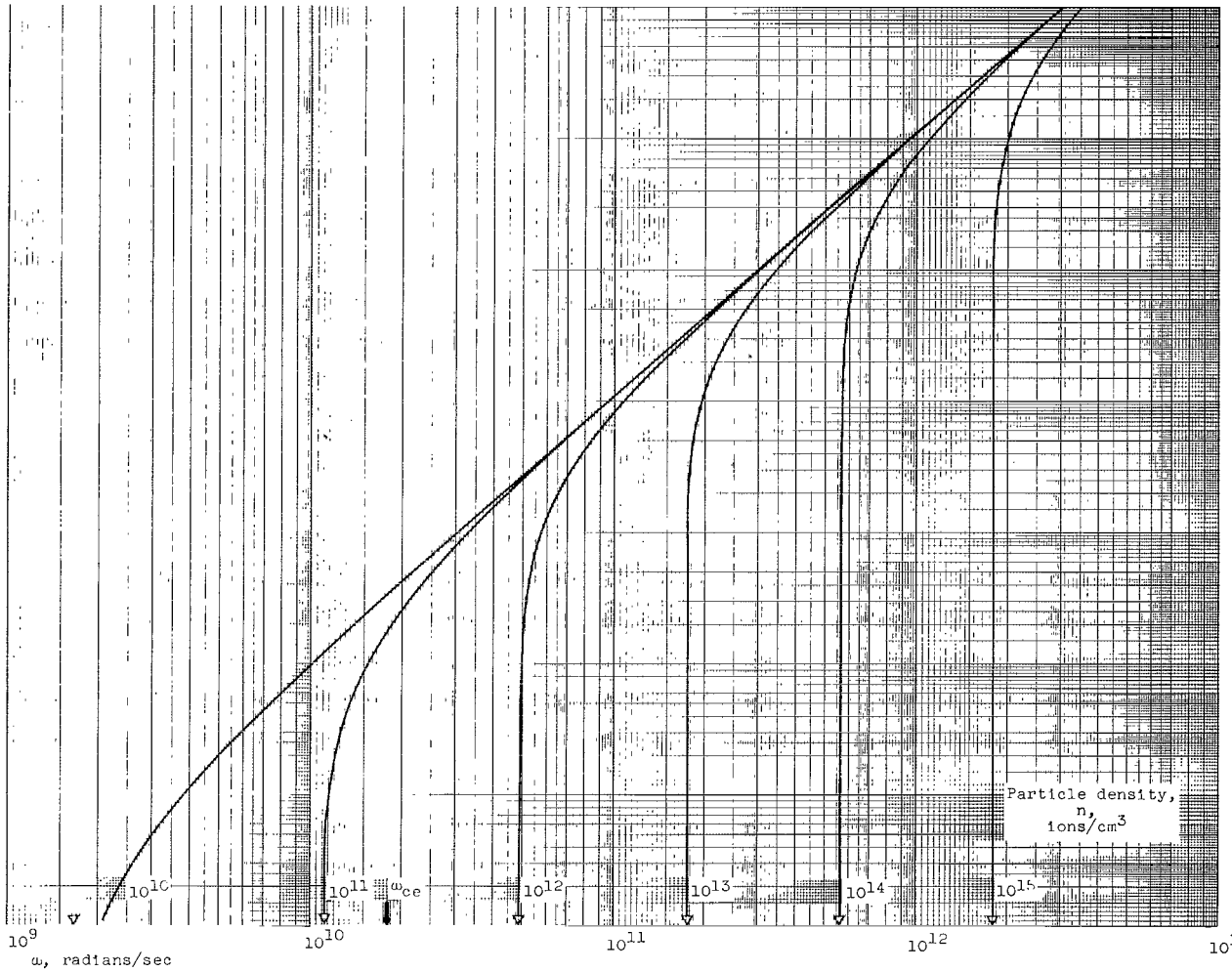

strength, 10^3 gauss.

wave propagation angle, 0°.

frequency. Wave propagation angles, 0° and 90°; Astrom's model.

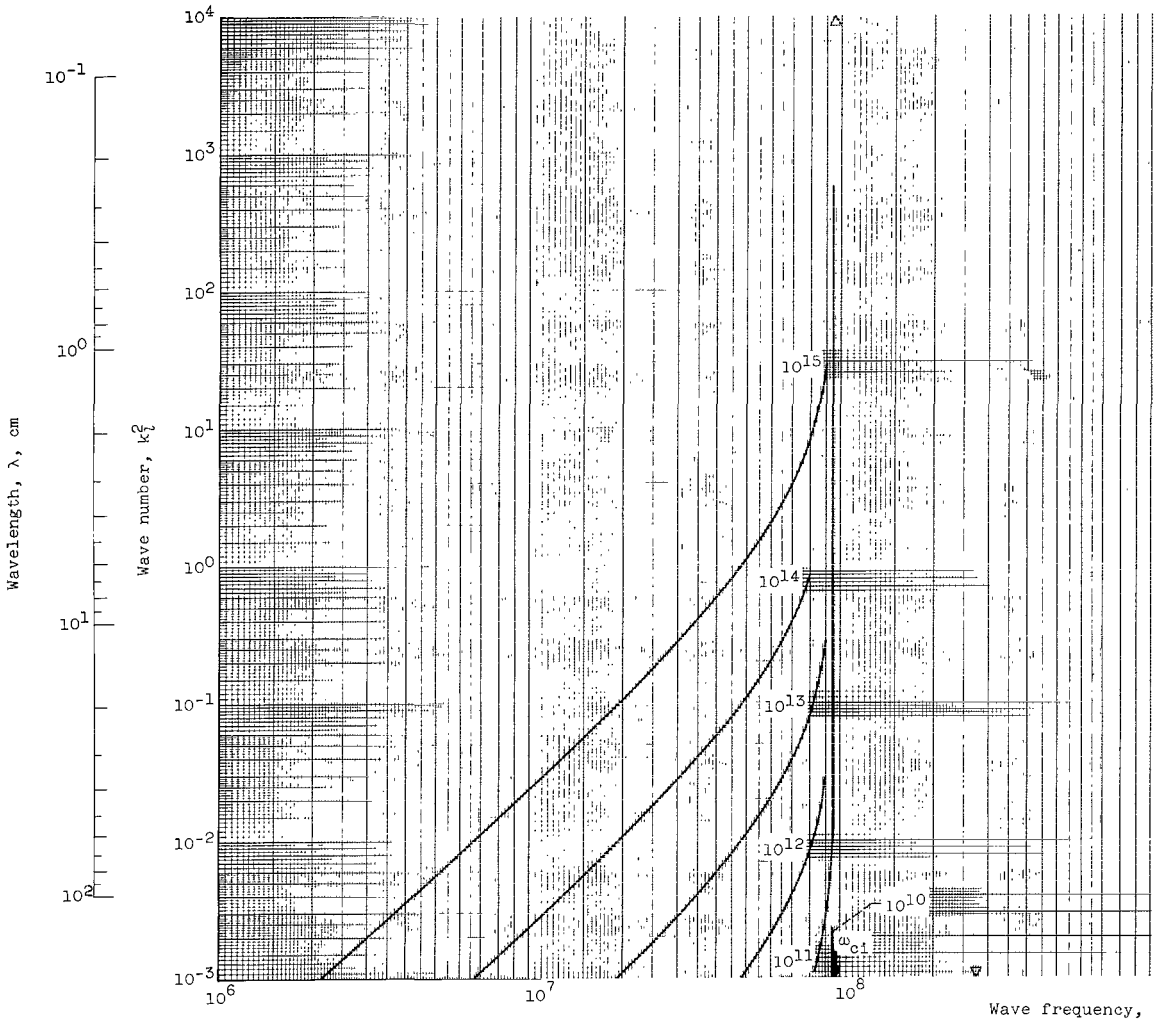

(b-3) Magnetic-field

(b) Continued. L mode;

Figure 1. - Continued. Wave number as function of

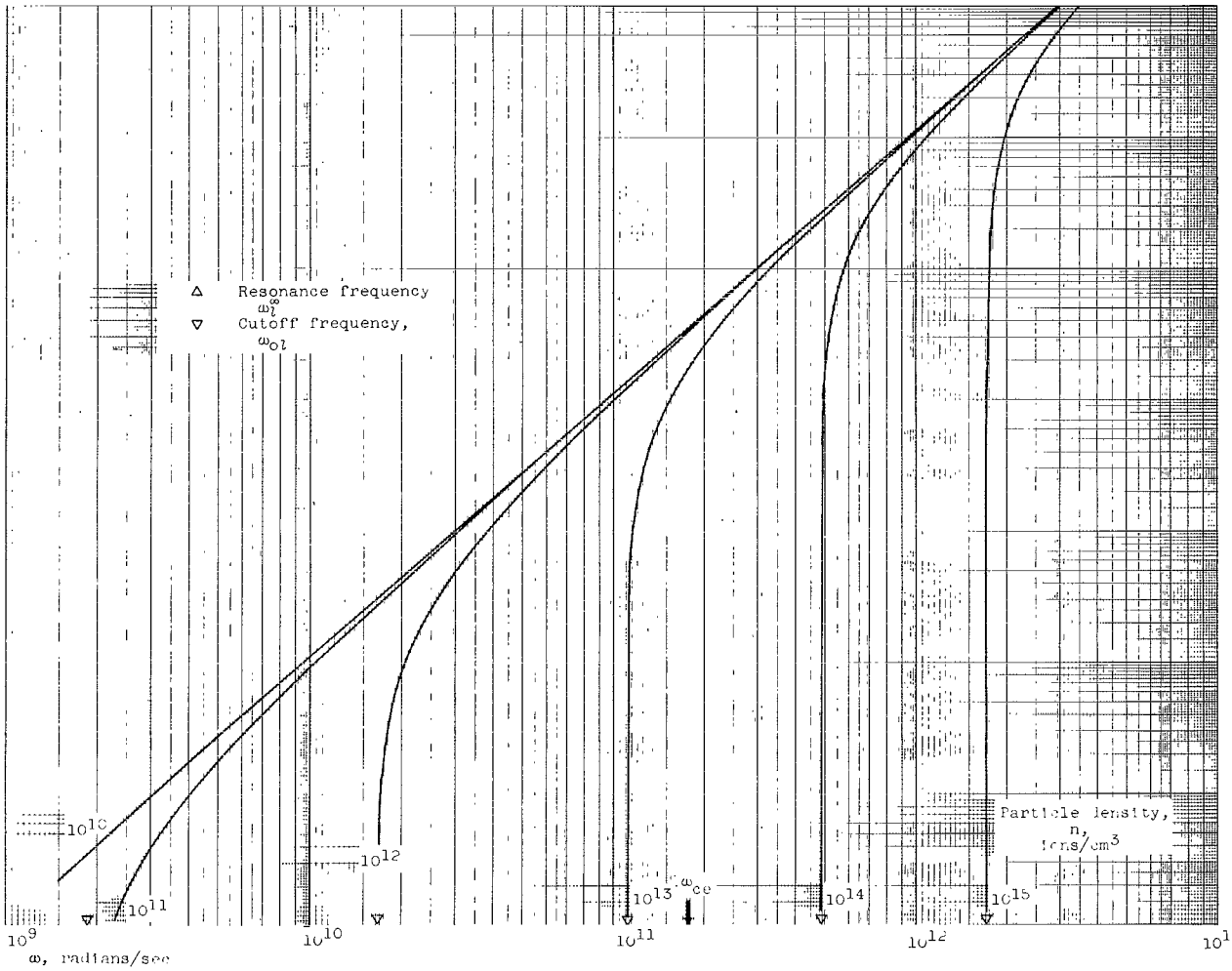

ω, radians/sec

strength, 10^4 gauss.

wave propagation angle, 0°.

frequency. Wave propagation angles, 0° and 90°; Astrom's model.

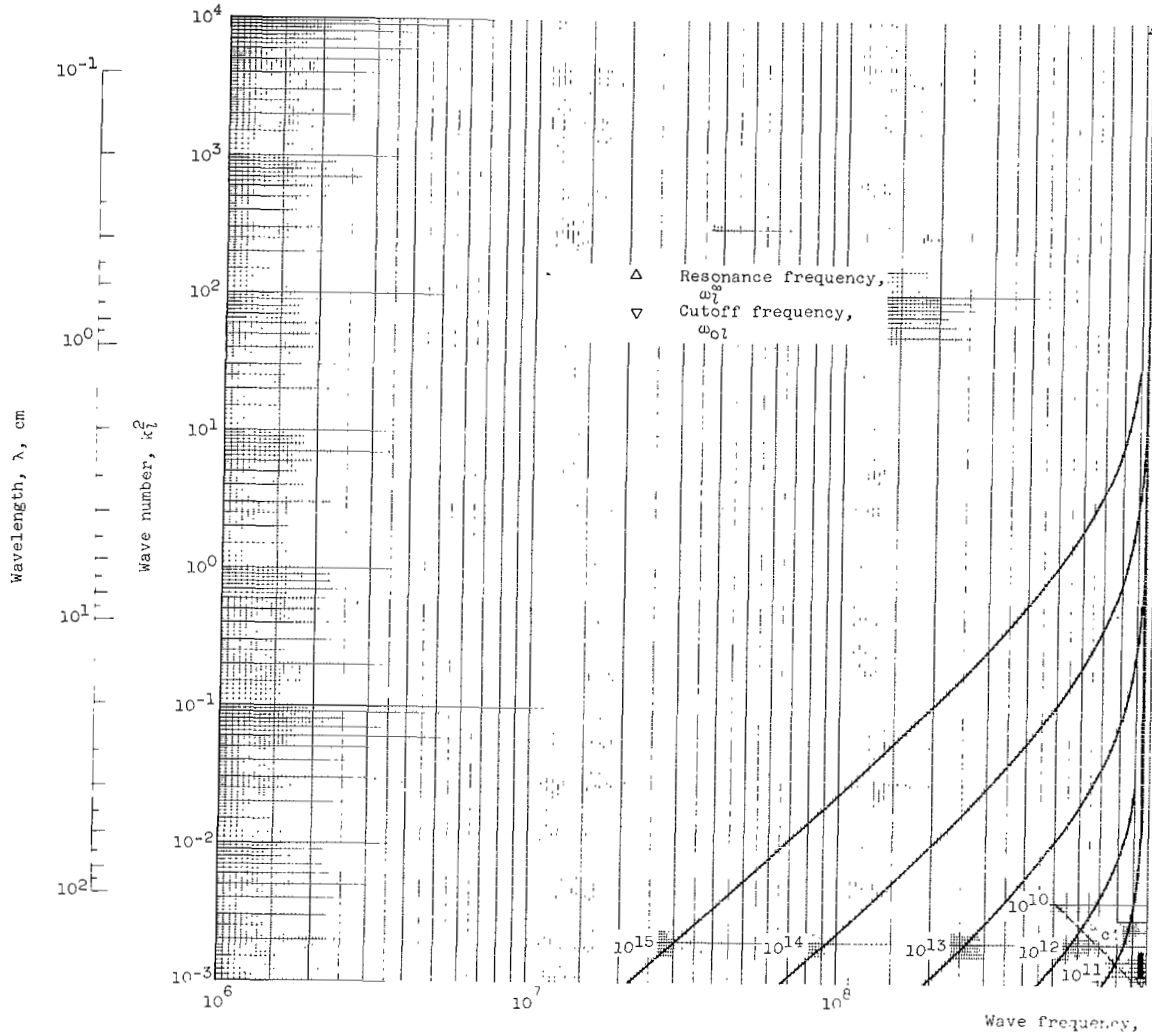

(b-4) Magnetic-field

(b) Concluded. L mode;

Figure 1. - Continued. Wave number as function of

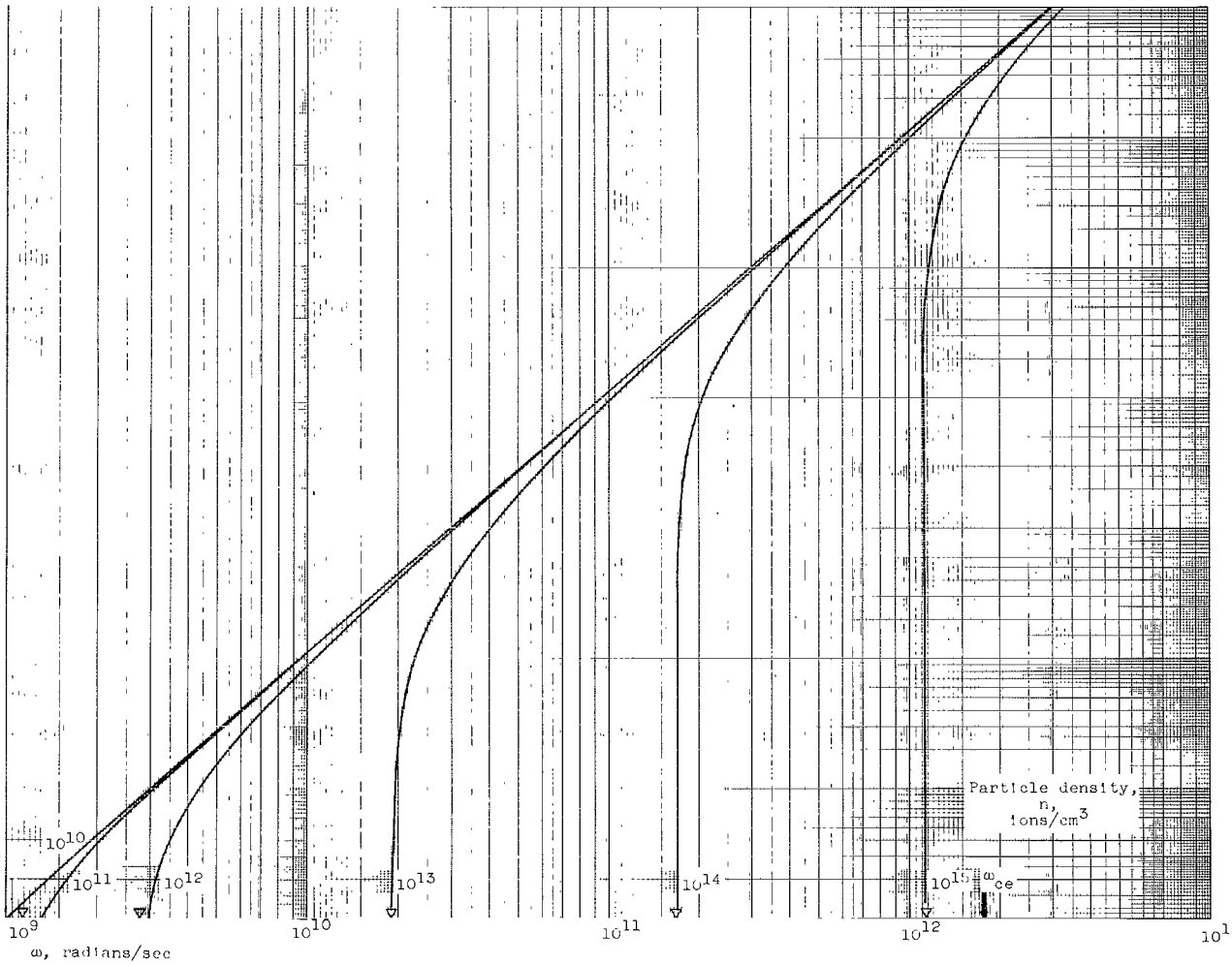

ω, radians/sec

strength, 10^5 gauss.

wave propagation angle, 0^o.

frequency. Wave propagation angles, 0^o and 90^o; Astrom's model.

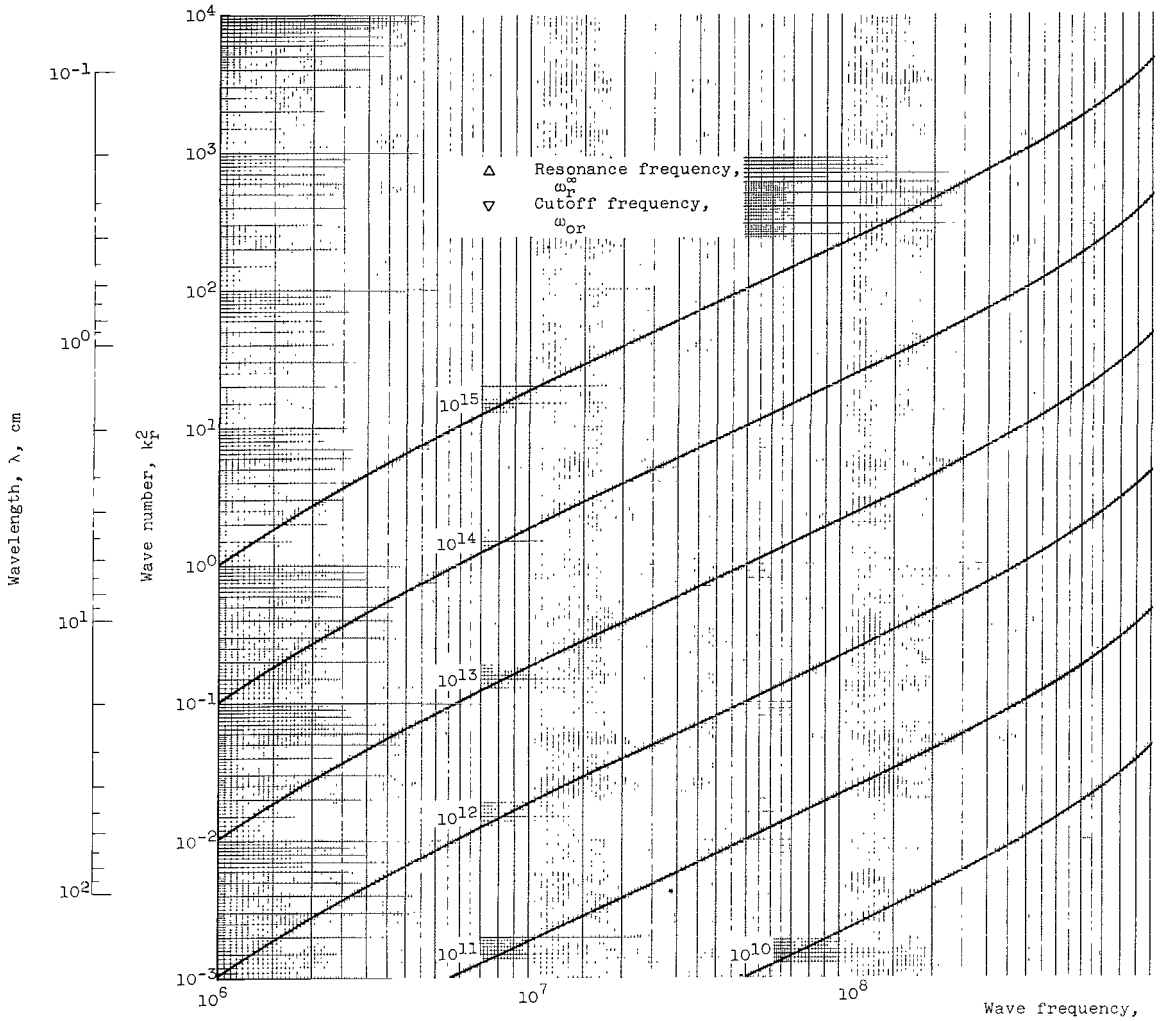

(c-1) Magnetic-field

(c) R mode; wave

Figure 1. - Continued. Wave number as function of

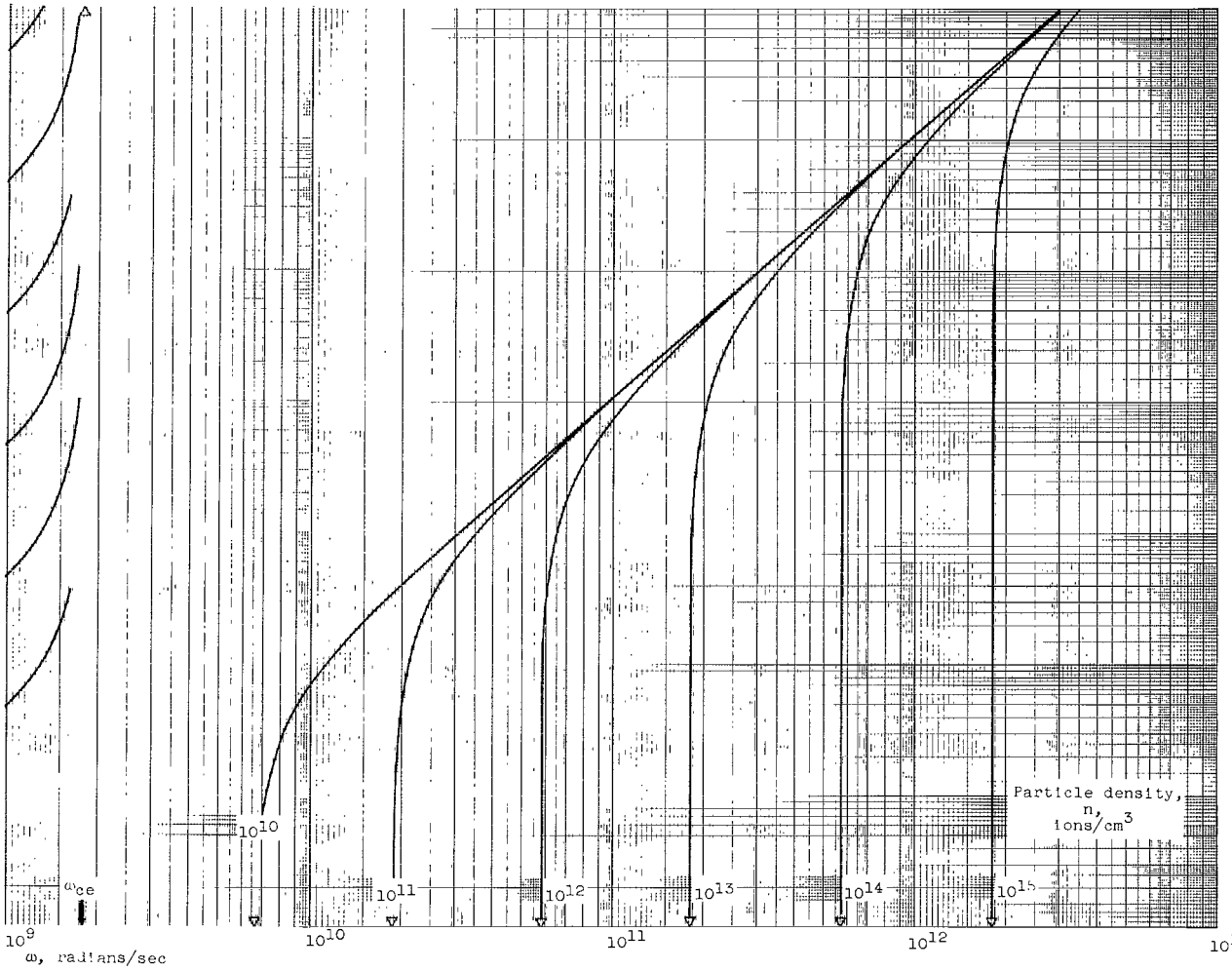

ω, radians/sec

strength, 10^2 gauss.

propagation angle, 0°.

frequency. Wave propagation angles, 0° and 90°; Astrom's model.

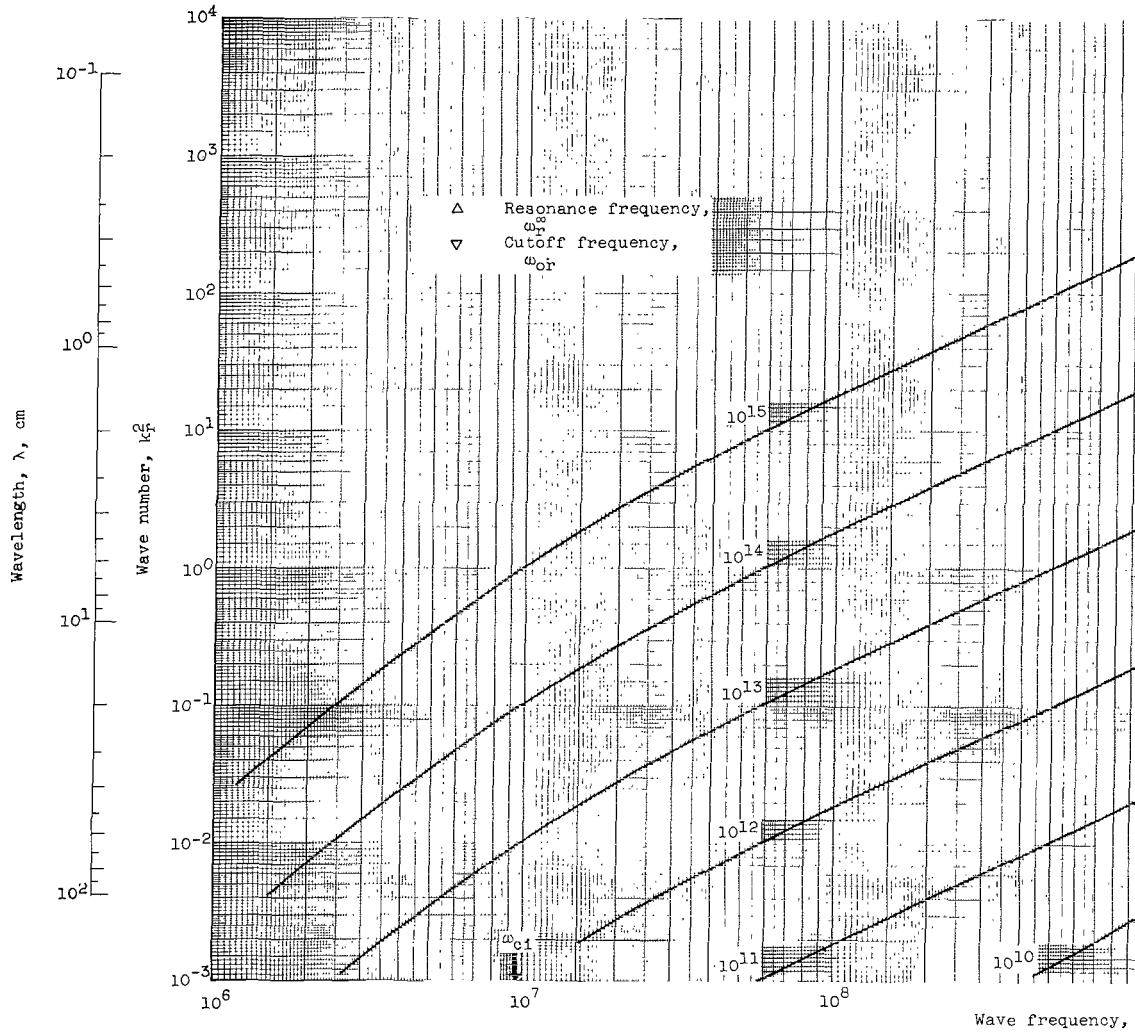

(c-2) Magnetic-field

(c) Continued. R mode;

Figure 1. - Continued. Wave number as function of

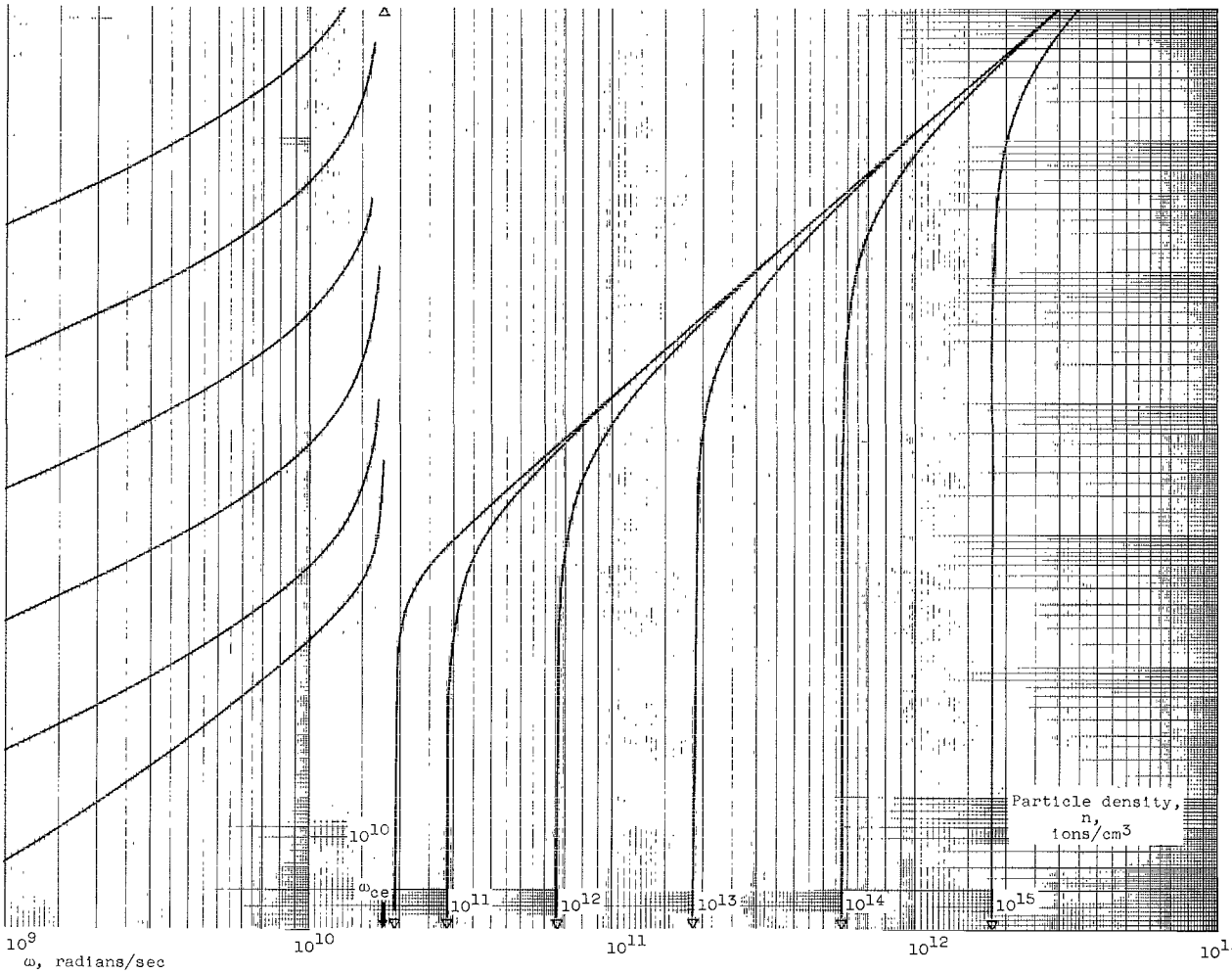

ω, radians/sec

strength, 10^3 gauss.

wave propagation angle, 0°.

frequency. Wave propagation angles, 0° and 90°; Astrom's model.

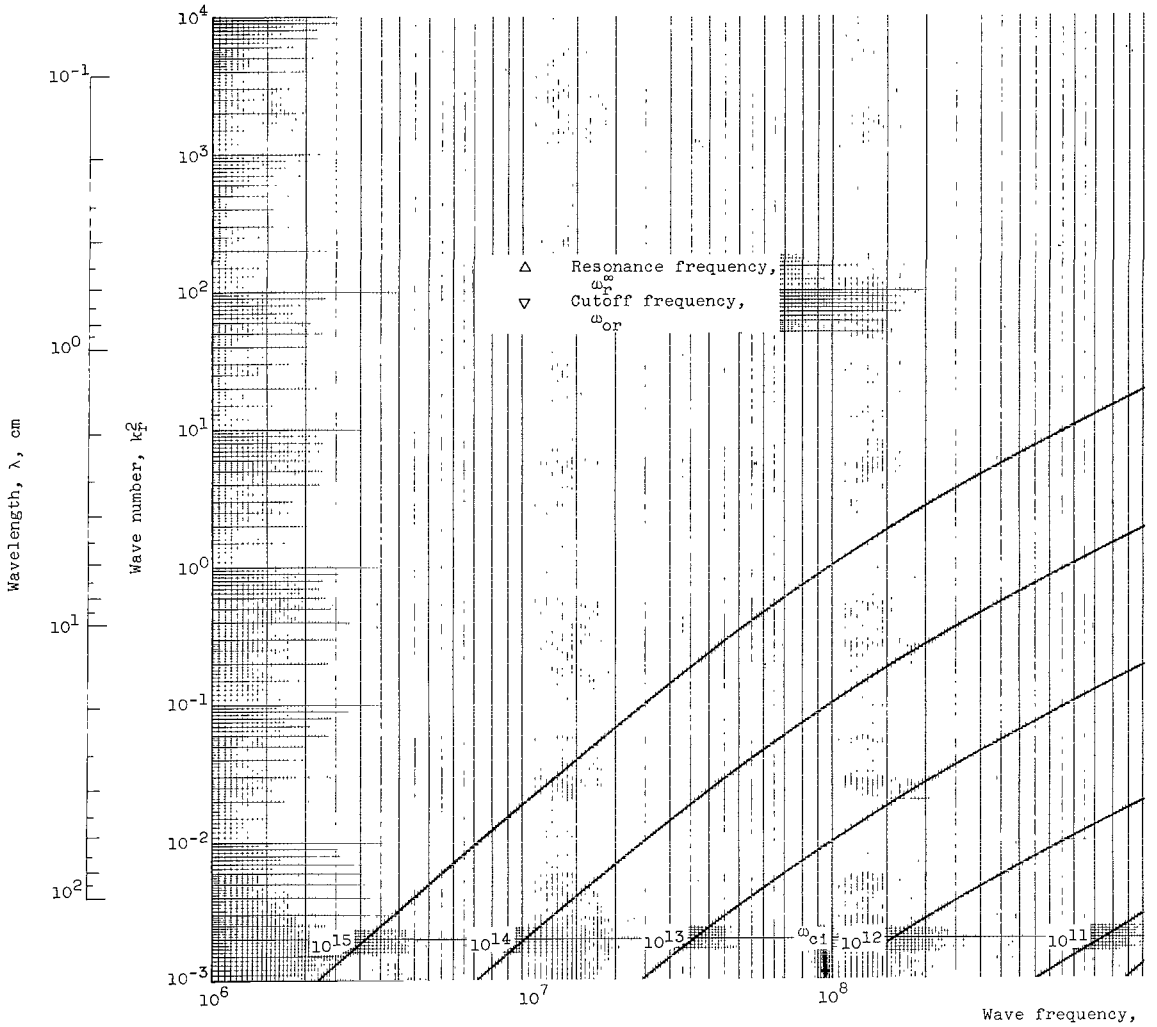

(c-3) Magnetic-field

(c) Continued. R mode;

Figure 1. - Continued. Wave number as function of

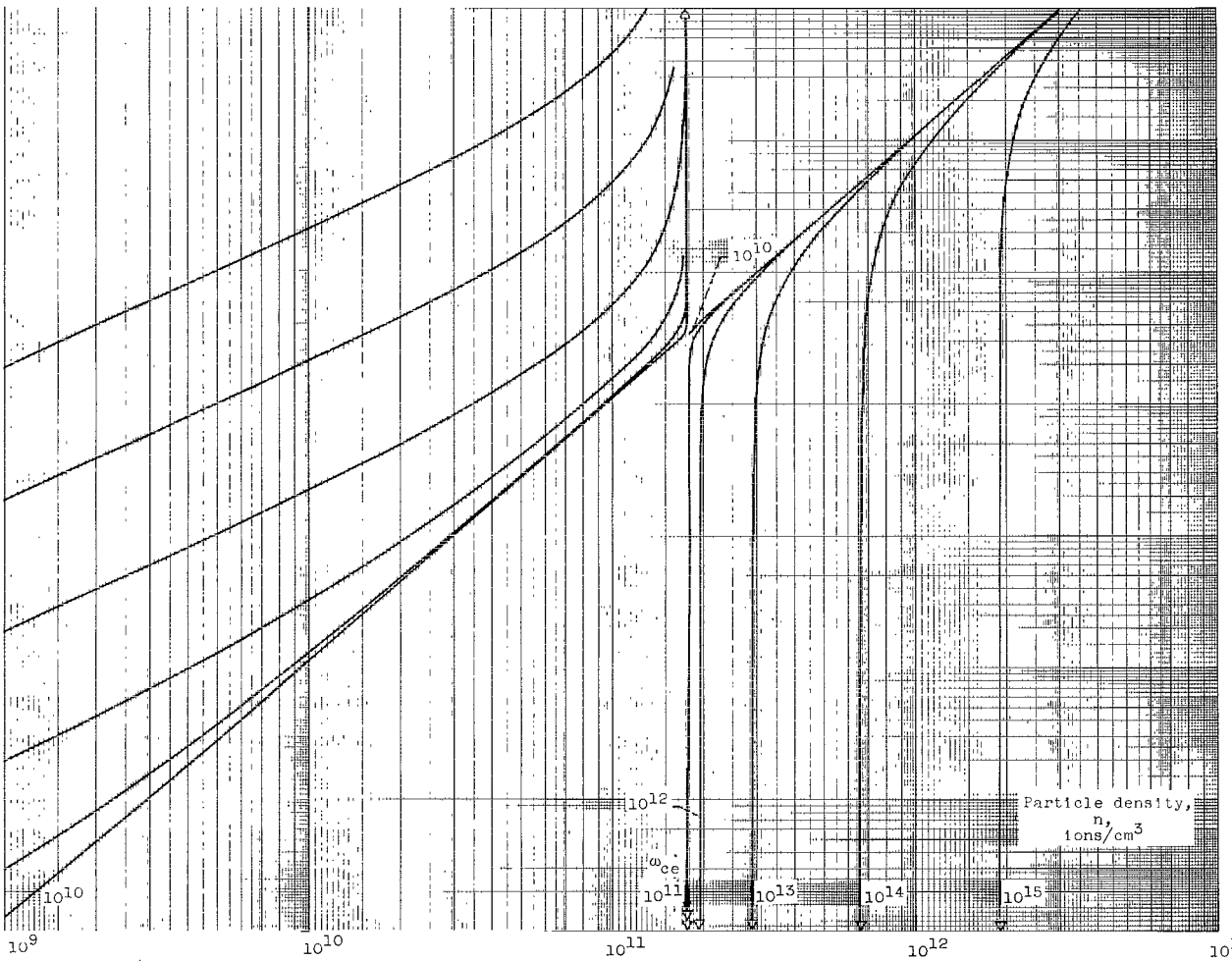

ω, radians/sec

strength, 10^4 gauss.

wave propagation angle, 0^o.

frequency. Wave propagation angles, 0^o and 90^o; Astrom's model.

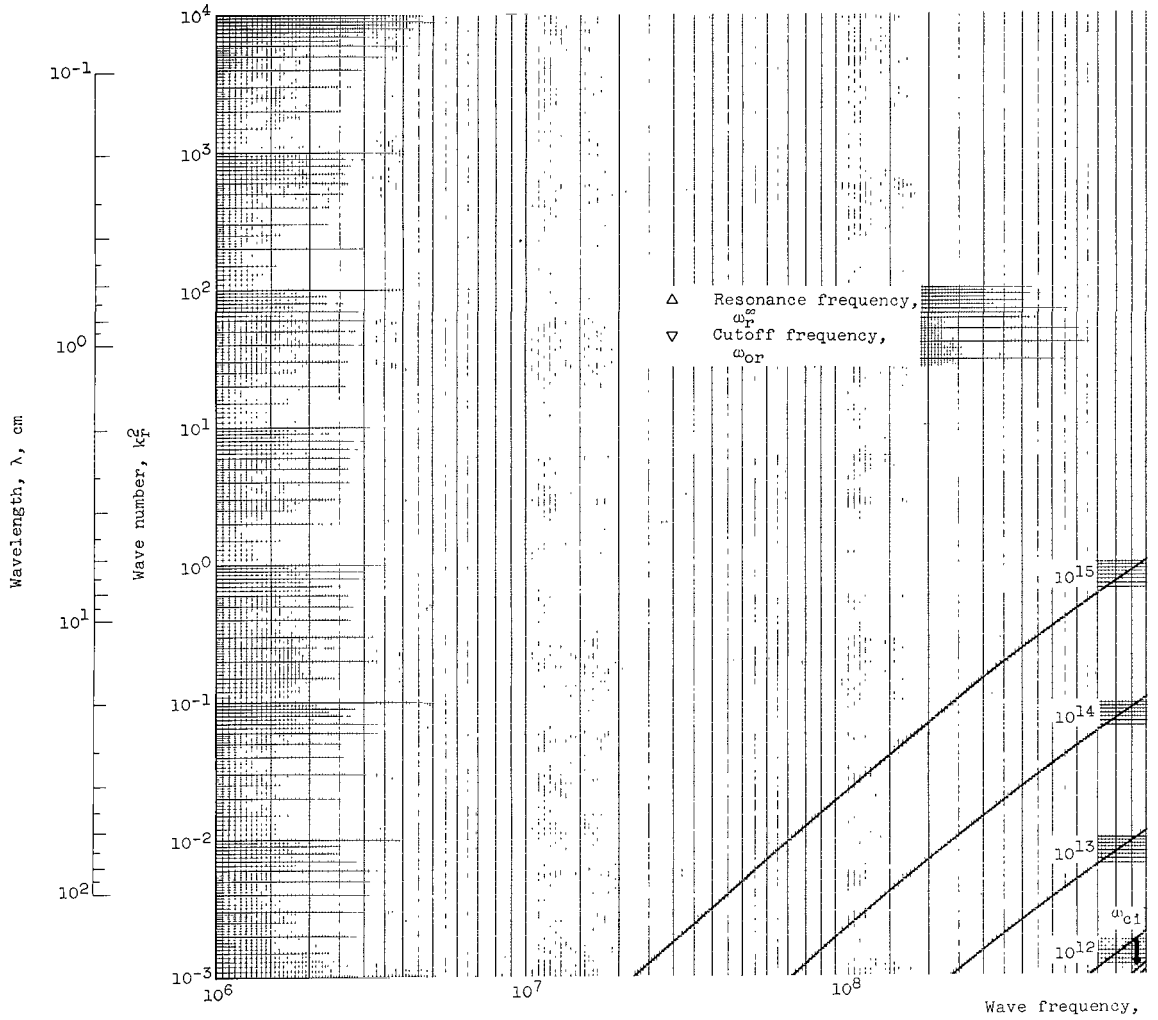

(c-4) Magnetic-field

(c) Concluded. R mode;

Figure 1. - Continued. Wave number as function of

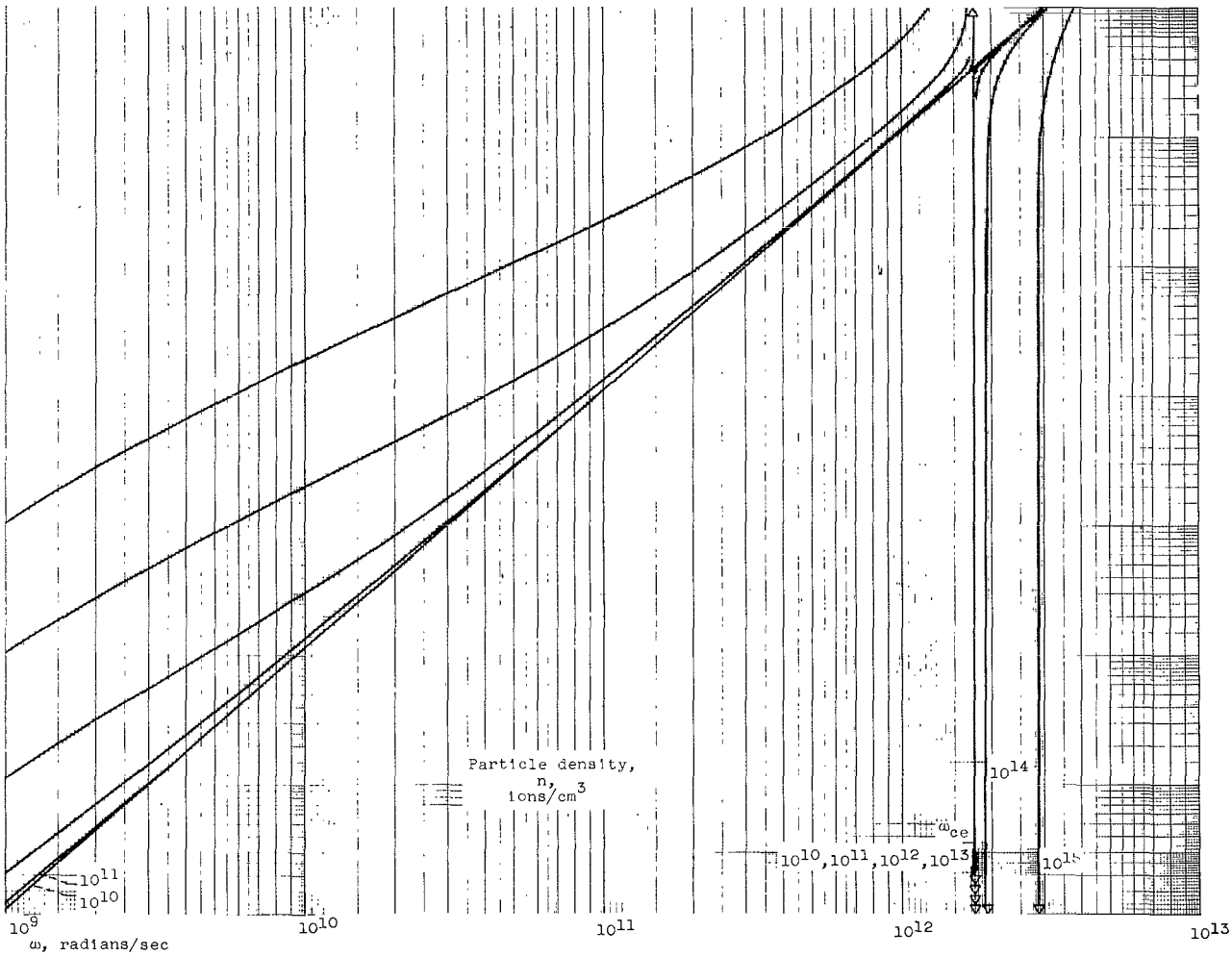

ω, radians/sec

strength, 10^5 gauss.

wave propagation angle, 0°.

frequency. Wave propagation angles, 0° and 90°; Astrom's model.

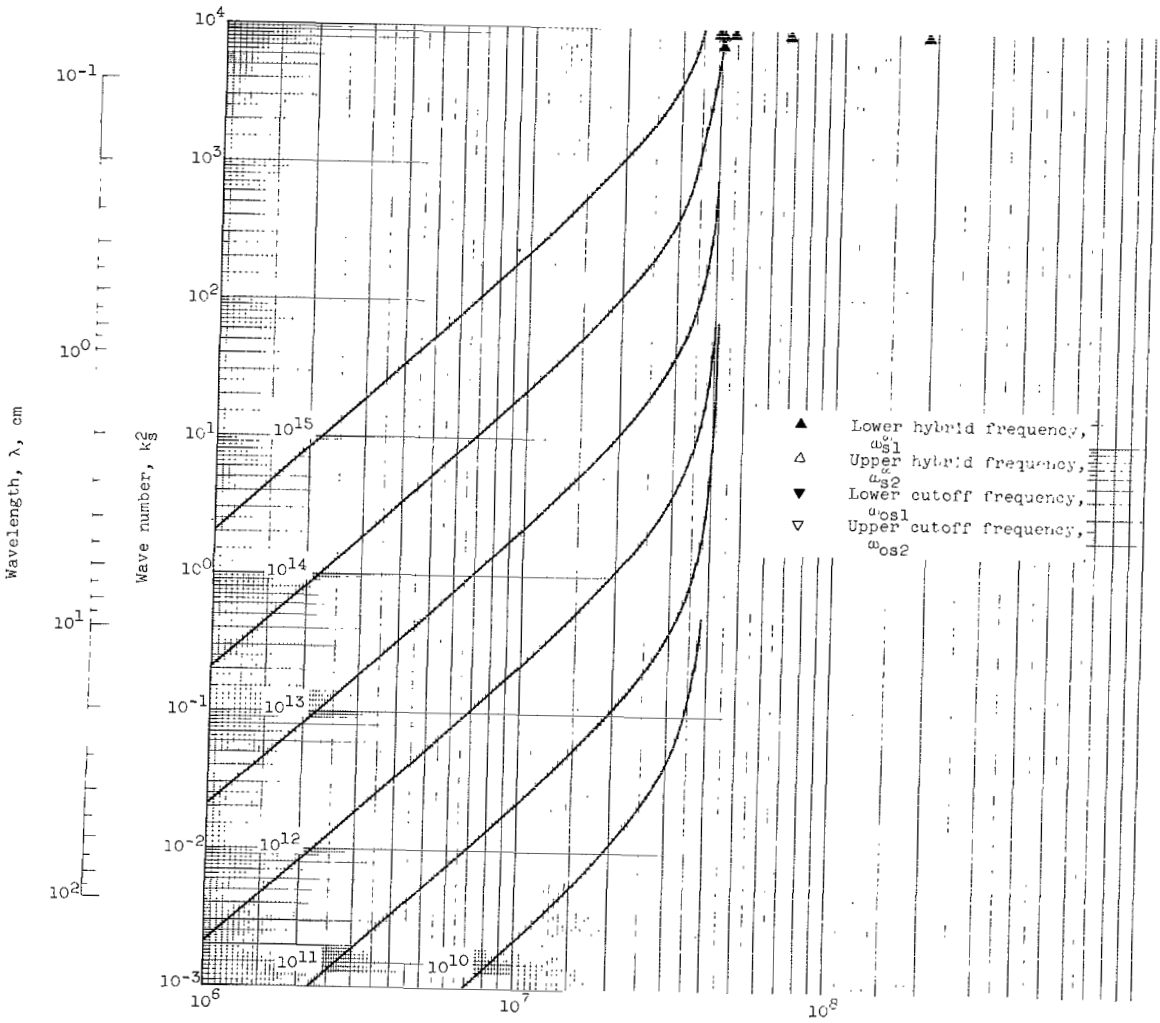

(d-1) Magnetic-field

(d) S mode; wave

Figure 1. - Continued. Wave number as function of

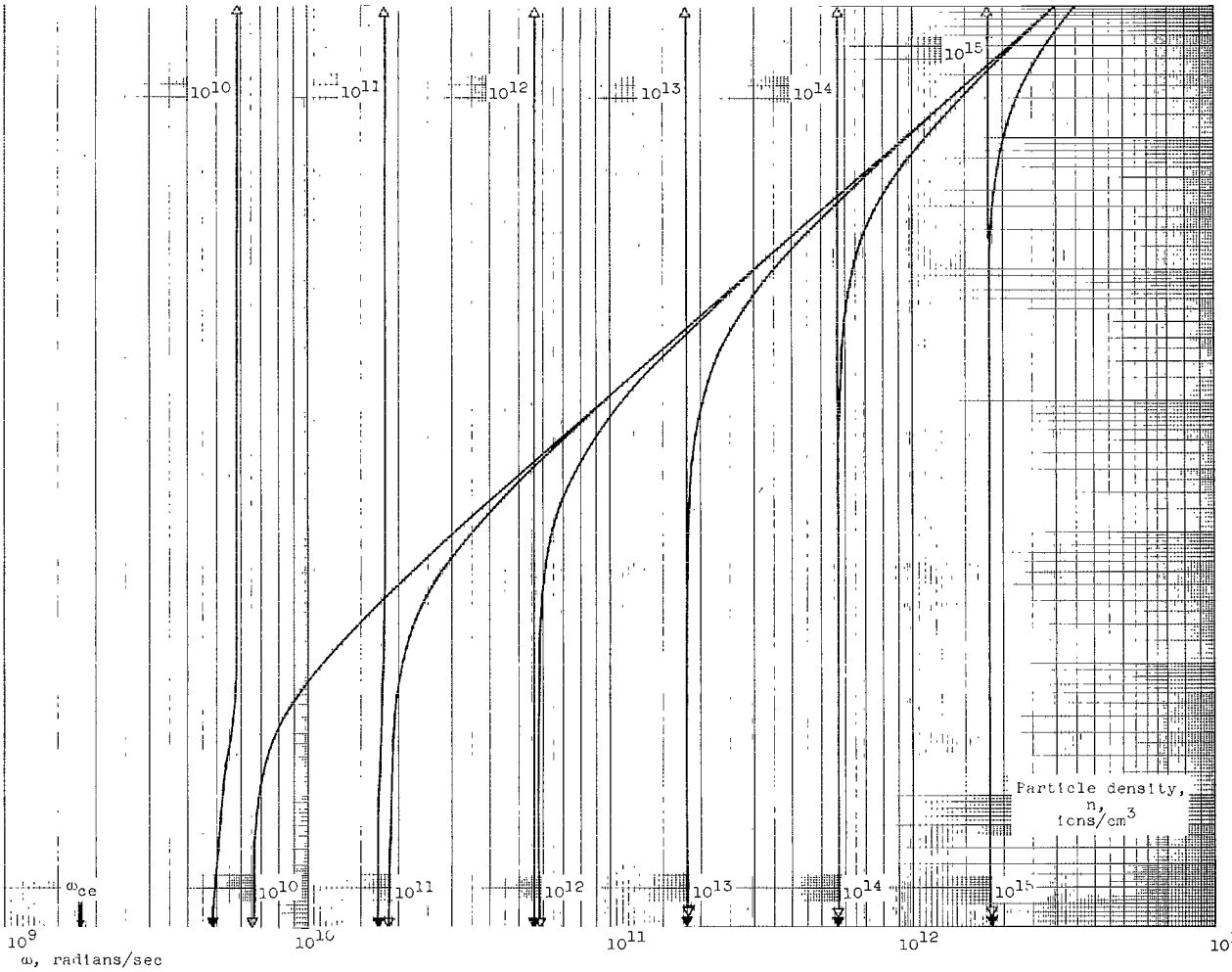

ω, radians/sec

strength, 10^2 gauss.

propagation angle, 90°.

frequency. Wave propagation angles, 0° and 90°; Astrom's model.

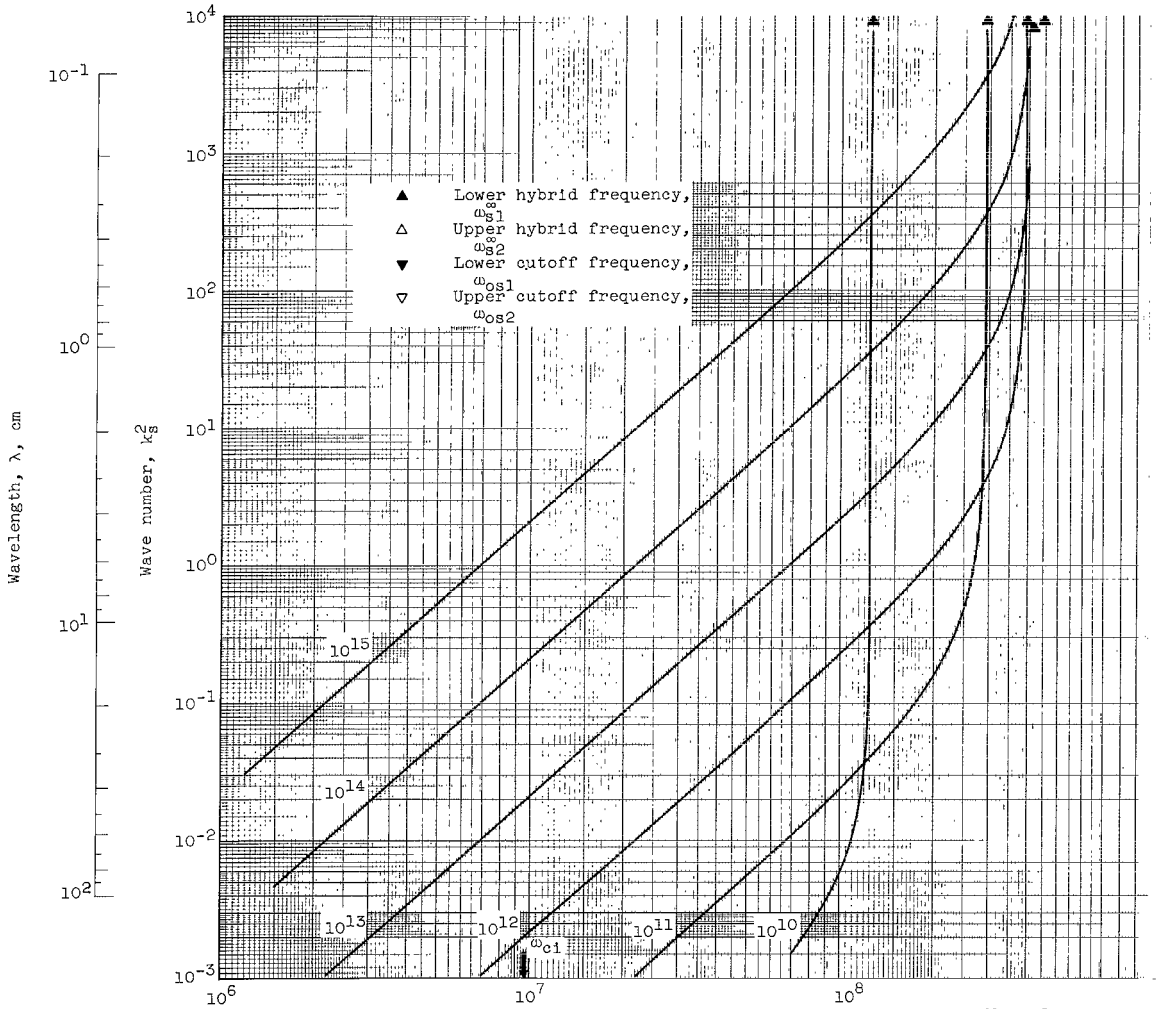

(d-2) Magnetic-field

(d) Continued. S mode;

Figure 1. - Continued. Wave number as function of

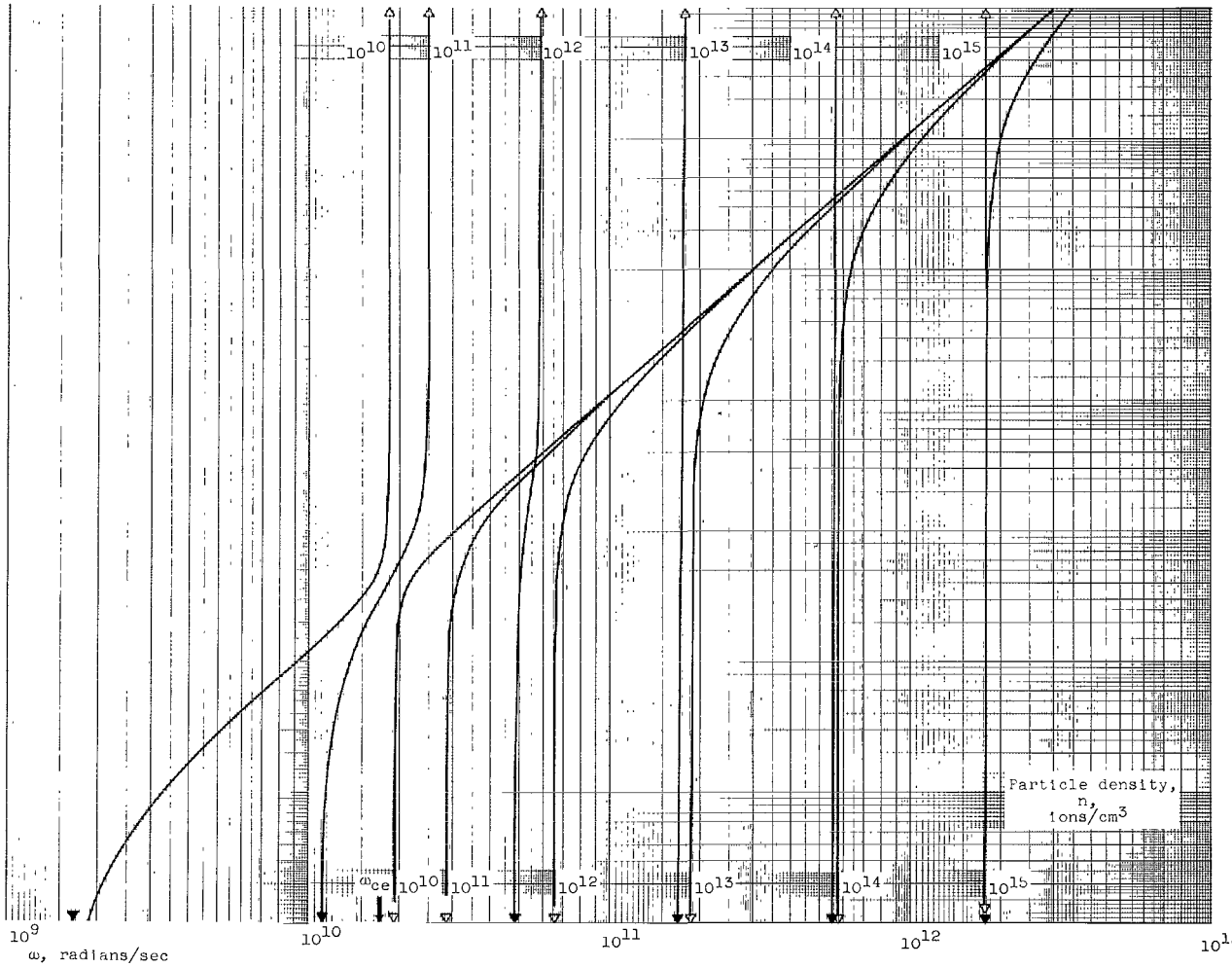

ω, radians/sec

strength, 10^3 gauss.

wave propagation angle, 90°.

frequency. Wave propagation angles, 0° and 90°; Astrom's model.

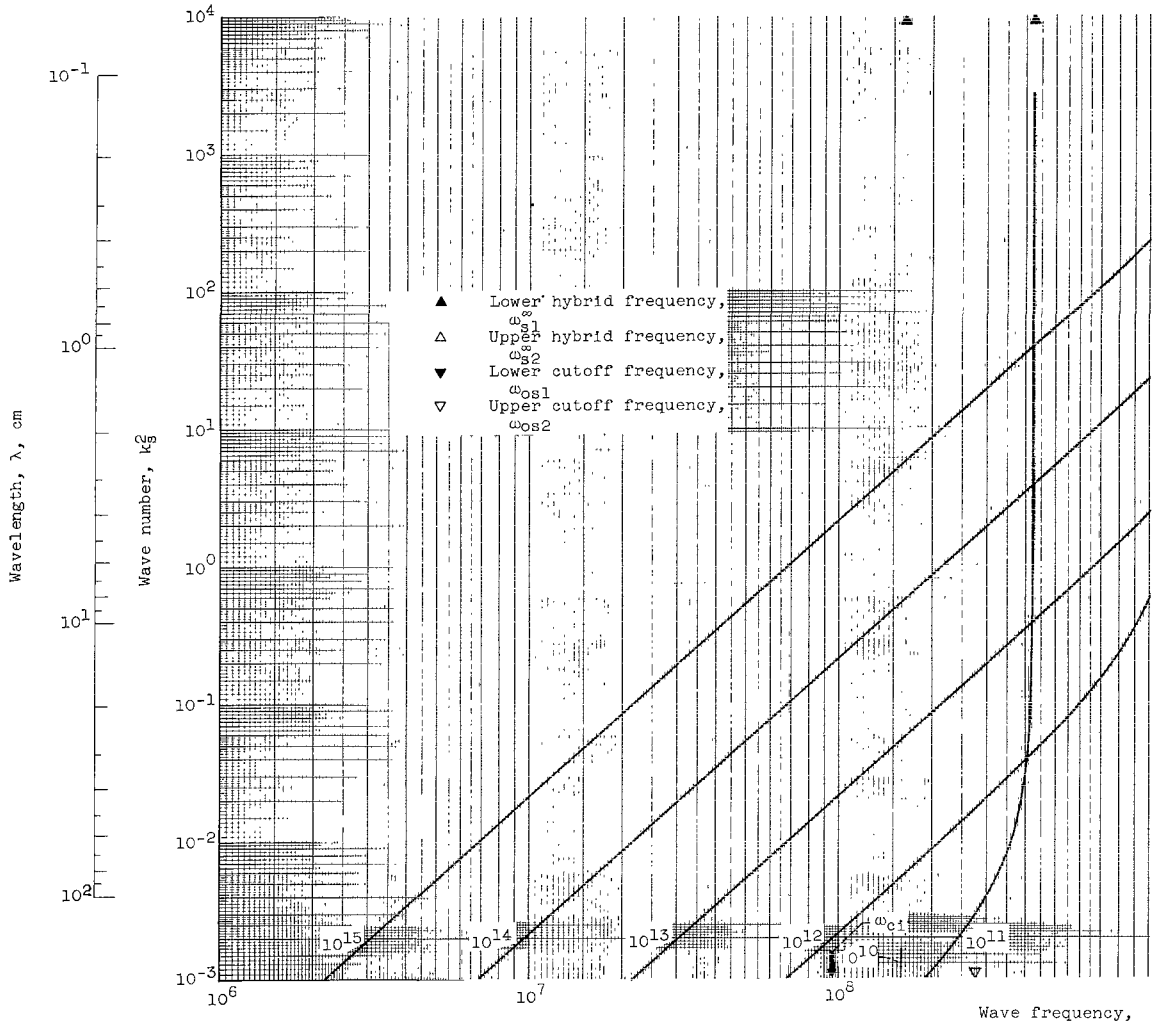

(d-3) Magnetic-field

(d) Continued. S mode;

Figure 1. - Continued. Wave number as function of

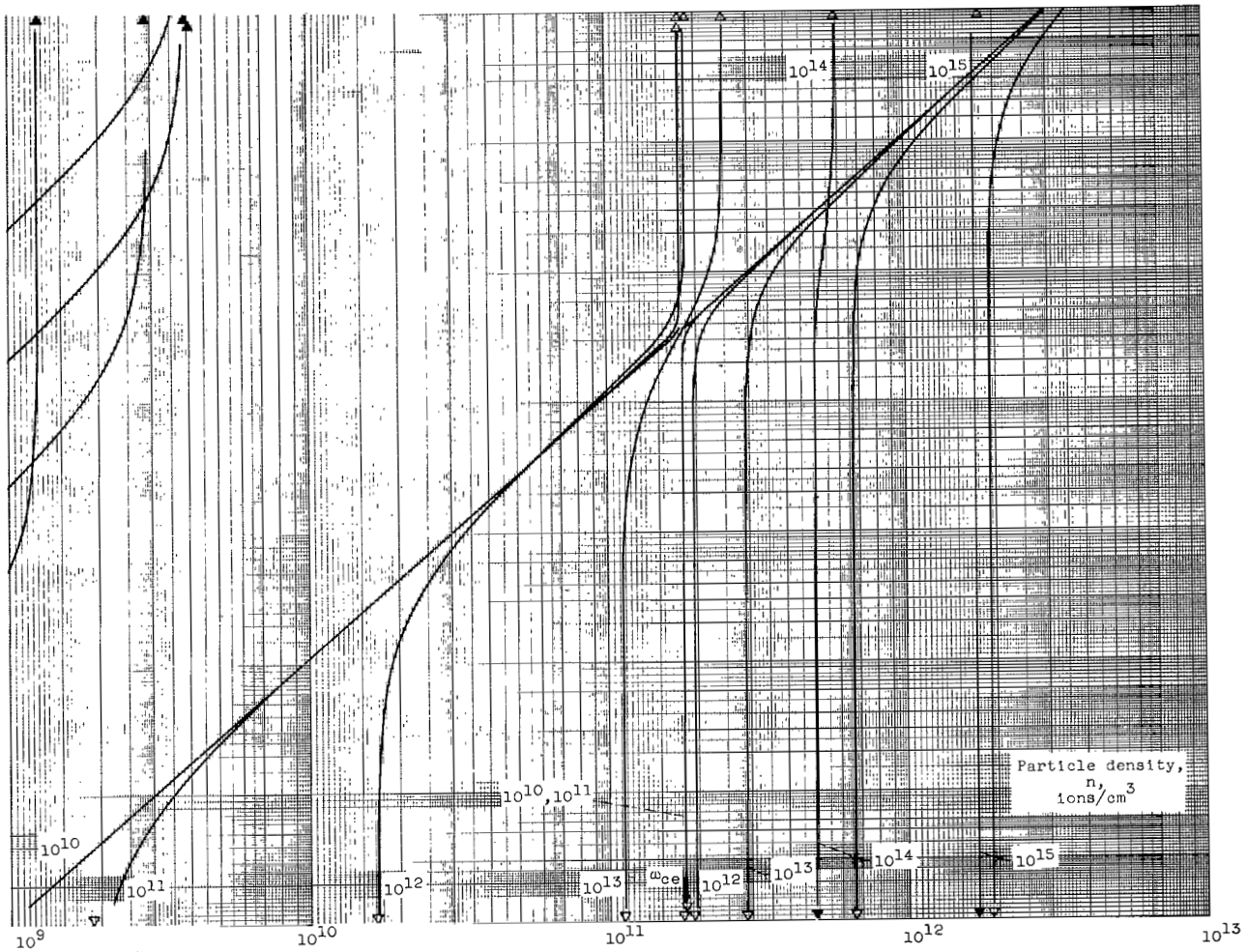

ω, radians/sec

strength, 10^4 gauss.

wave propagation angle, 90°.

frequency. Wave propagation angles, 0° and 90°; Astrom's model.

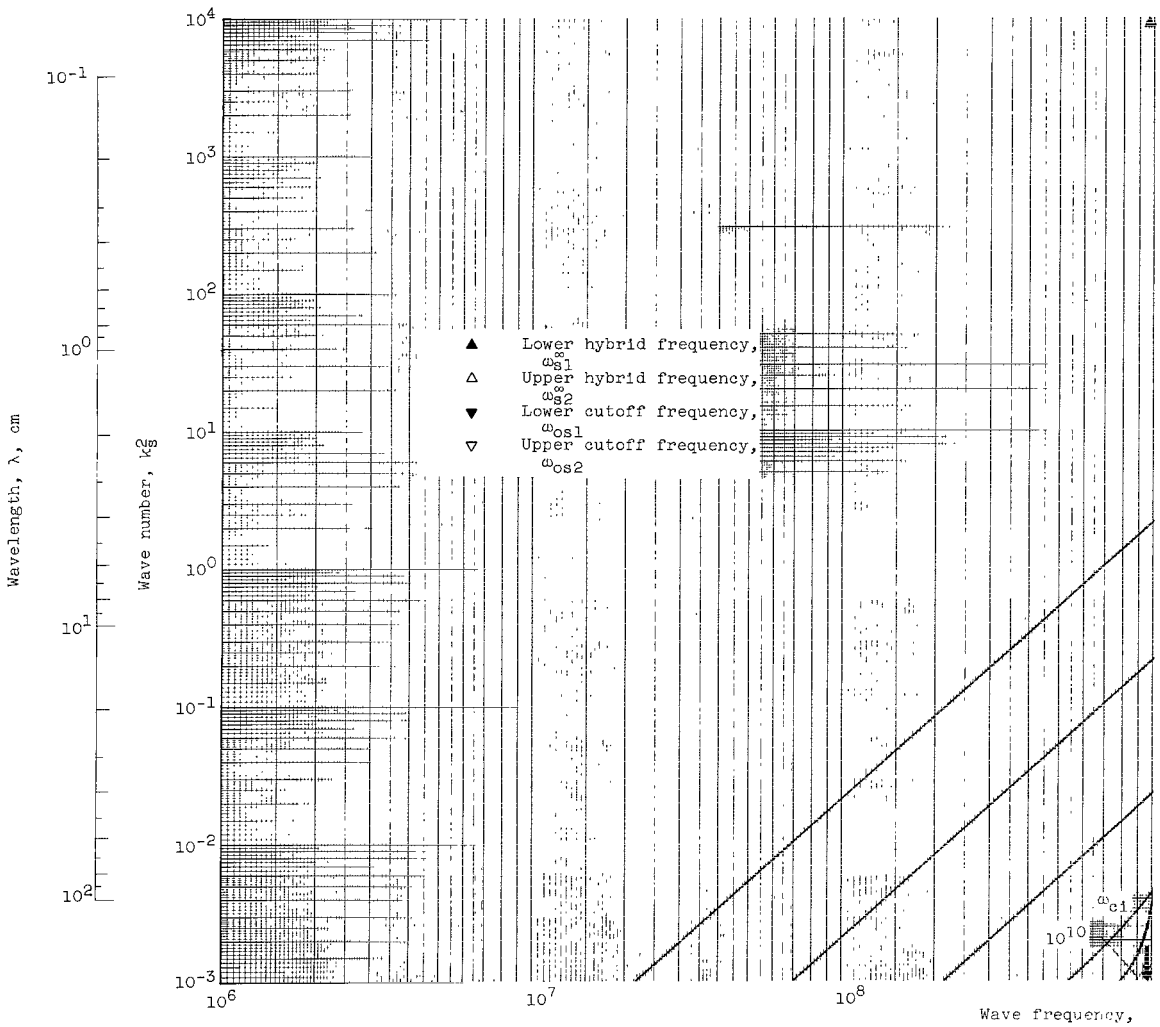

(d-4) Magnetic-field

(d) Concluded. S mode;

Figure 1. - Concluded. Wave number as function of

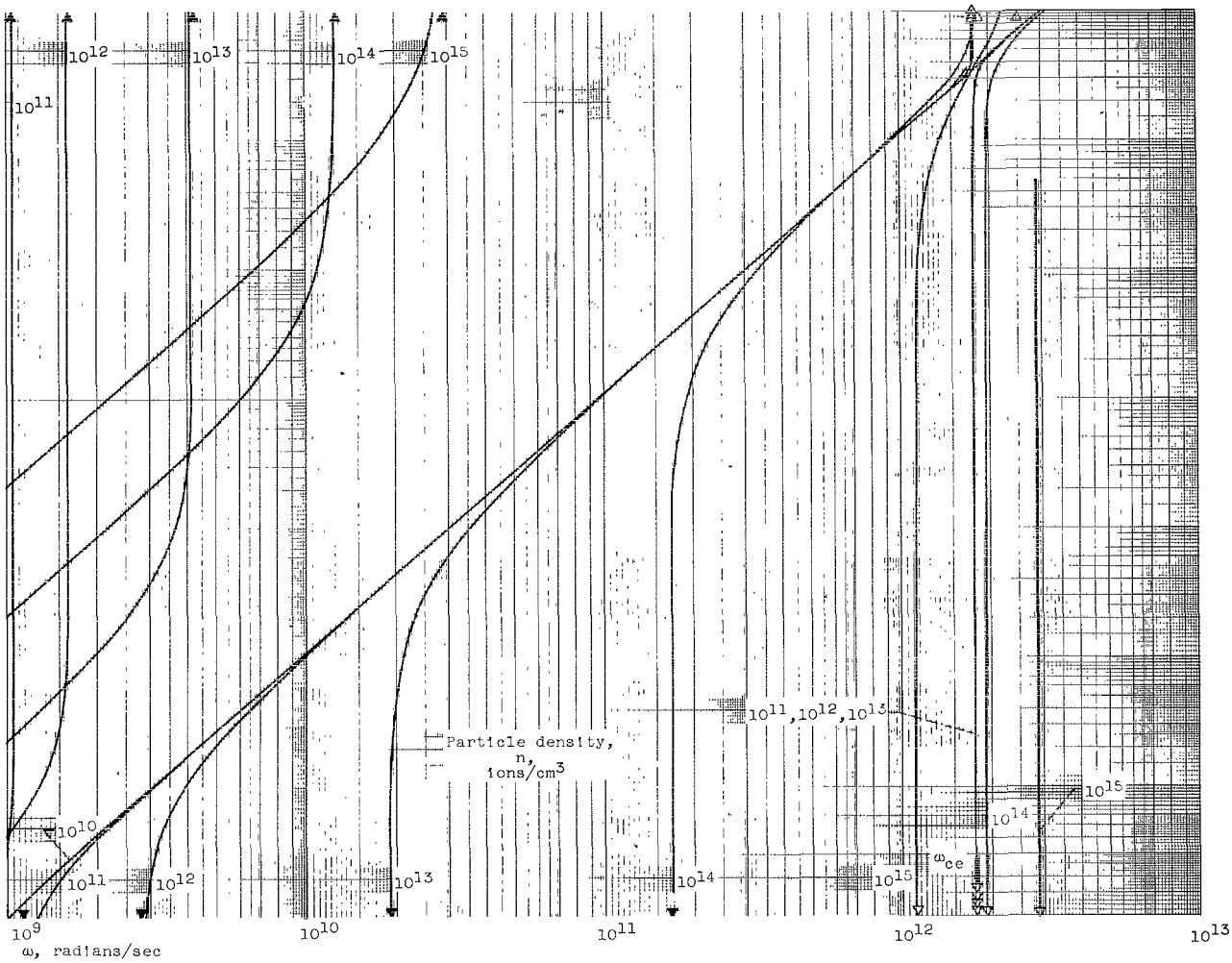

ω, radians/sec

strength, 10^5 gauss.

wave propagation angle, 90°.

frequency. Wave propagation angles, 0° and 90°; Astrom's model.

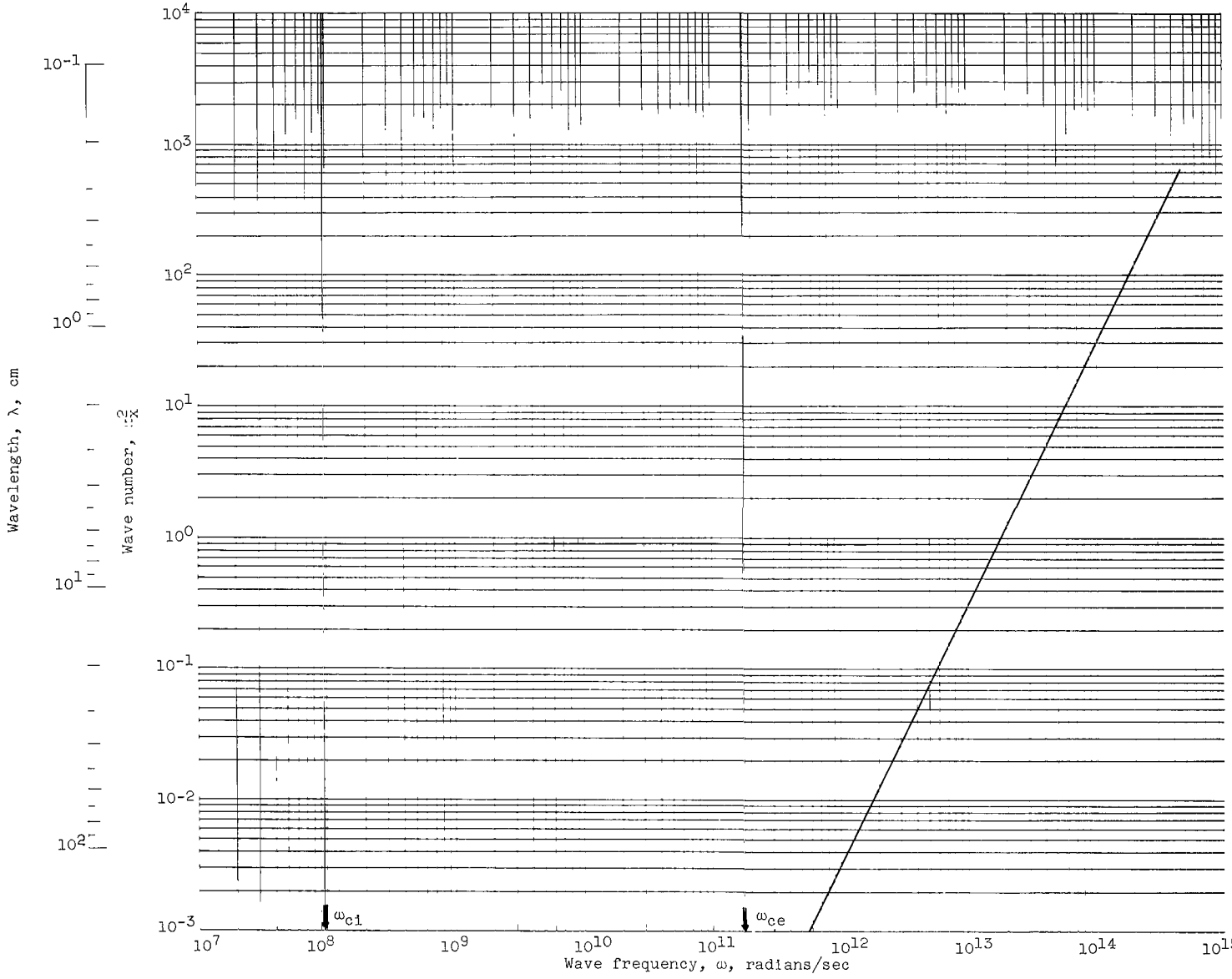

(a) x-component.

Figure 2. - Wave number as function of frequency. Wave propagation angle, 0.1^{o}; magnetic-field strength, 10^{4} gauss; particle density, 10^{13} ions per cubic centimeter; Astrom's model.

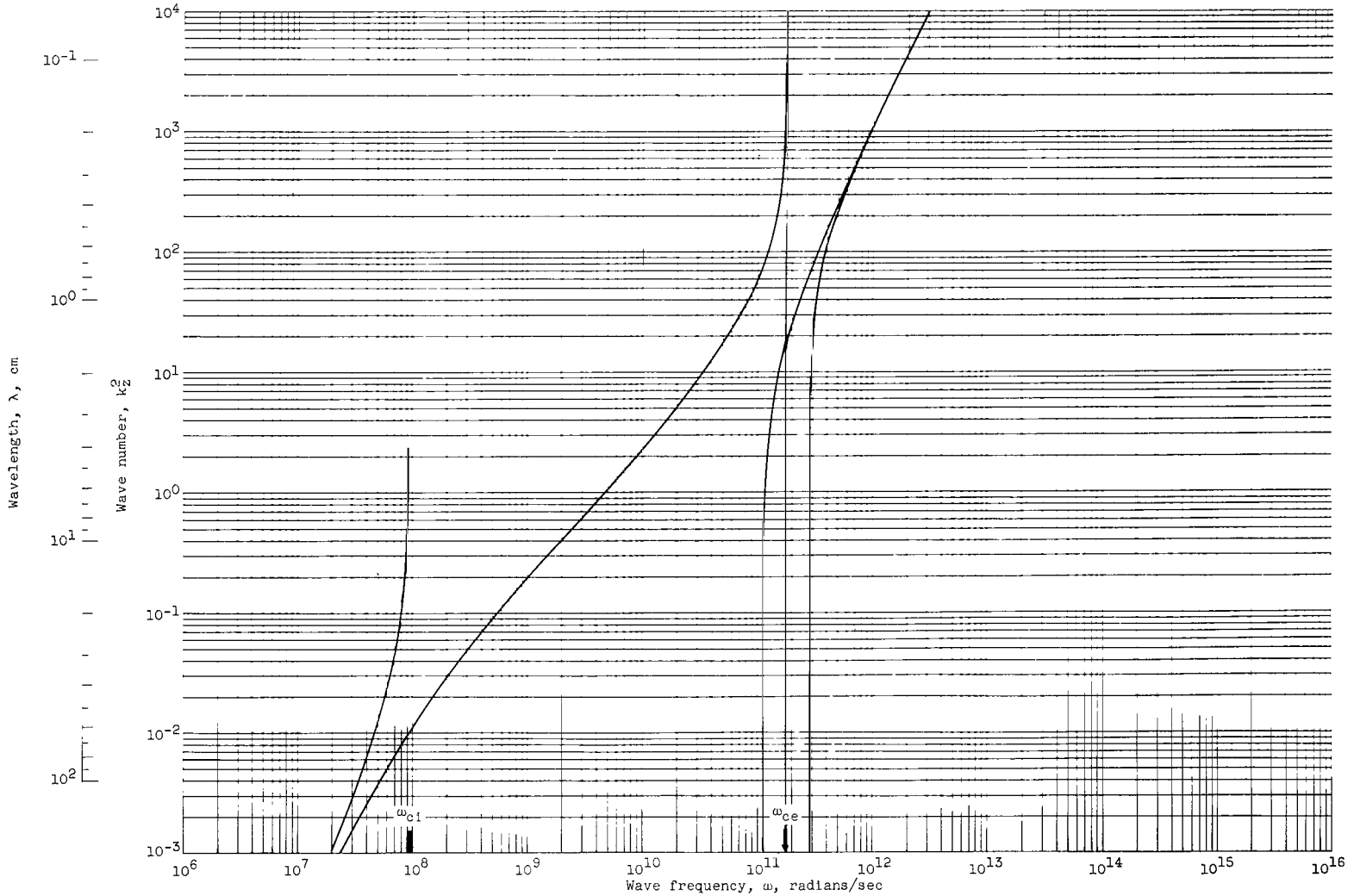

(b) z-component.

Figure 2. - Concluded. Wave number as function of frequency. Wave propagation angle, 0.1°; magnetic-field strength, 10^4 gauss; particle density, 10^{13} ions per cubic centimeter; Astrom's model.

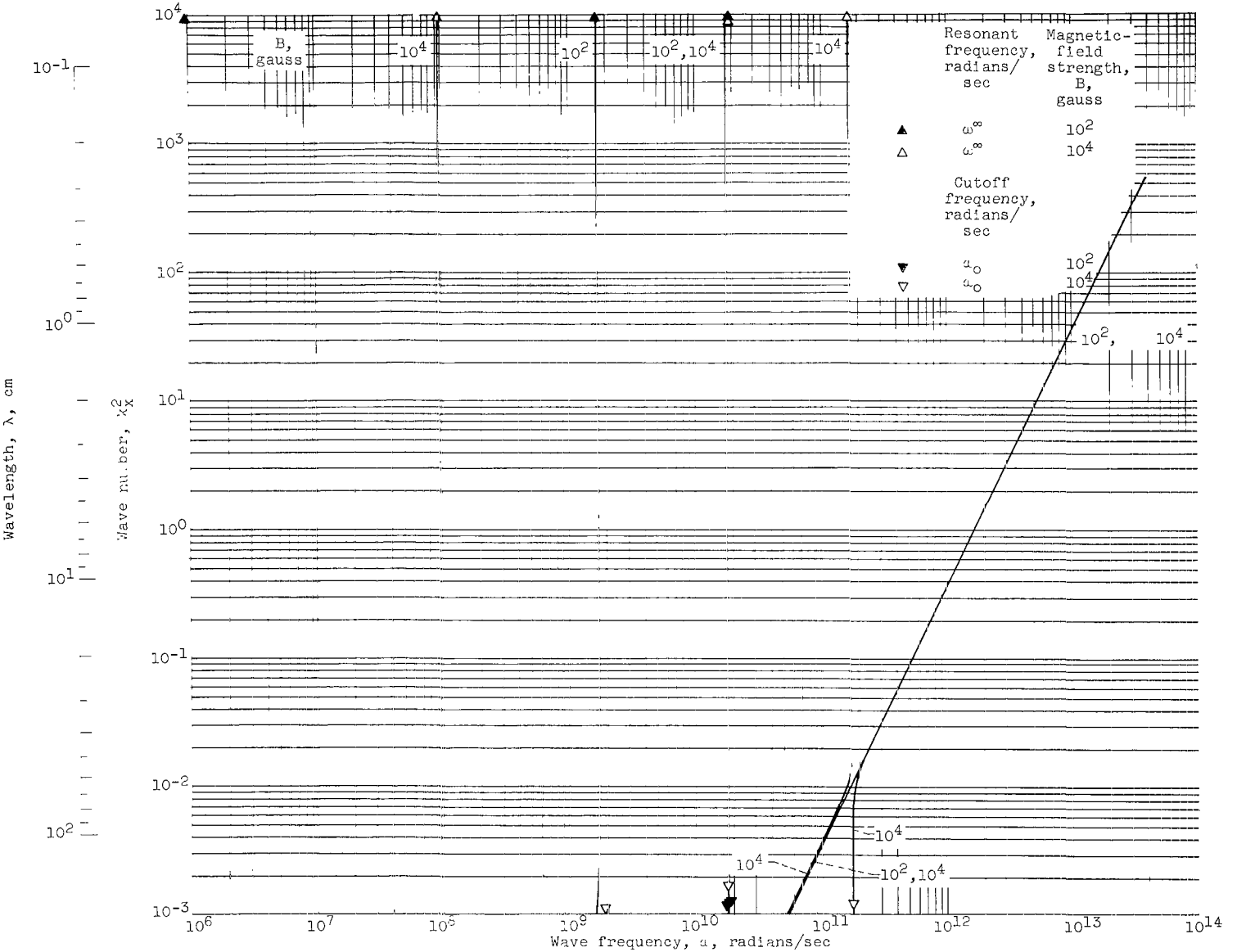

(a-1) x-component.

(a) Particle density, 10^{11} ions per cubic centimeter.

Figure 3. - Wave number as function of frequency. Wave propagation angle, 1°; Astrom's model.

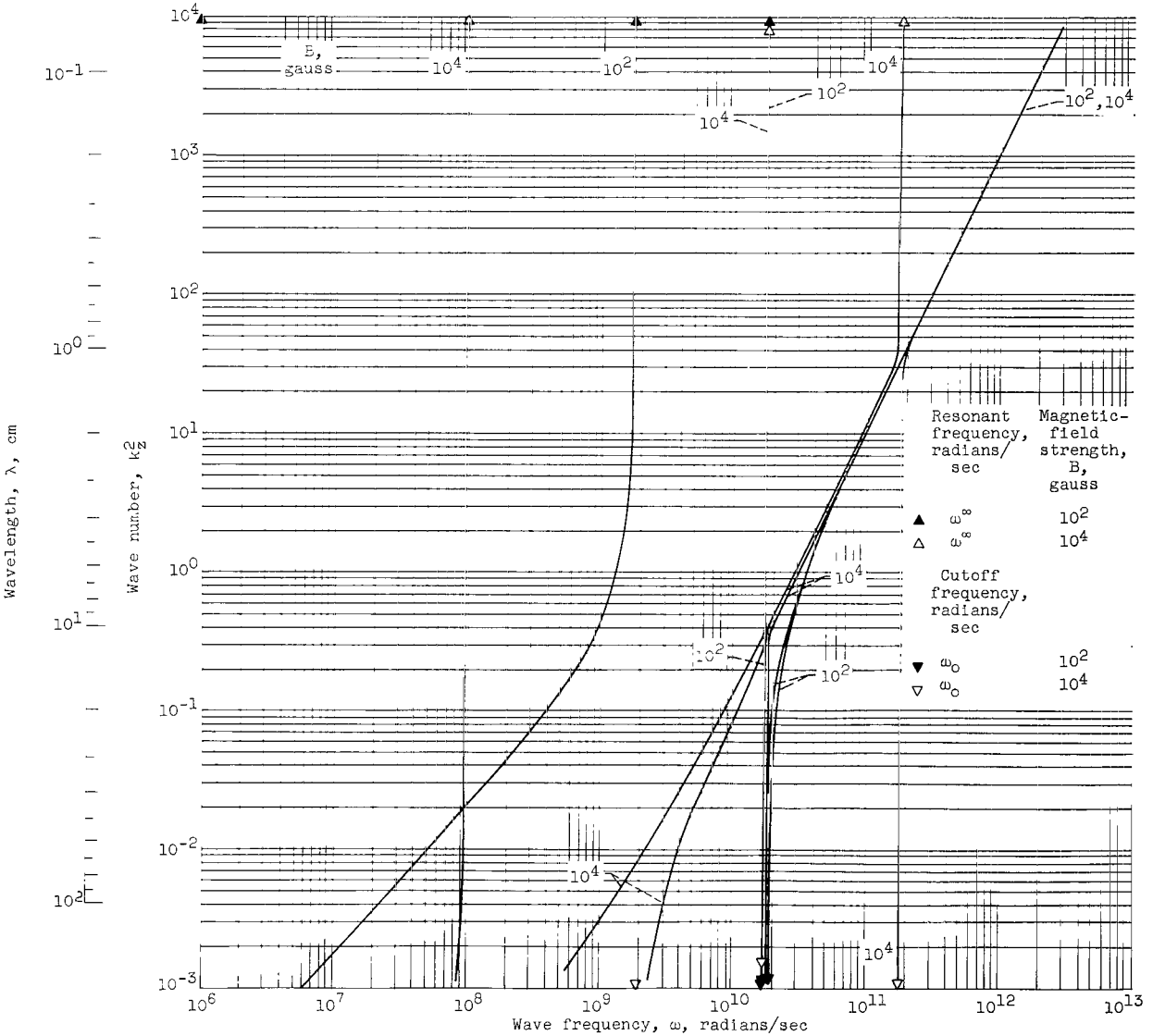

(a-2) z-component.

(a) Concluded. Particle density, 10^{11} ions per cubic centimeter.

Figure 3. - Continued. Wave number as function of frequency. Wave propagation angle, 1°; Astrom's model.

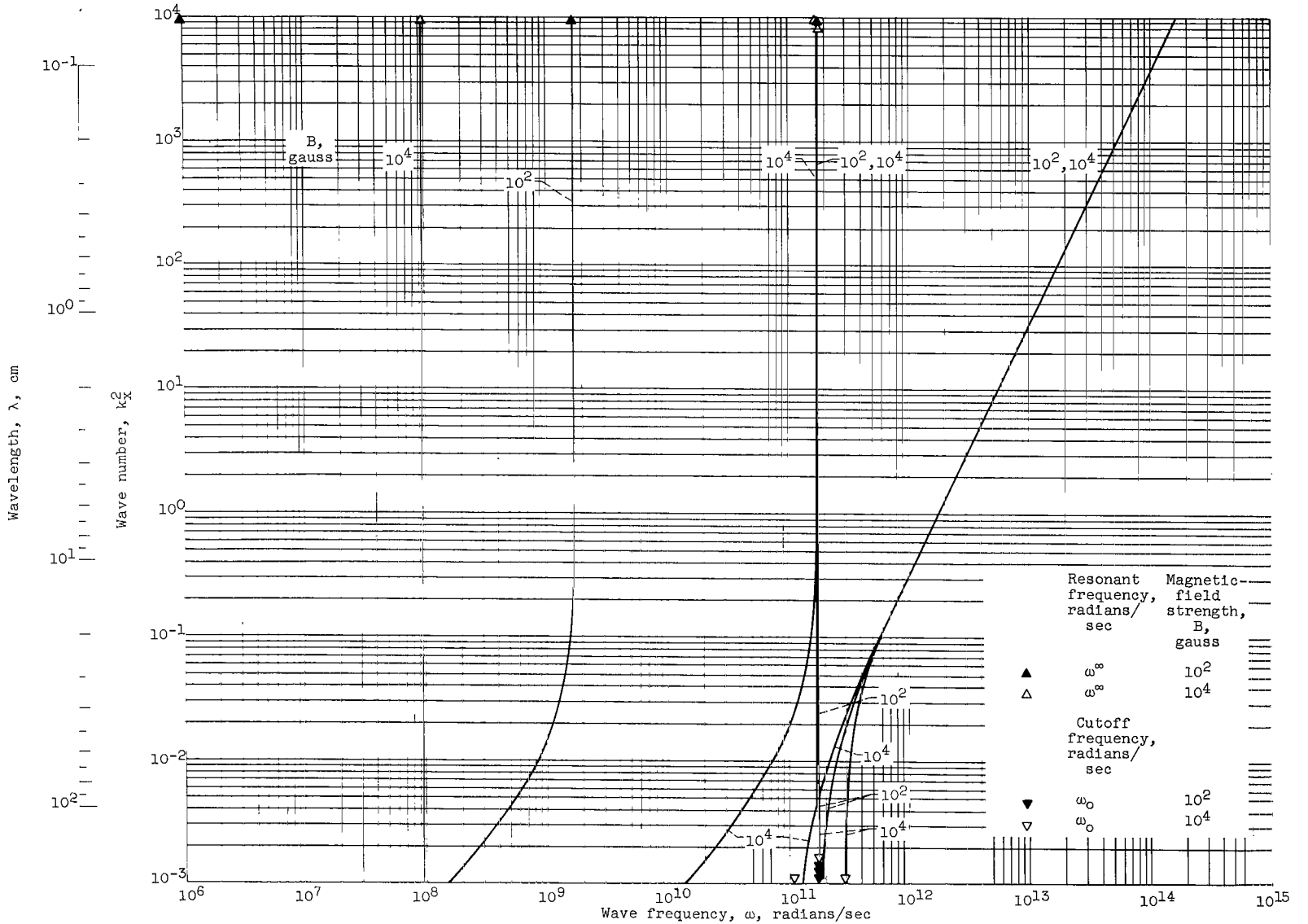

(b-1) x-component.

(b) Particle density, 10^{13} ions per cubic centimeter.

Figure 3. - Continued. Wave number as function of frequency. Wave propagation angle, 1°; Astrom's model.

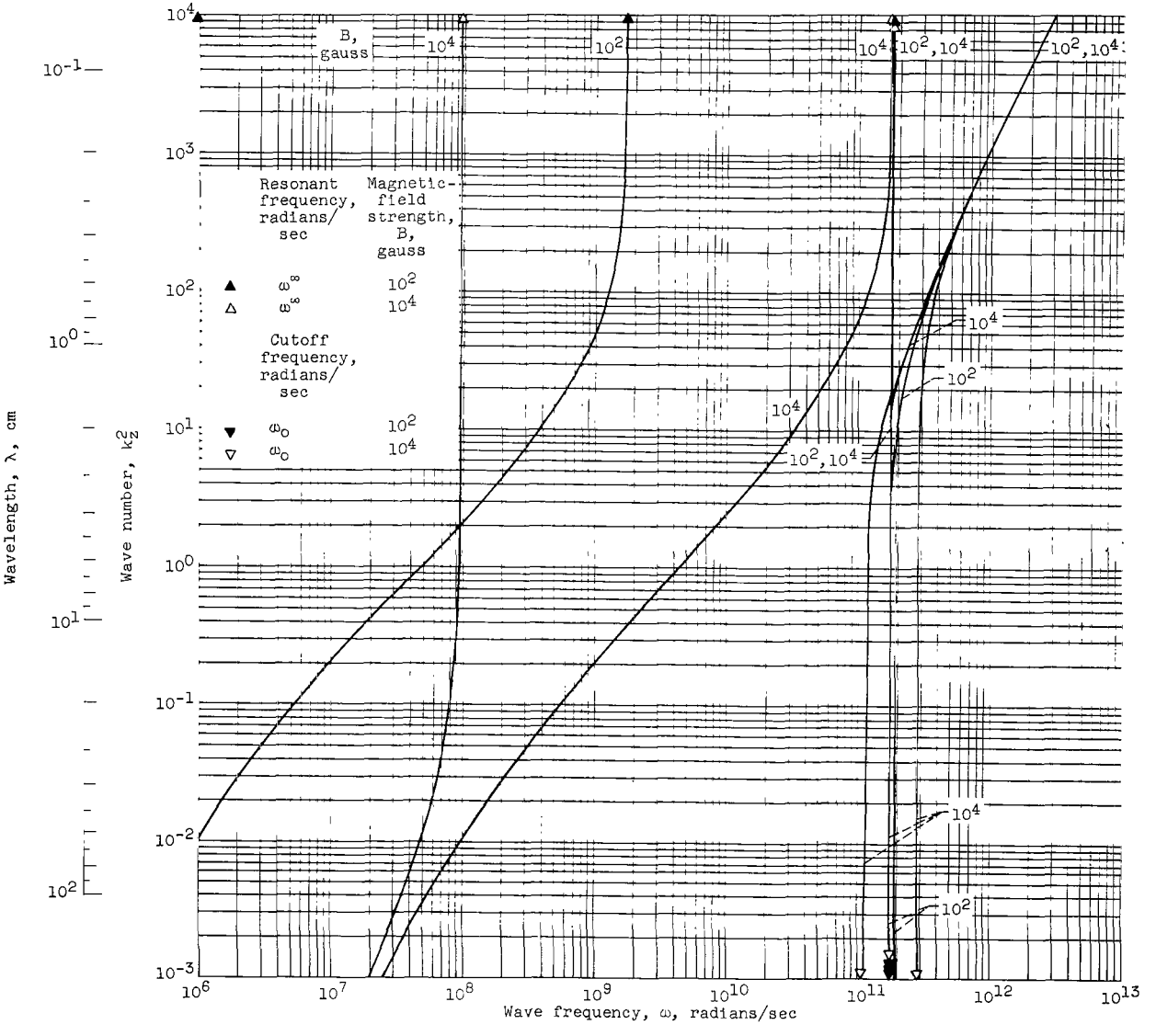

(b-2) z-component.

(b) Concluded. Particle density, 10^{13} ions per cubic centimeter.

Figure 3. - Concluded. Wave number as function of frequency. Wave propagation angle, 1°; Astrom's model.

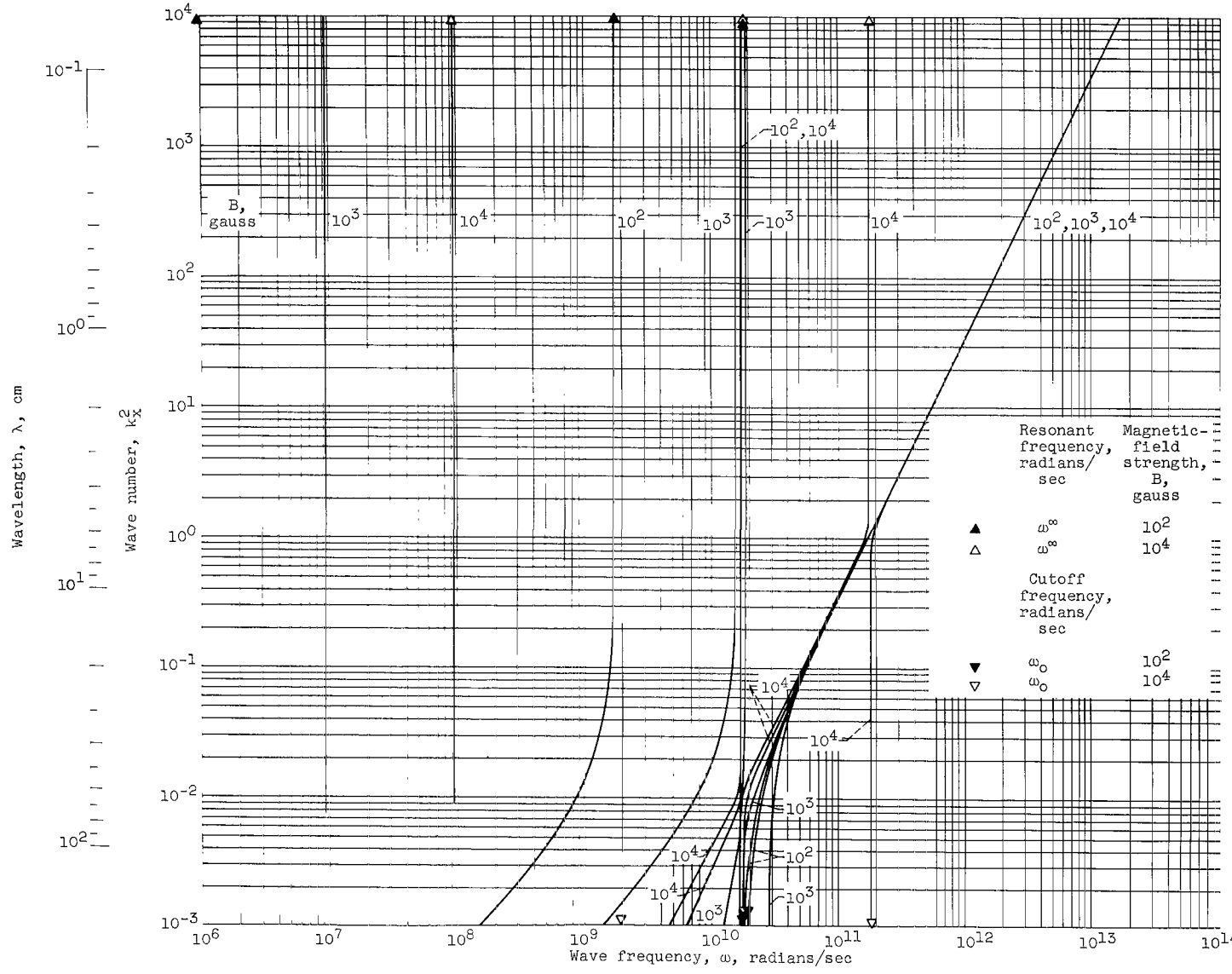

(a-1) x-component.

(a) Particle density, 10^{11} ions per cubic centimeter.

Figure 4. - Wave number as function of frequency. Wave propagation angle, 10^{o}; Astrom's model.

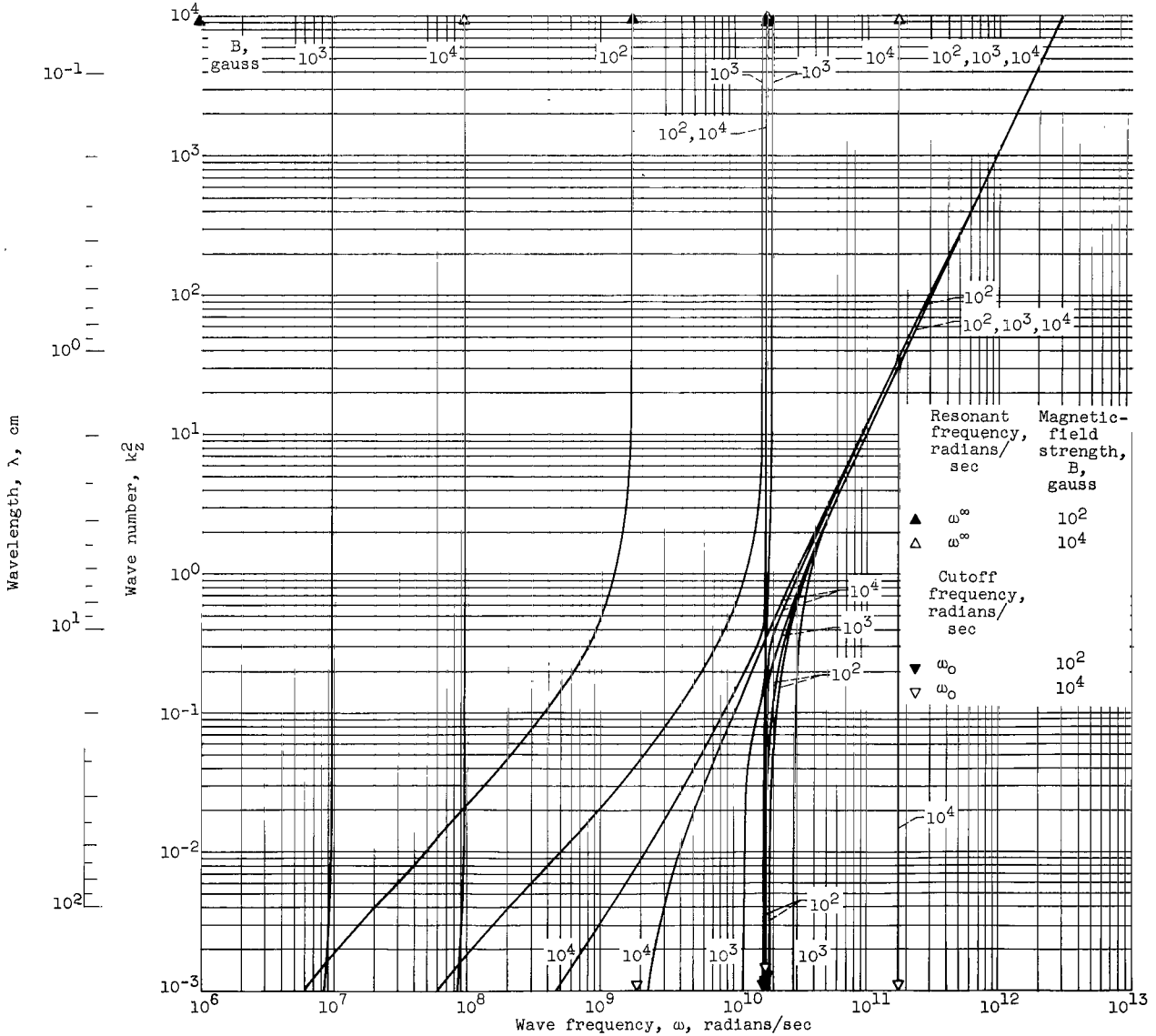

(a-2) z-component.

(a) Concluded. Particle density, 10^{11} ions per cubic centimeter.

Figure 4. - Continued. Wave number as function of frequency. Wave propagation angle, 16°; Astrom's model.

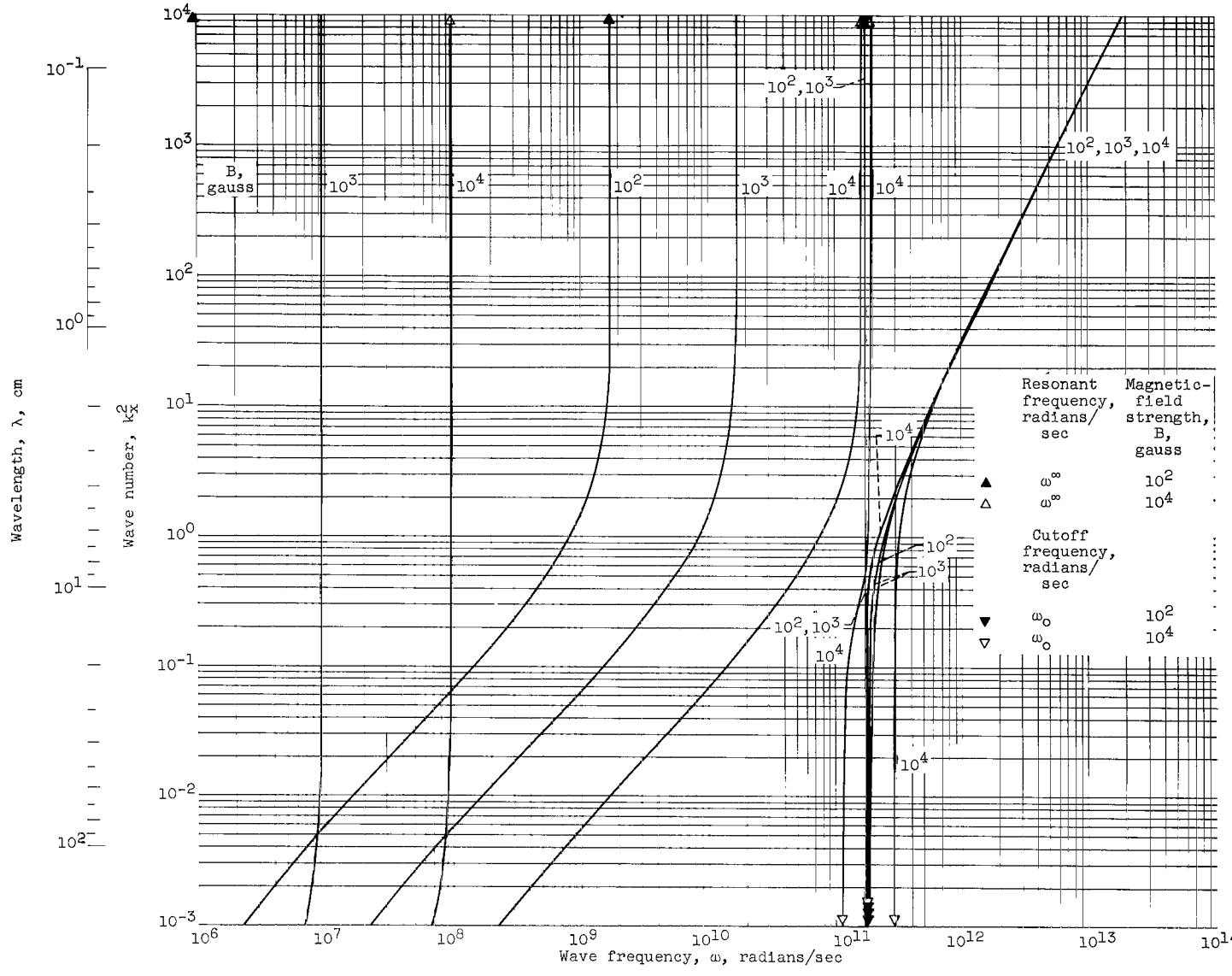

(b-1) x-component.

(b) Particle density, 10^{13} ions per cubic centimeter.

Figure 4. - Continued. Wave number as function of frequency. Wave propagation angle, 10^{o}; Astrom's model.

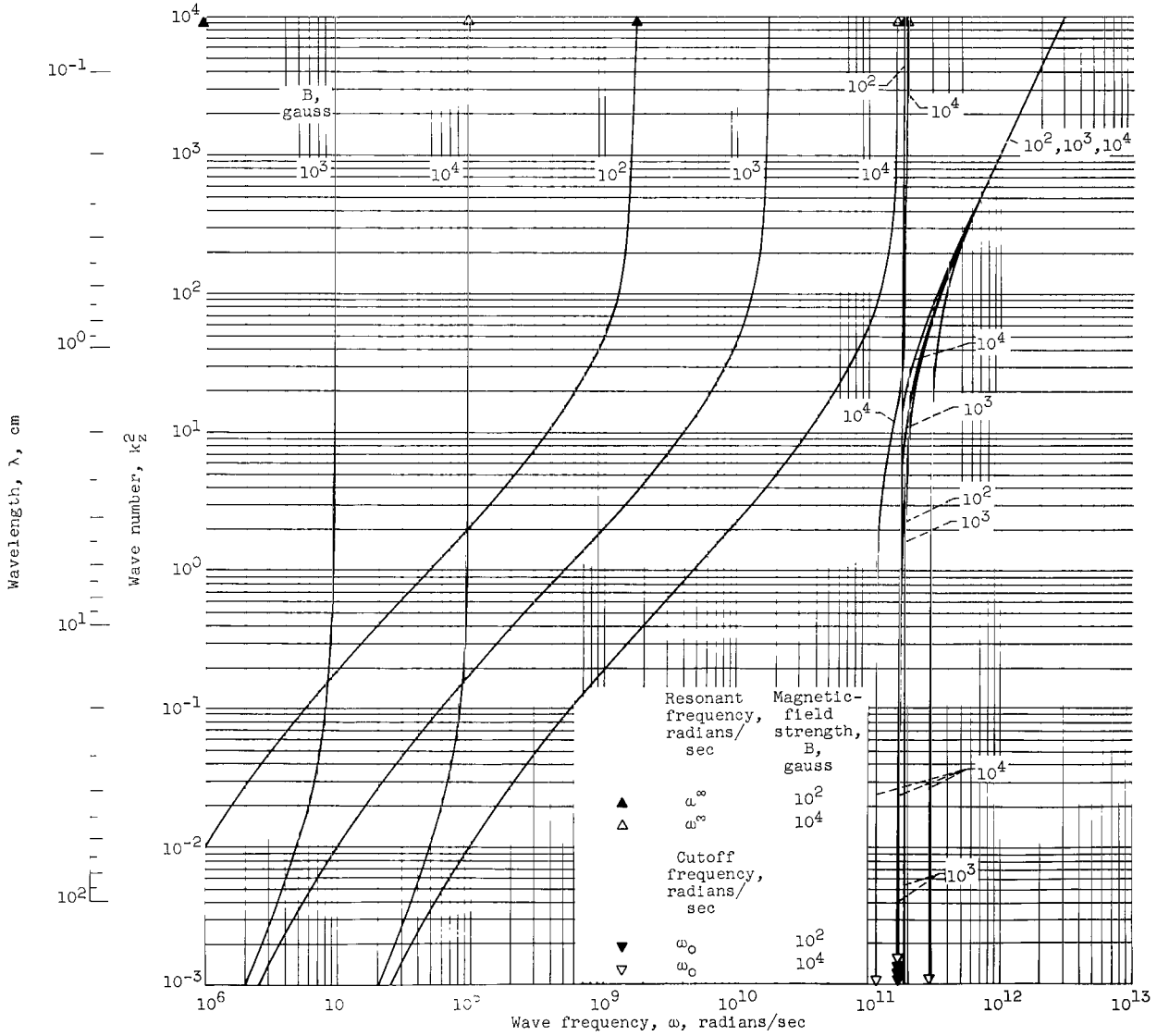

(b-2) z-component.

(b) Concluded. Particle density, 10^{13} ions per cubic centimeter.

Figure 4. - Concluded. Wave number as function of frequency. Wave propagation angle, 10^{o}; Astrom's model.

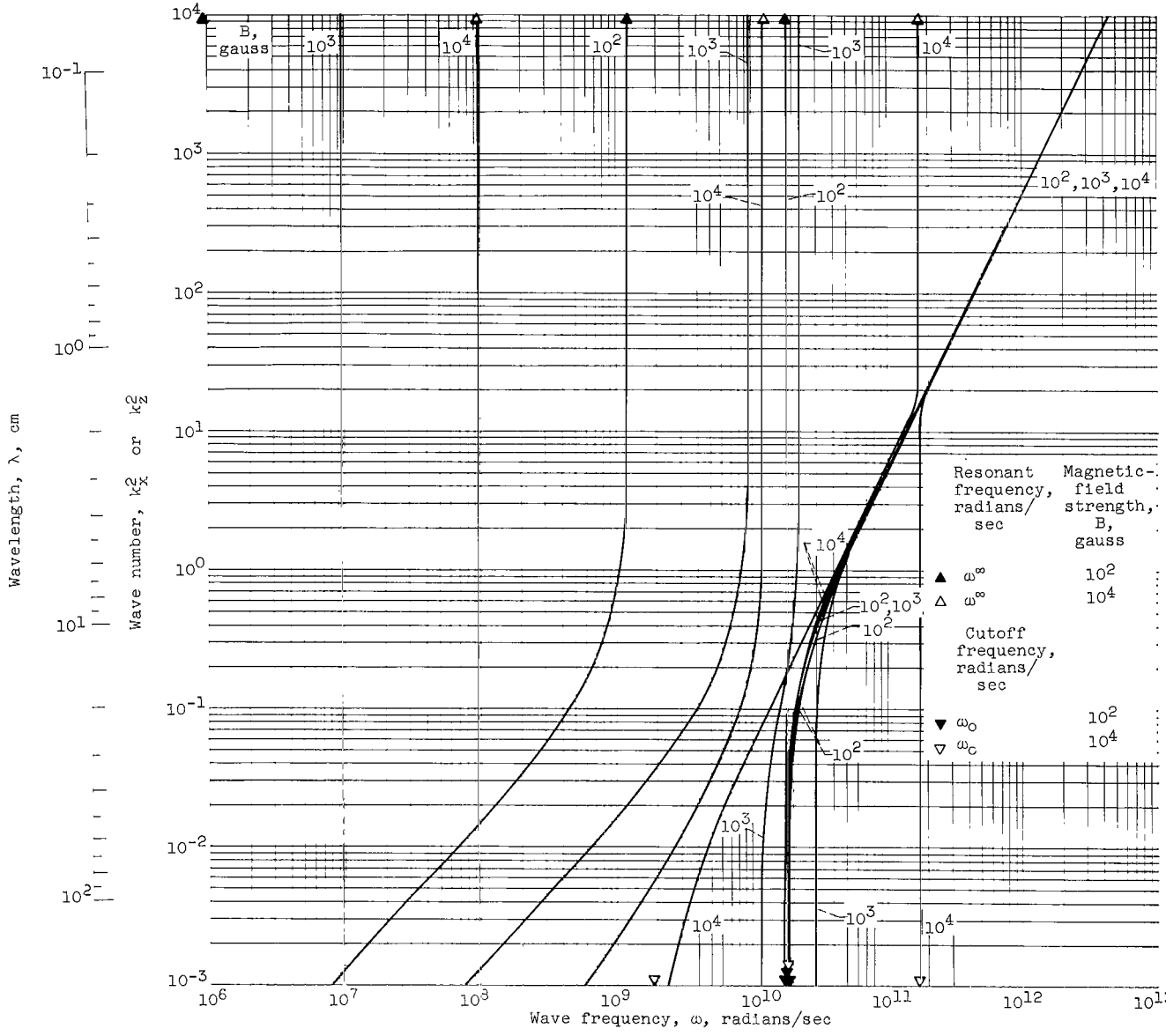

(a) Particle density, 10^{11} ions per cubic centimeter.

Figure 5. - Wave number as function of frequency. Wave propagation angle, 45°; Astrom's model.

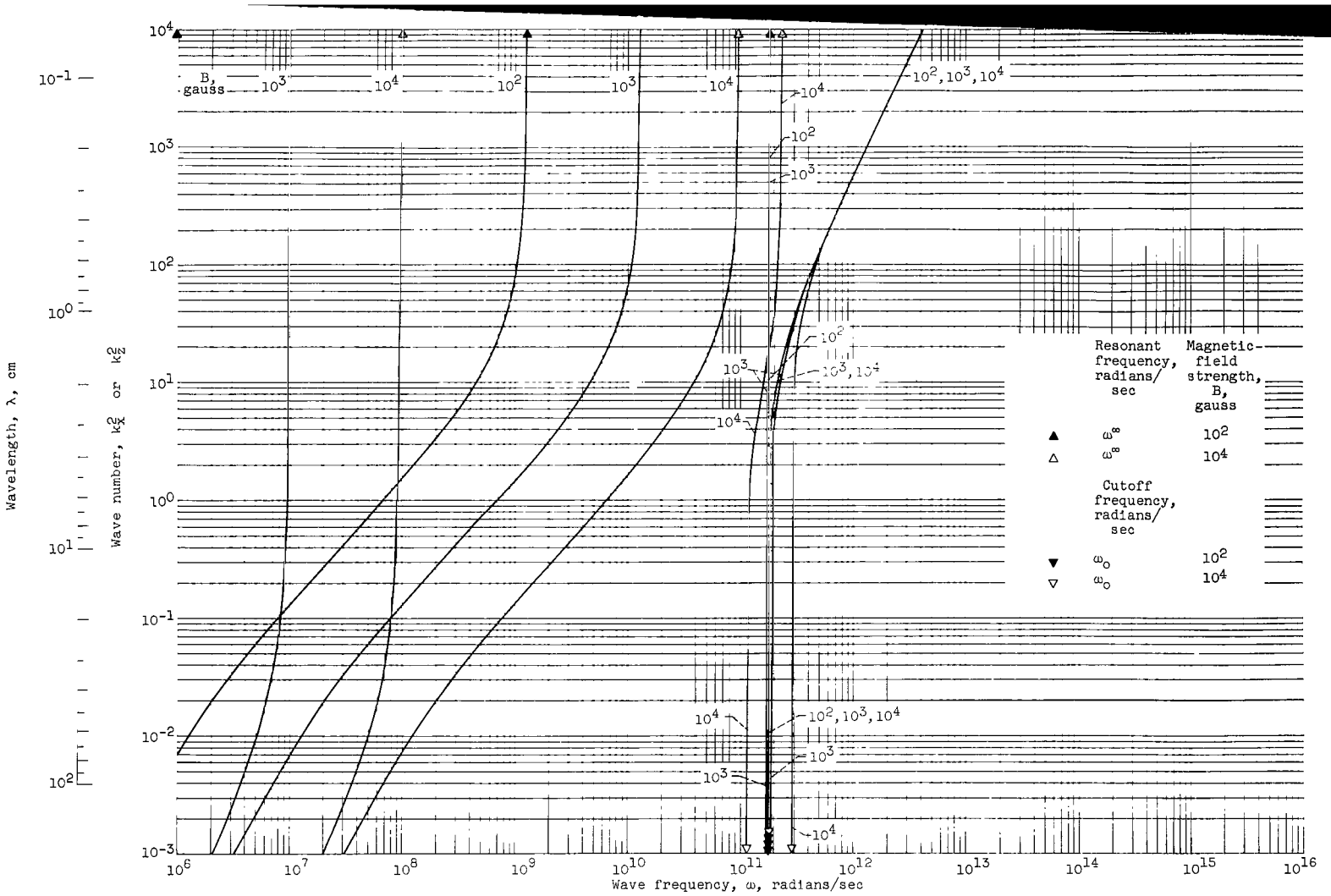

(b) Particle density, 10^{13} ions per cubic centimeter.

Figure 5. - Concluded. Wave number as function of frequency. Wave propagation angle, 45°; Astrom's model.

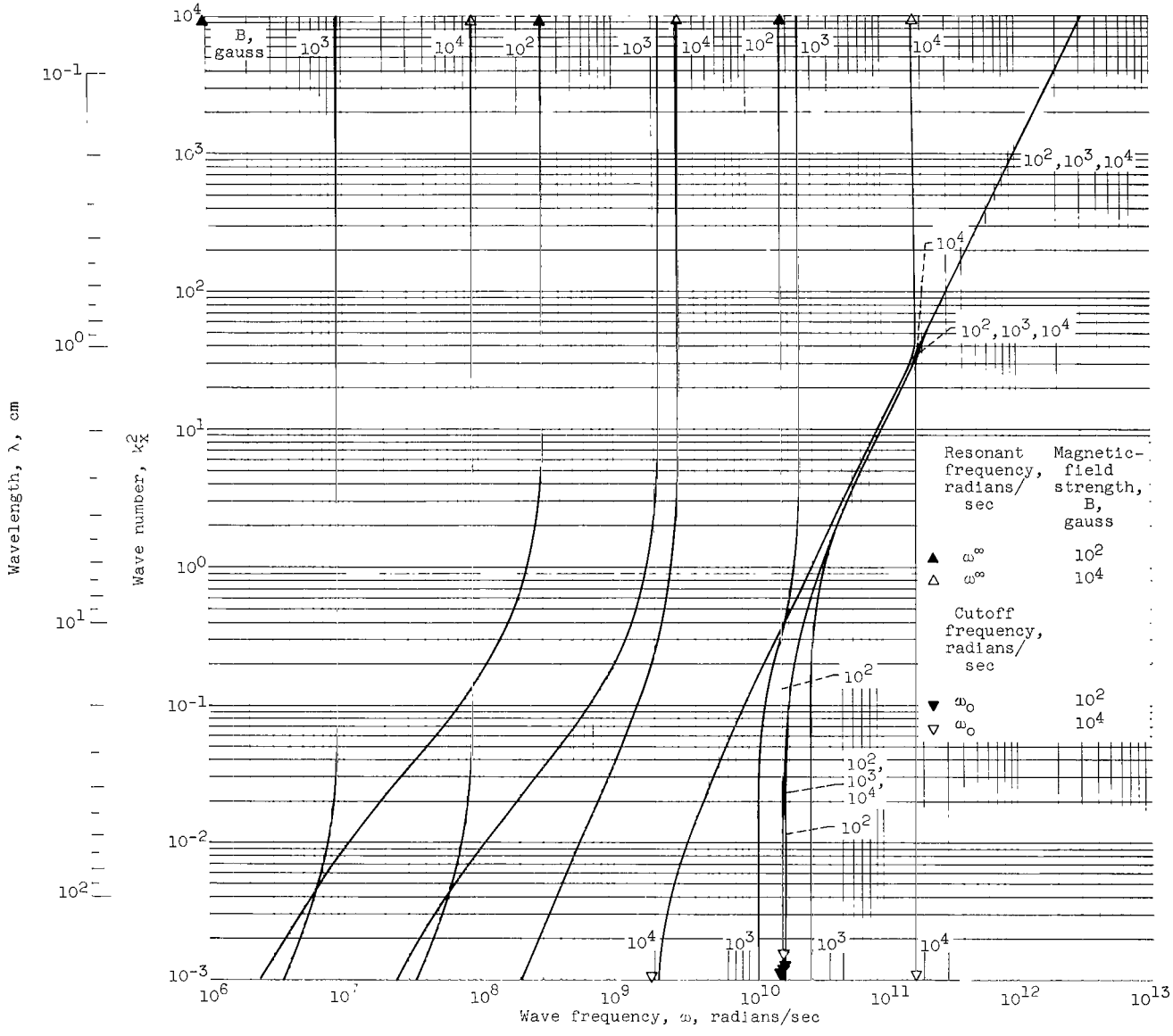

(a-1) x-component.

(a) Particle density, 10^{11} ions per cubic centimeter.

Figure 6. - Wave number as function of frequency. Wave propagation angle, 90°; Astrom's model.

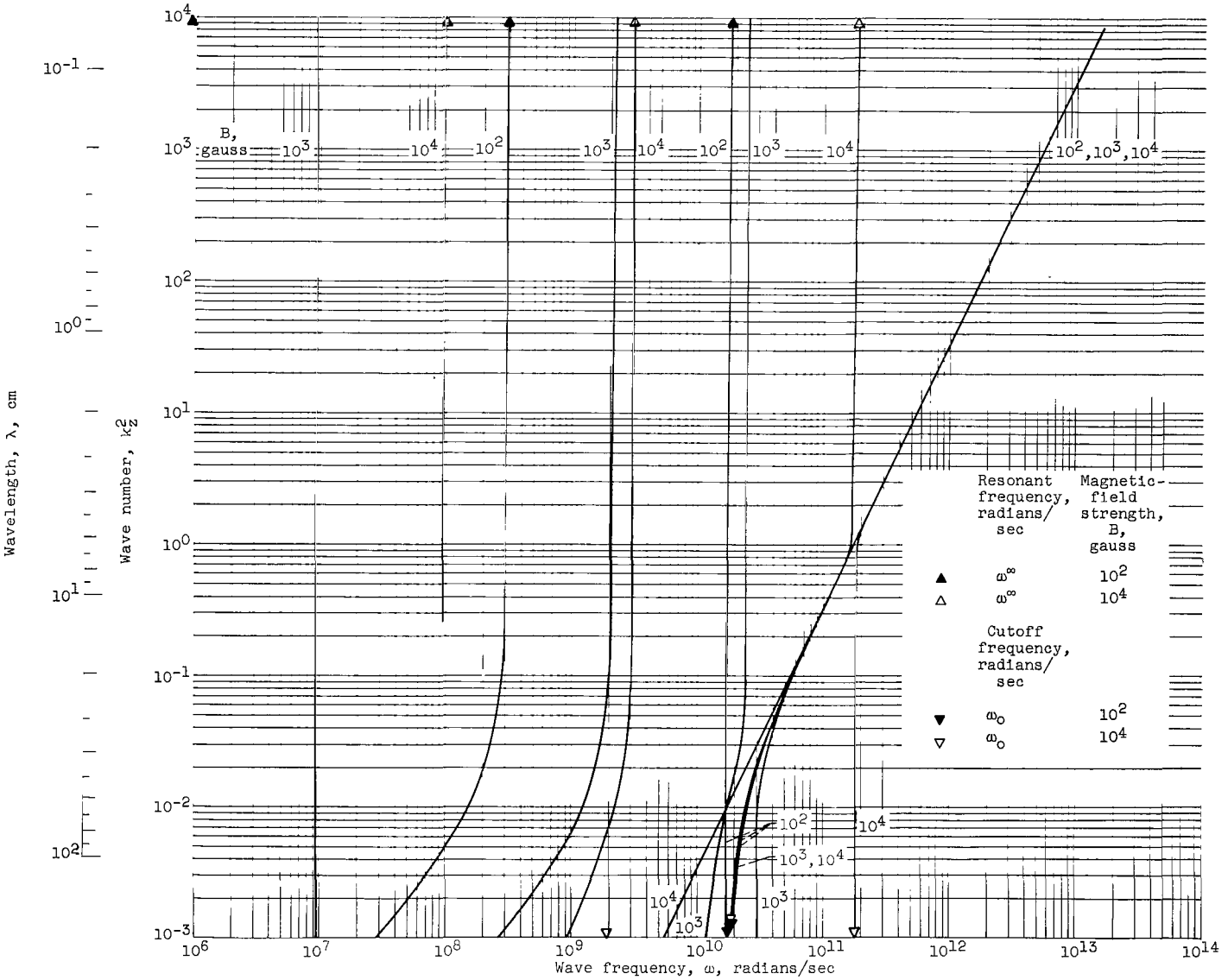

(a-2) z-component.

(a) Concluded. Particle density, 10^{11} ions per cubic centimeter.

Figure 6. - Continued. Wave number as function of frequency. Wave propagation angle, 80°; Astrom's model.

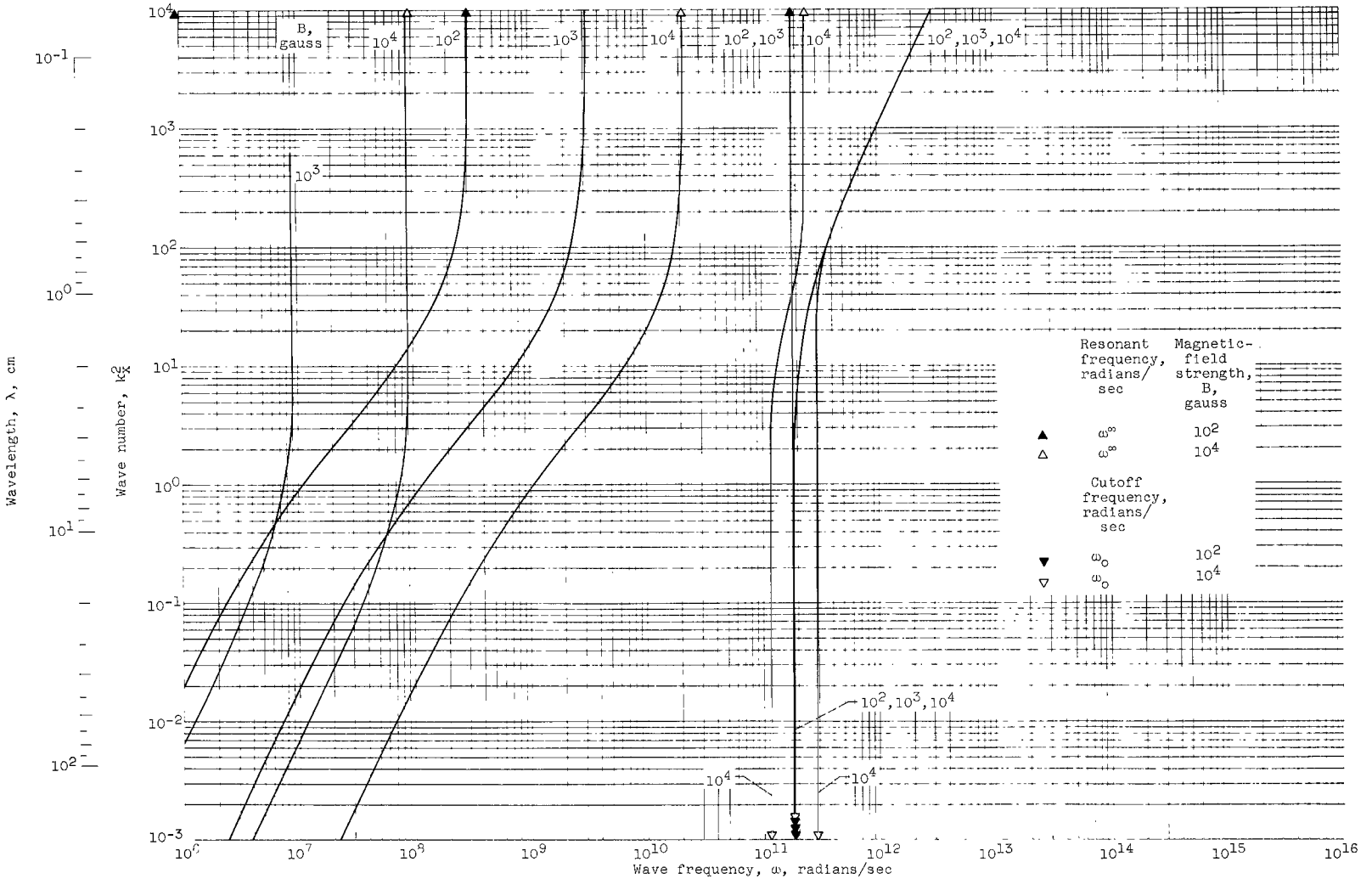

(b-1) x-component.

(b) Particle density, 10^{13} ions per cubic centimeter.

Figure 6. - Continued. Wave number as function of frequency. Wave propagation angle, 80°; Astrom's model.

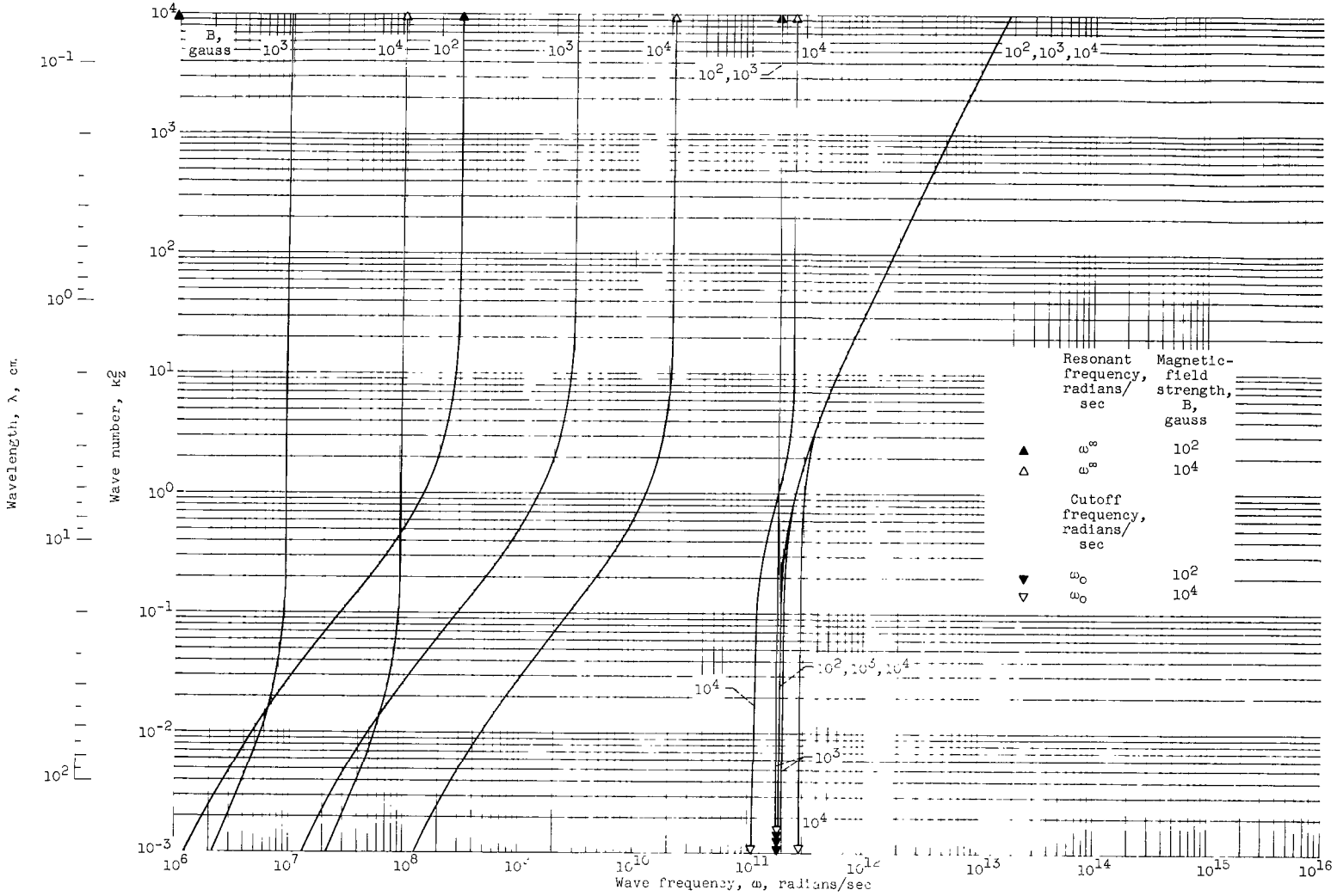

(c-2) z-component.

(b) Concluded. Particle density, 10^{13} ions per cubic centimeter.

Figure 6. - Concluded. Wave number as function of frequency. Wave propagation angle, 80°; Astrom's model.

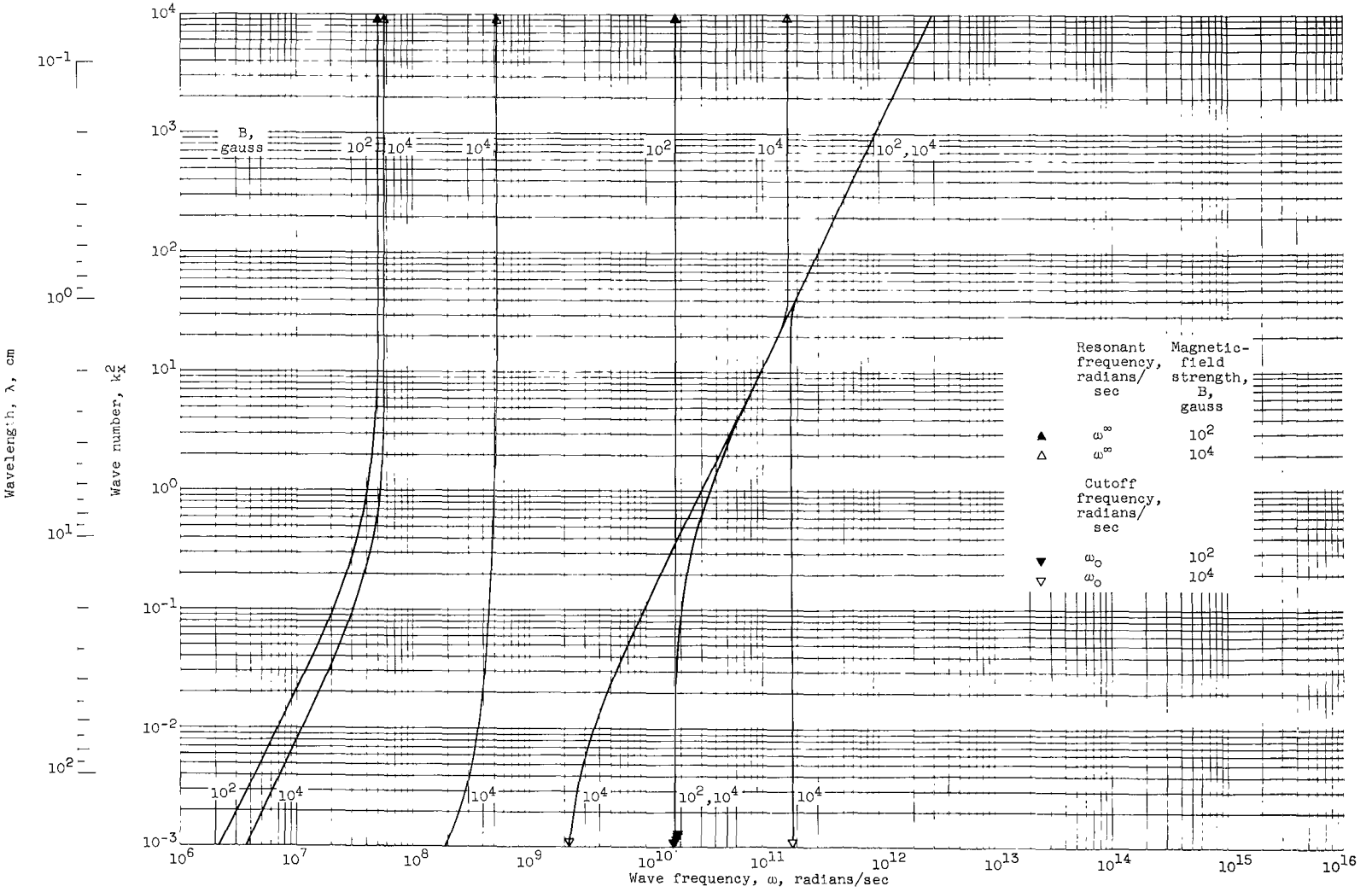

(a-1) x-component.

(a) Particle density, 10^{11} ions per cubic centimeter.

Figure 7. - Wave number as function of frequency. Wave propagation angle, 89°; Astrom's model.

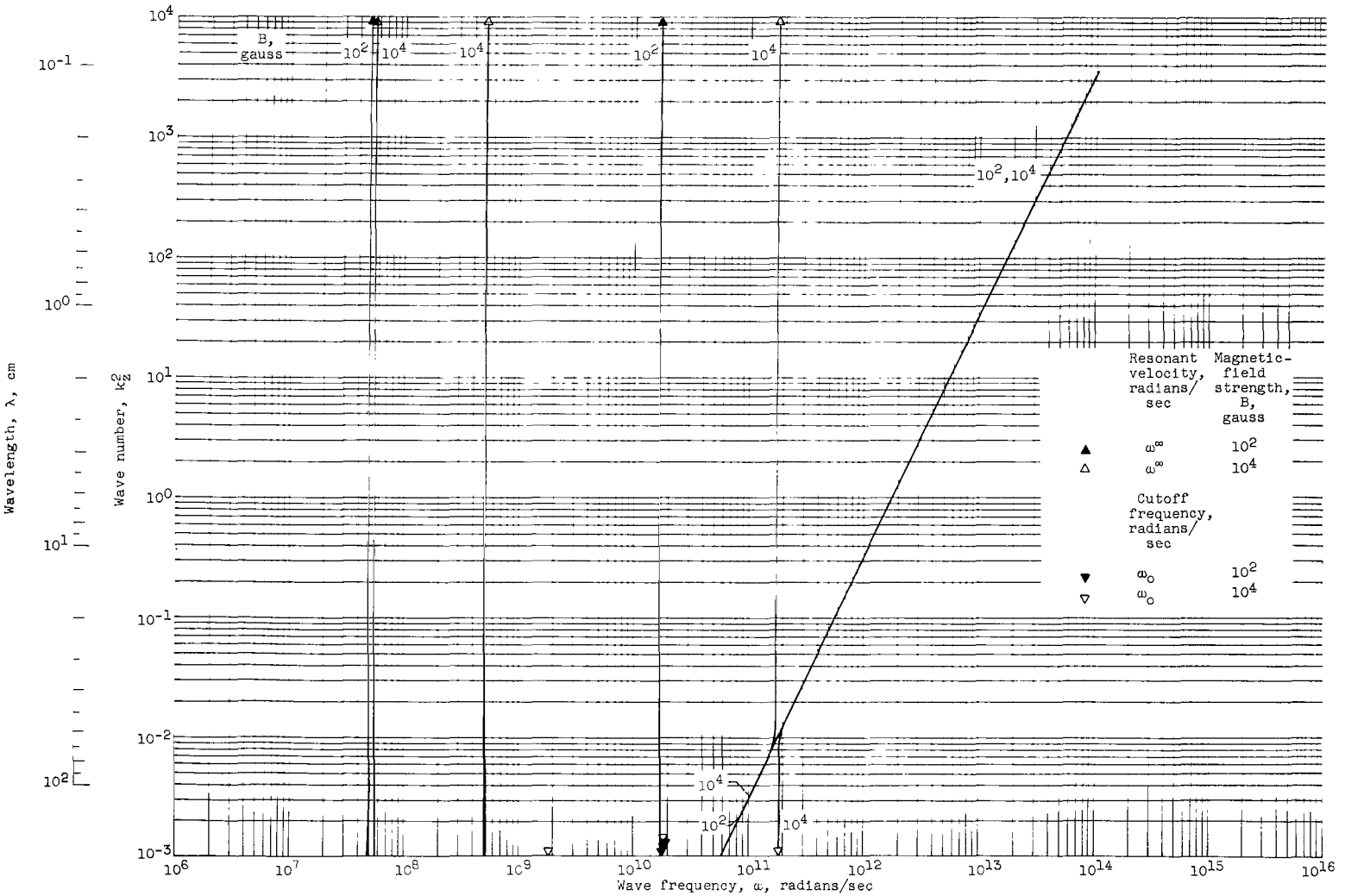

(a-2) z-component.

(a) Concluded. Particle density, 10^{11} ions per cubic centimeter.

Figure 7. - Continued. Wave number as function of frequency. Wave propagation angle, 89°; Astrom's model.

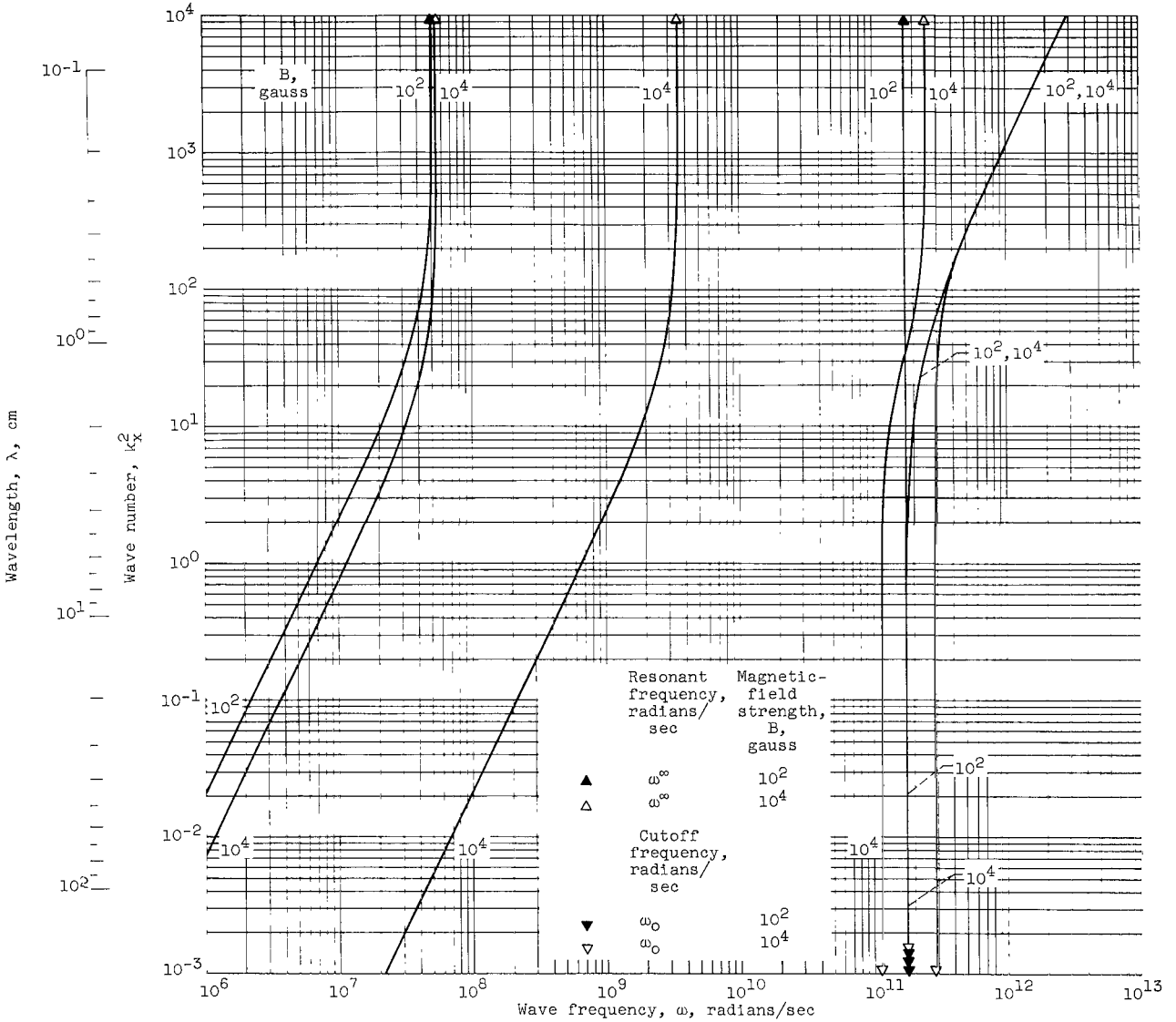

(b-1) x-component.

(b) Particle density, 10^{13} ions per cubic centimeter.

Figure 7. - Continued. Wave number as function of frequency. Wave propagation angle, 89°; Astrom's model.

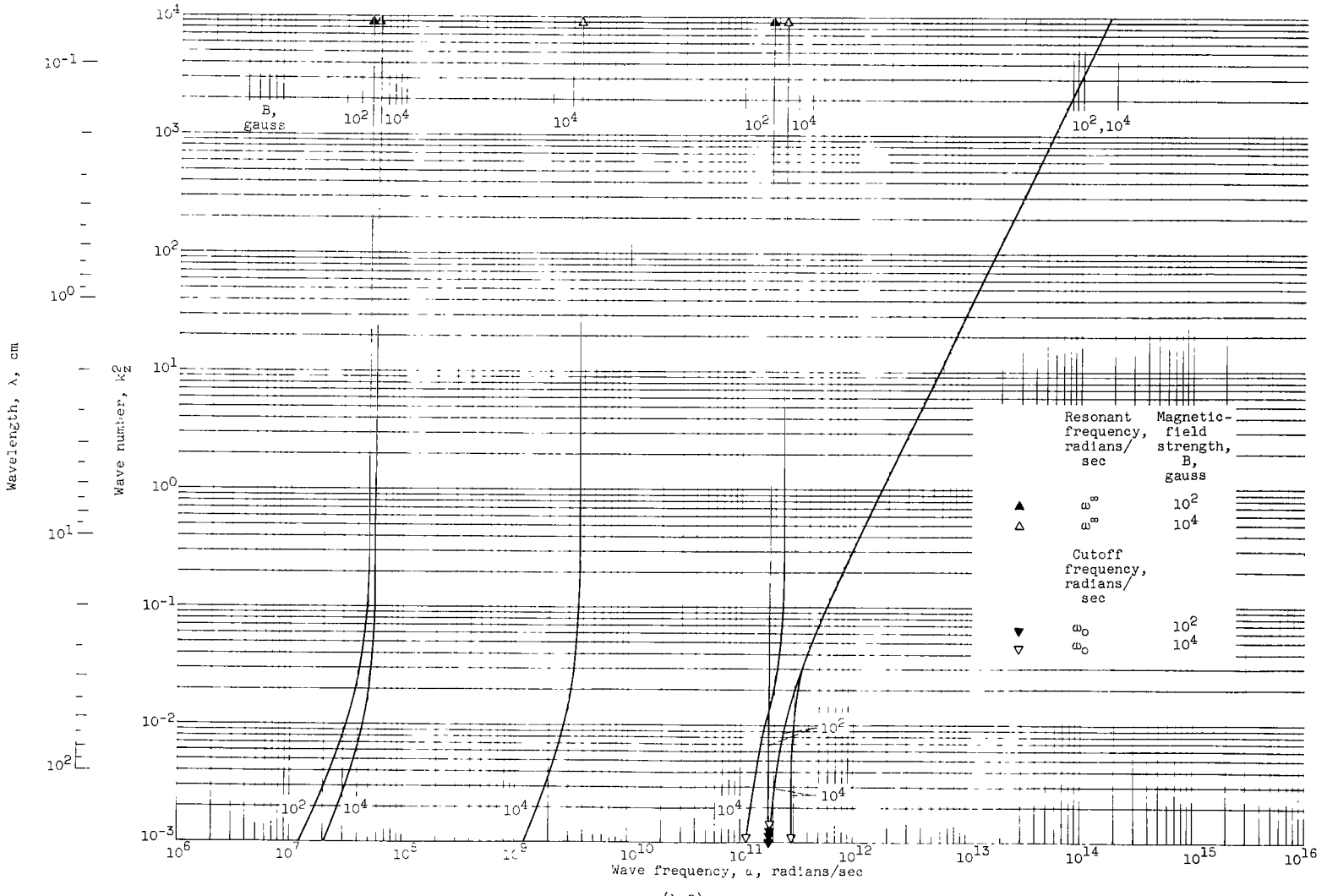

(b-2) z-component.

(b) Concluded. Particle density, 10^{13} ions per cubic centimeter.

Figure 7. - Concluded. Wave number as function of frequency. Wave propagation angle, 89°; Astrom's model.

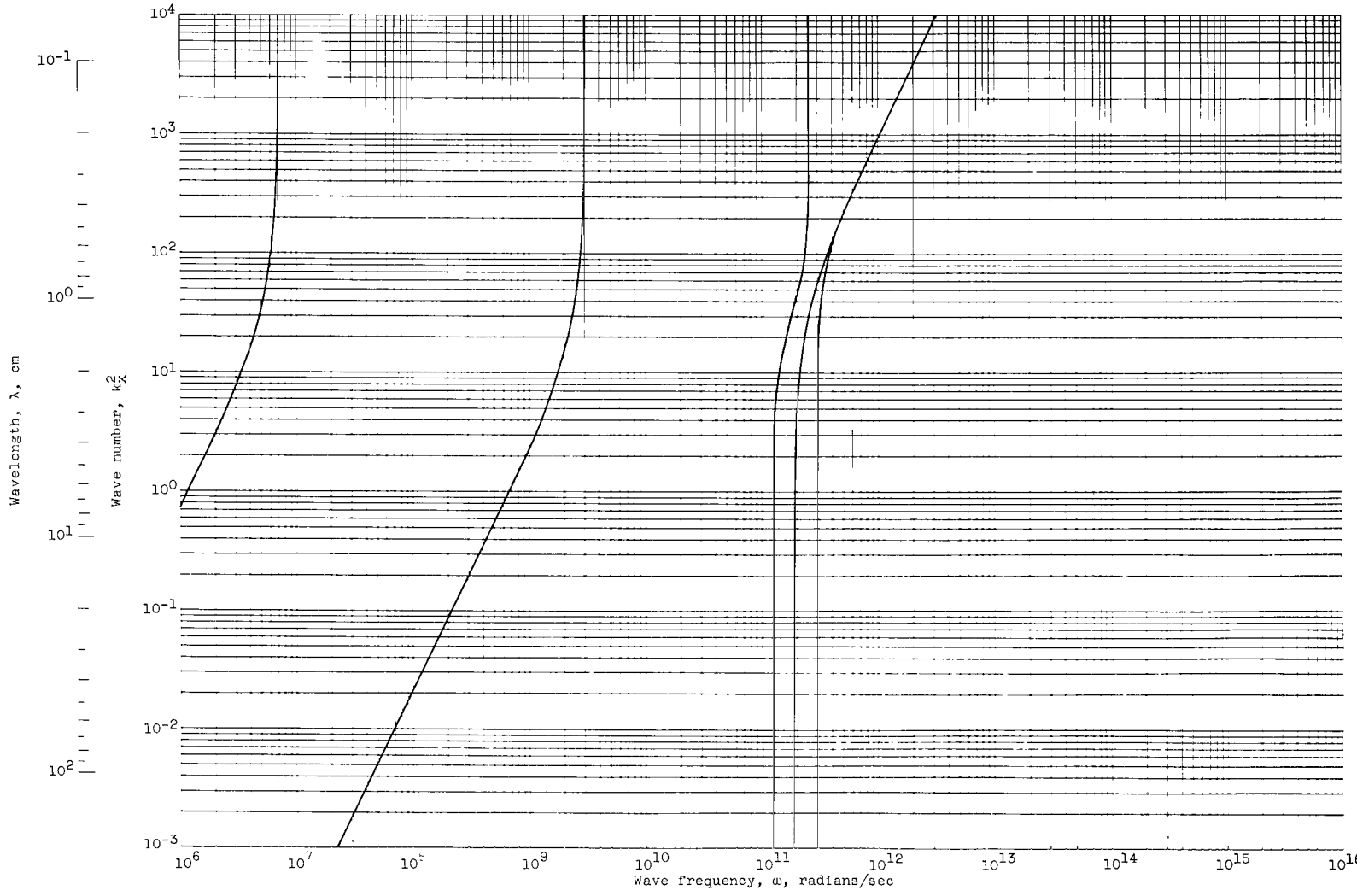

(a) x-component.

Figure 8. - Wave number as function of frequency. Wave propagation angle, 89.9°; magnetic-field strength, 10^4 gauss; particle density, 10^{13} ions per cubic centimeter; Astrom's model.

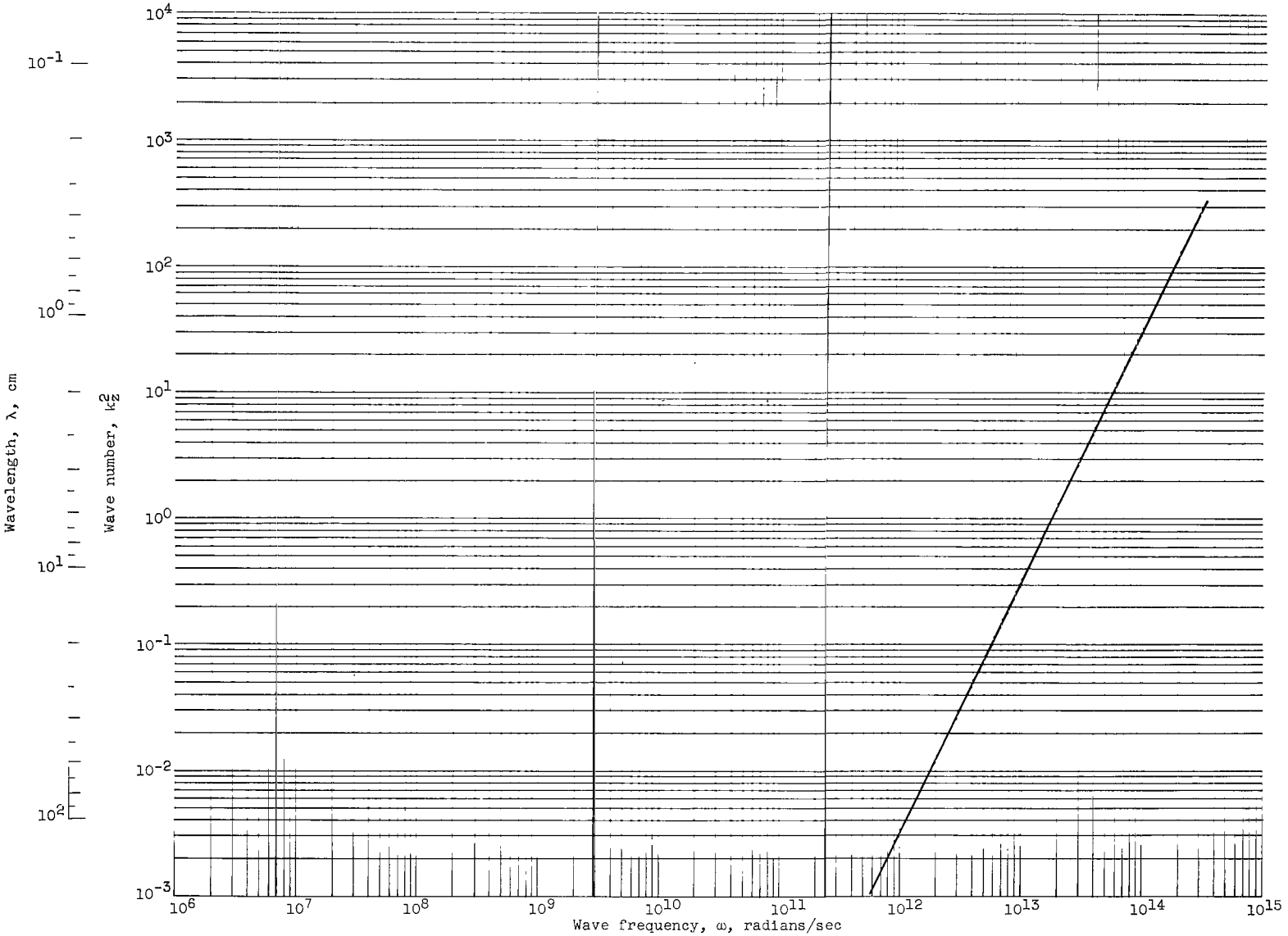

(b) z-component.

Figure 8. - Concluded. Wave number as function of frequency. Wave propagation angle, 89.9°; magnetic-field strength, 10^4 gauss; particle density, 10^{13} ions per cubic centimeter; Astrom's model.

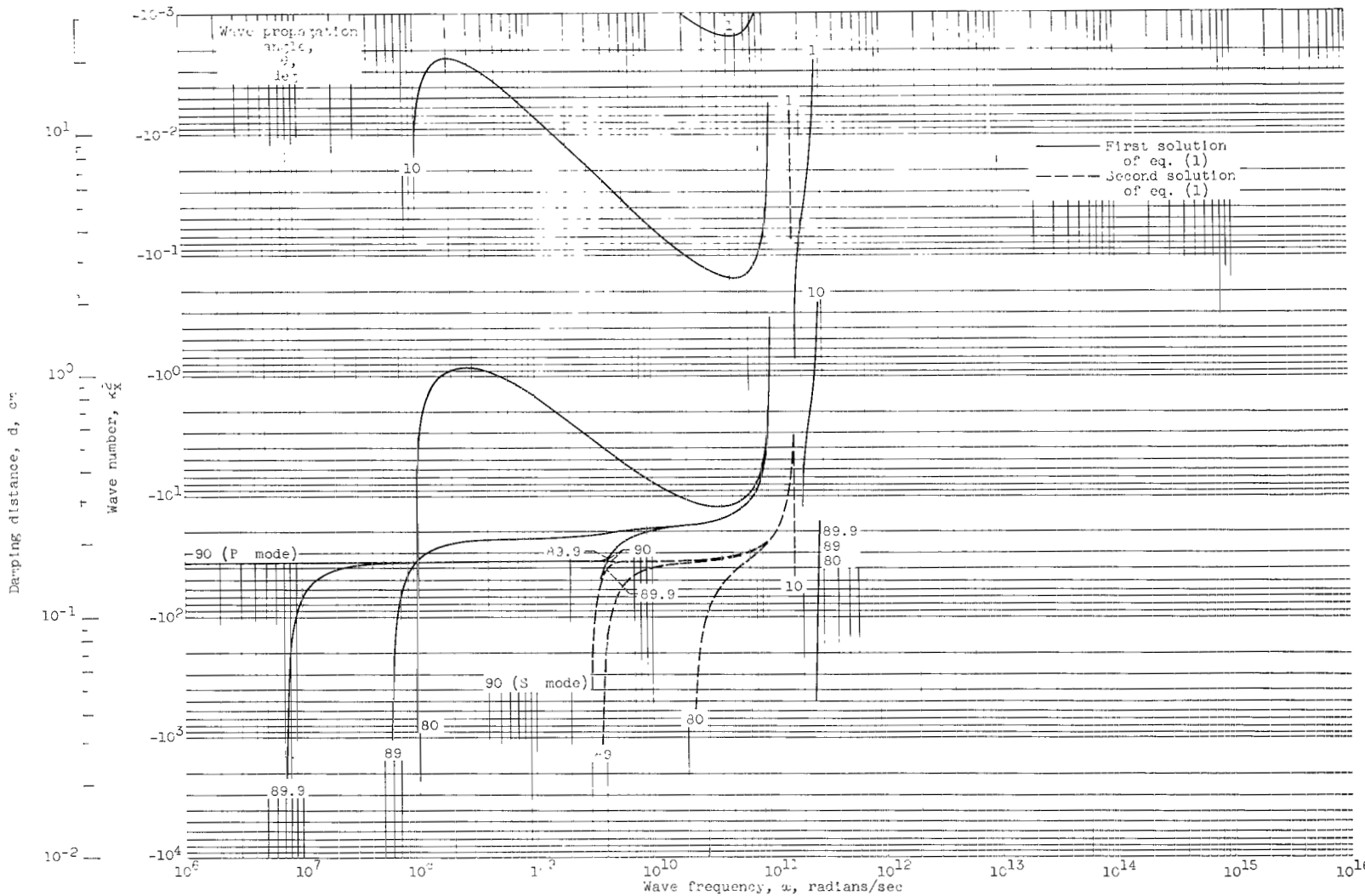

(a) x-component.

Figure 9. - Wave numbers in imaginary (nonpropagating) region as functions of frequency for various oblique angles. Magnetic-field strength, 10^4 gauss; particle density, 10^{13} ions per cubic centimeter.

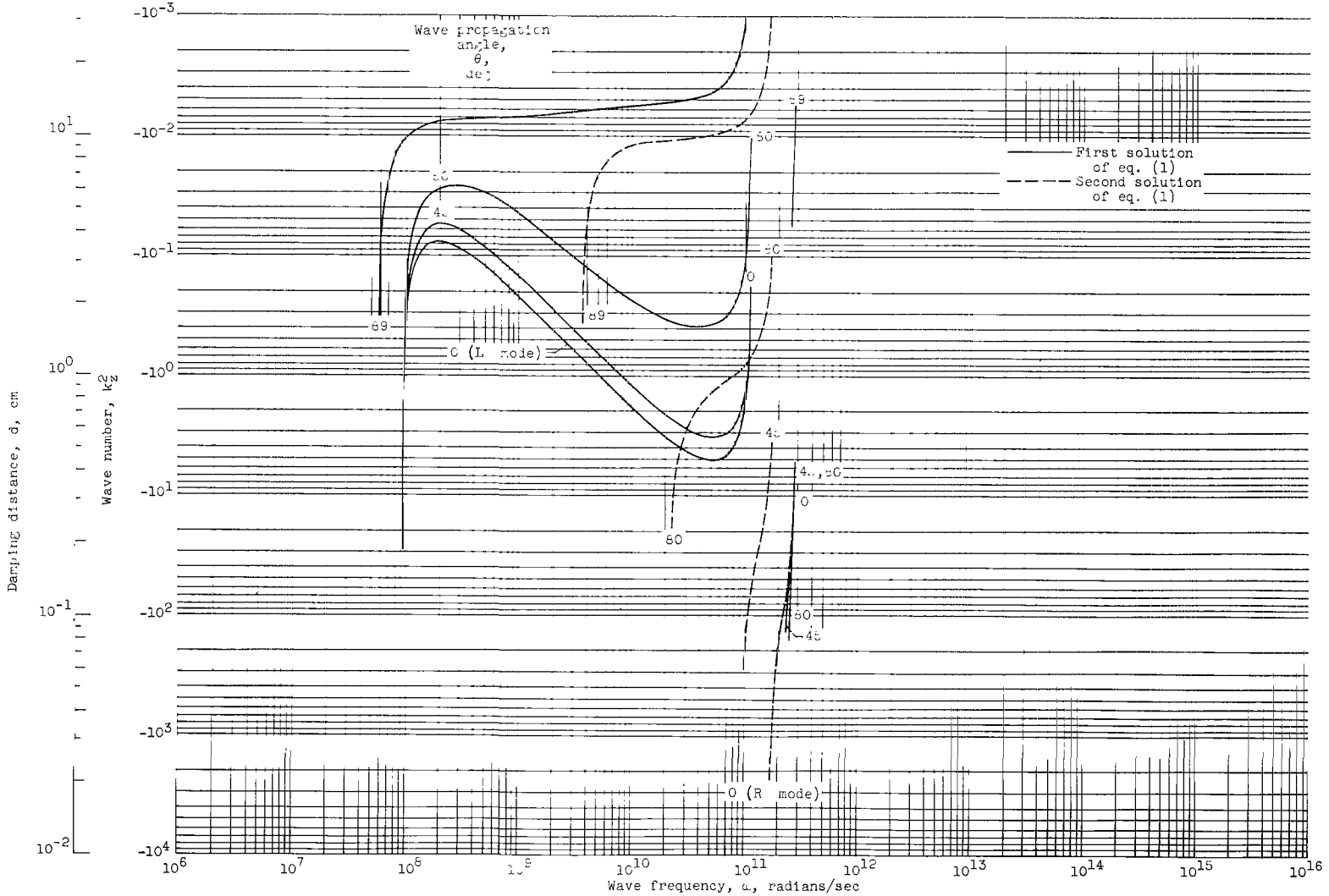

(b) z-component.

Figure 9. - Concluded. Wave numbers in imaginary (nonpropagating) region as functions of frequency for various oblique angles. Magnetic-field strength, 10^4 gauss; particle density, 10^{13} ions per cubic centimeter.

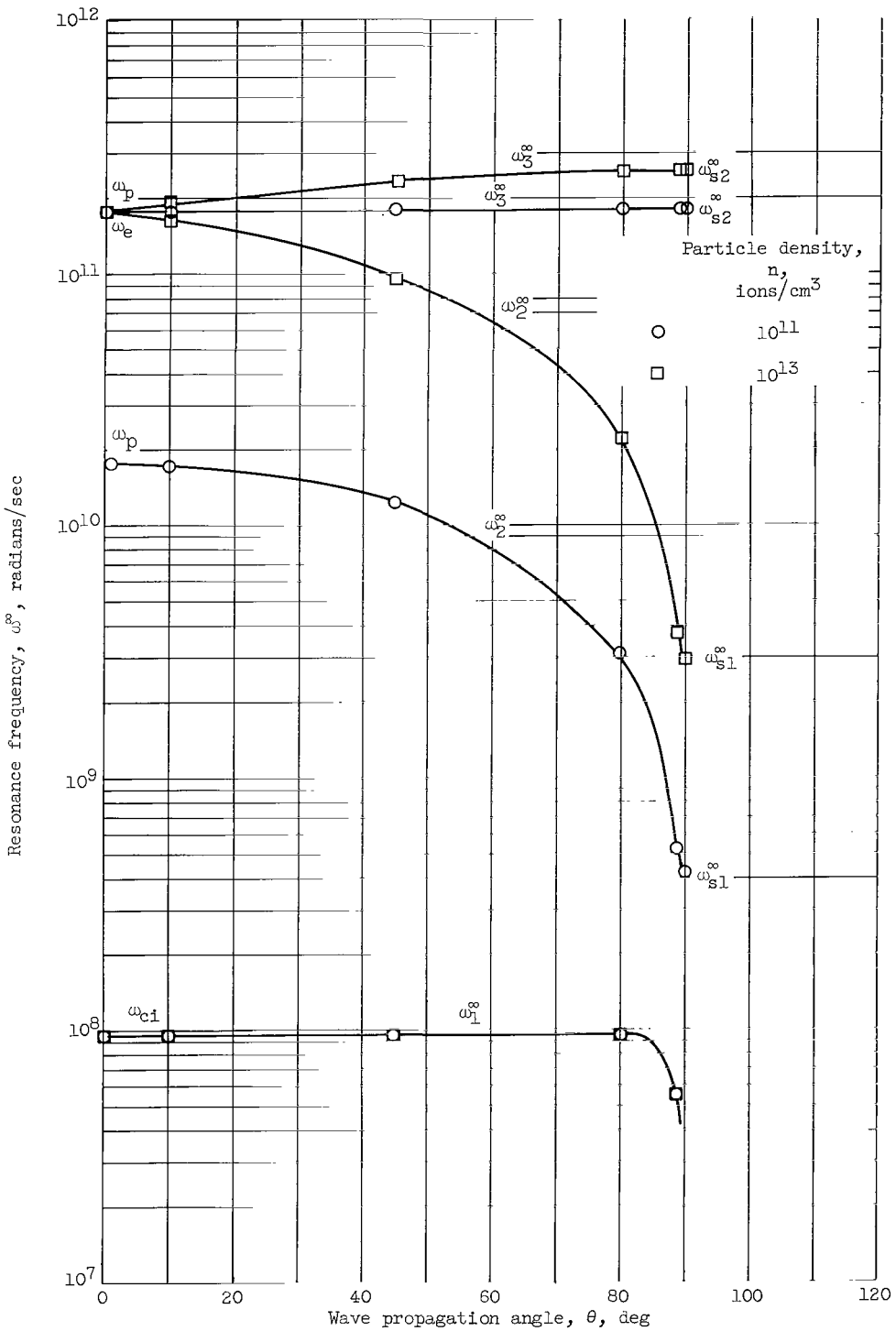

(a) Magnetic-field strength, 10^4 gauss.

Figure 10. - Resonant frequency as function of oblique wave propagation angle. Astrom's model.

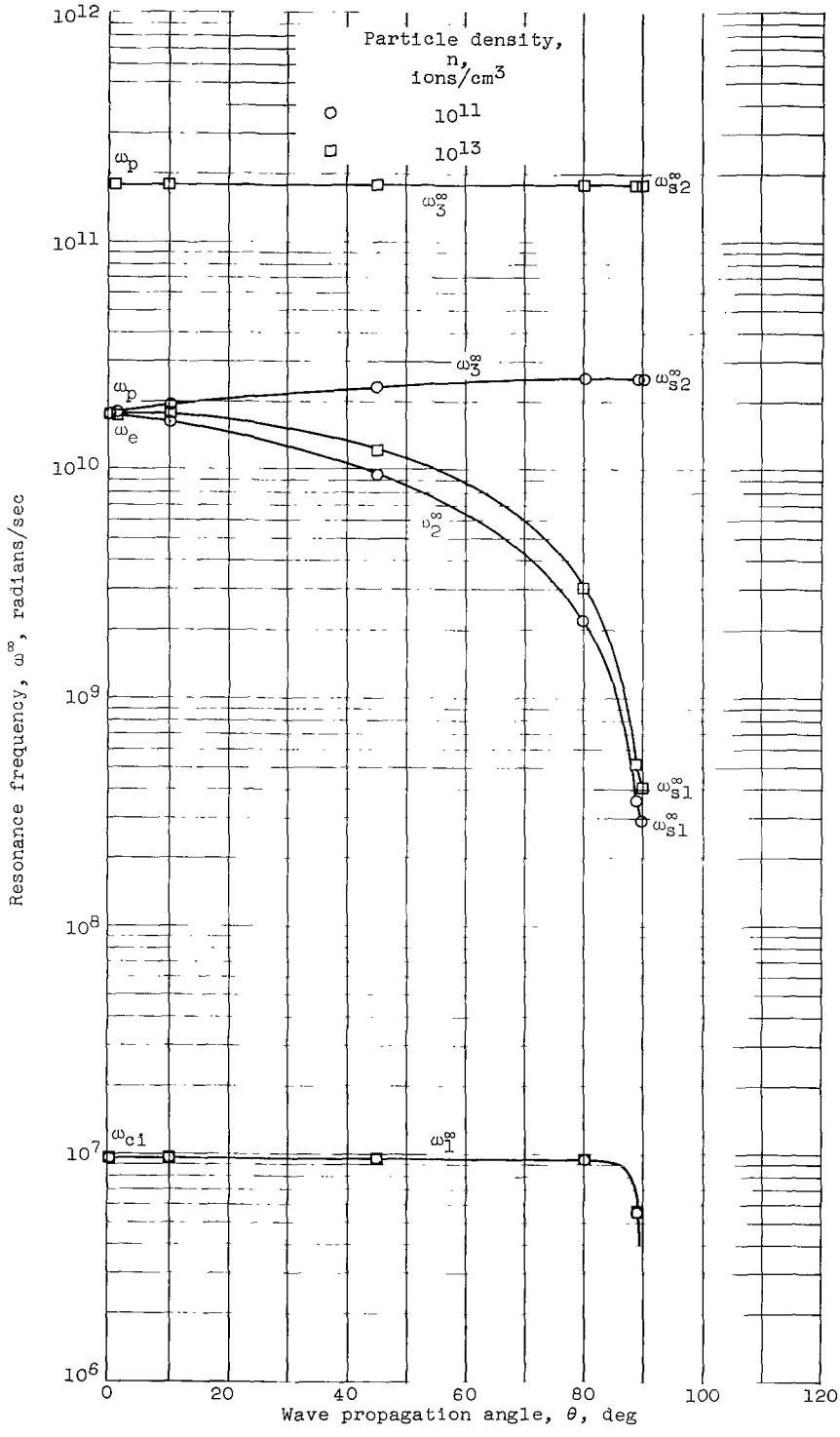

(b) Magnetic-field strength, 10^3 gauss.

Figure 10. - Continued. Resonant frequency as function of oblique wave propagation angle. Astrom's model.

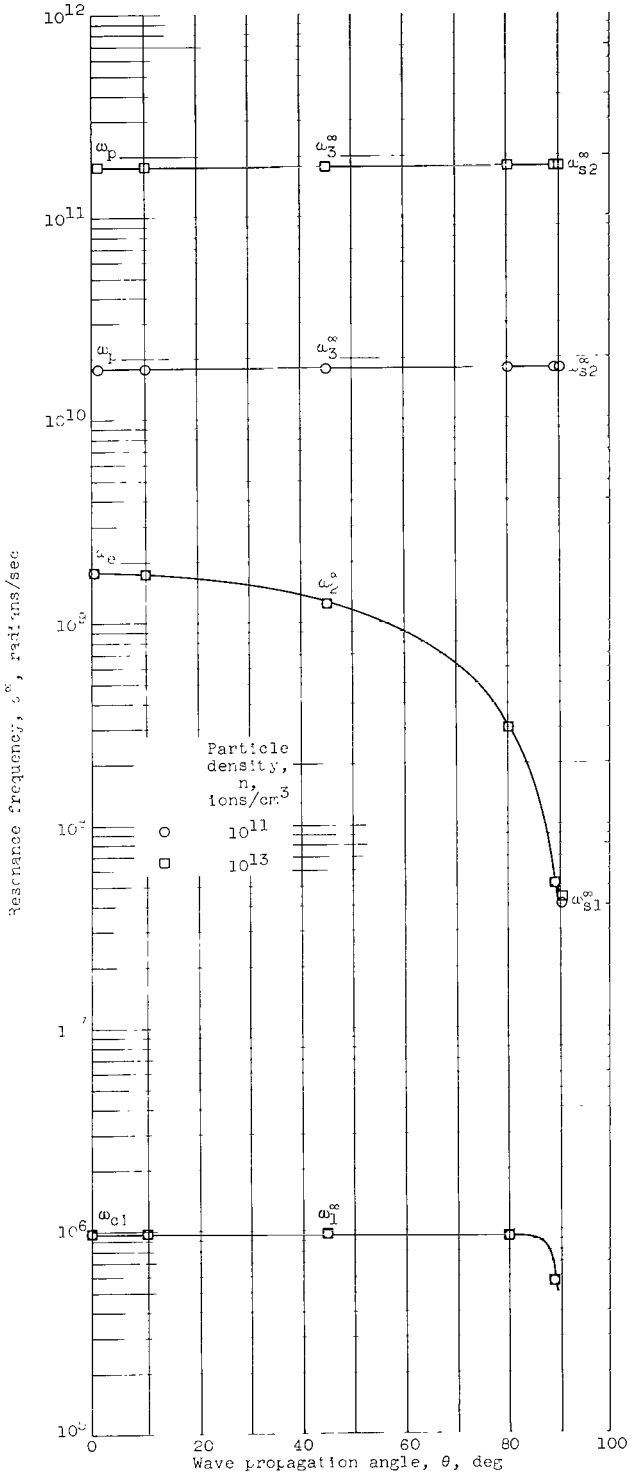

(c) Magnetic-field strength, 10^2 gauss.

Figure 10. - Concluded. Resonant frequency as function of oblique wave propagation angle. Astron's model.

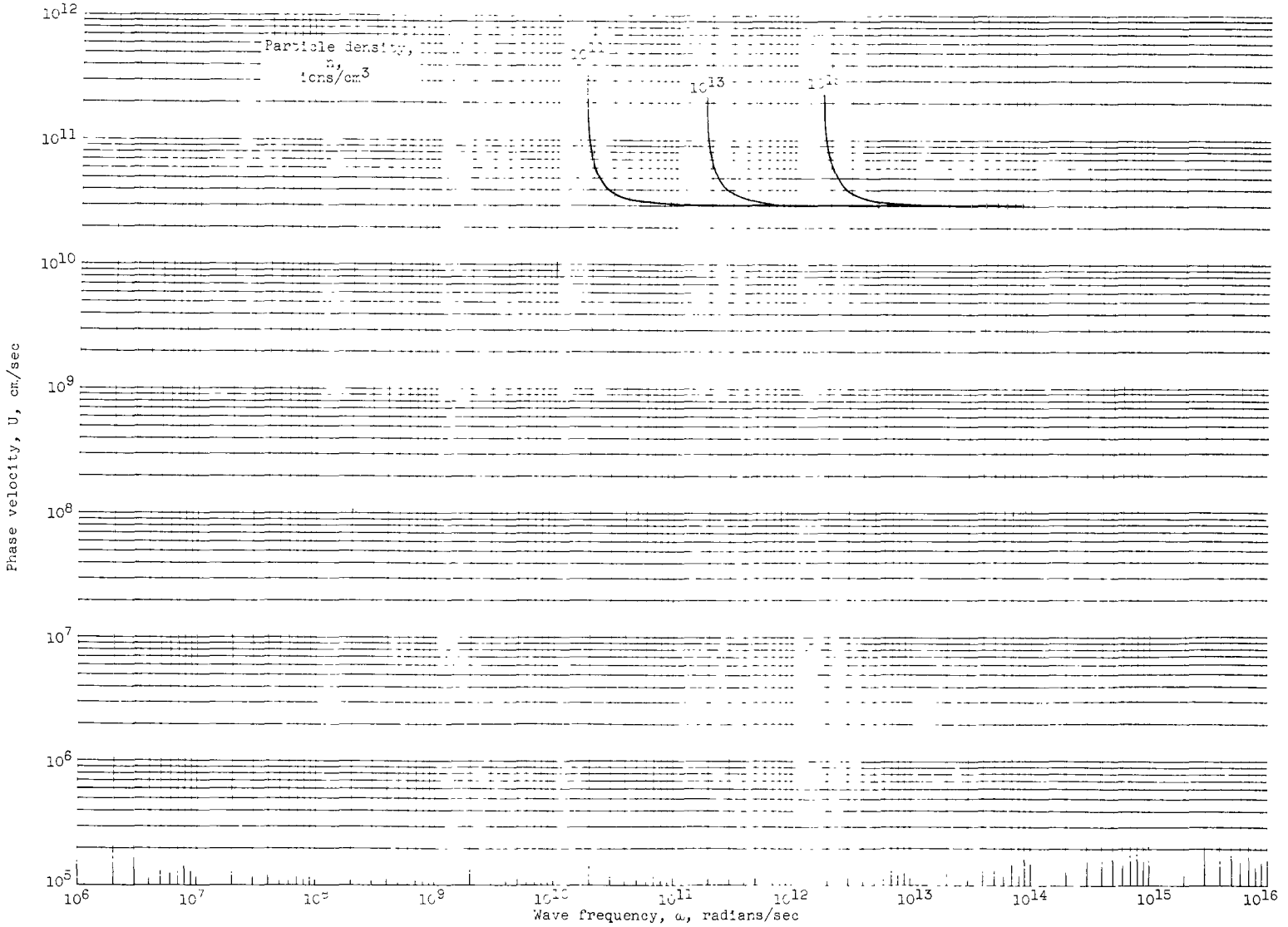

(a) P mode; wave propagation angle, 90°.

Figure 11. - Phase velocity as function of wave frequency. Astrom's model.

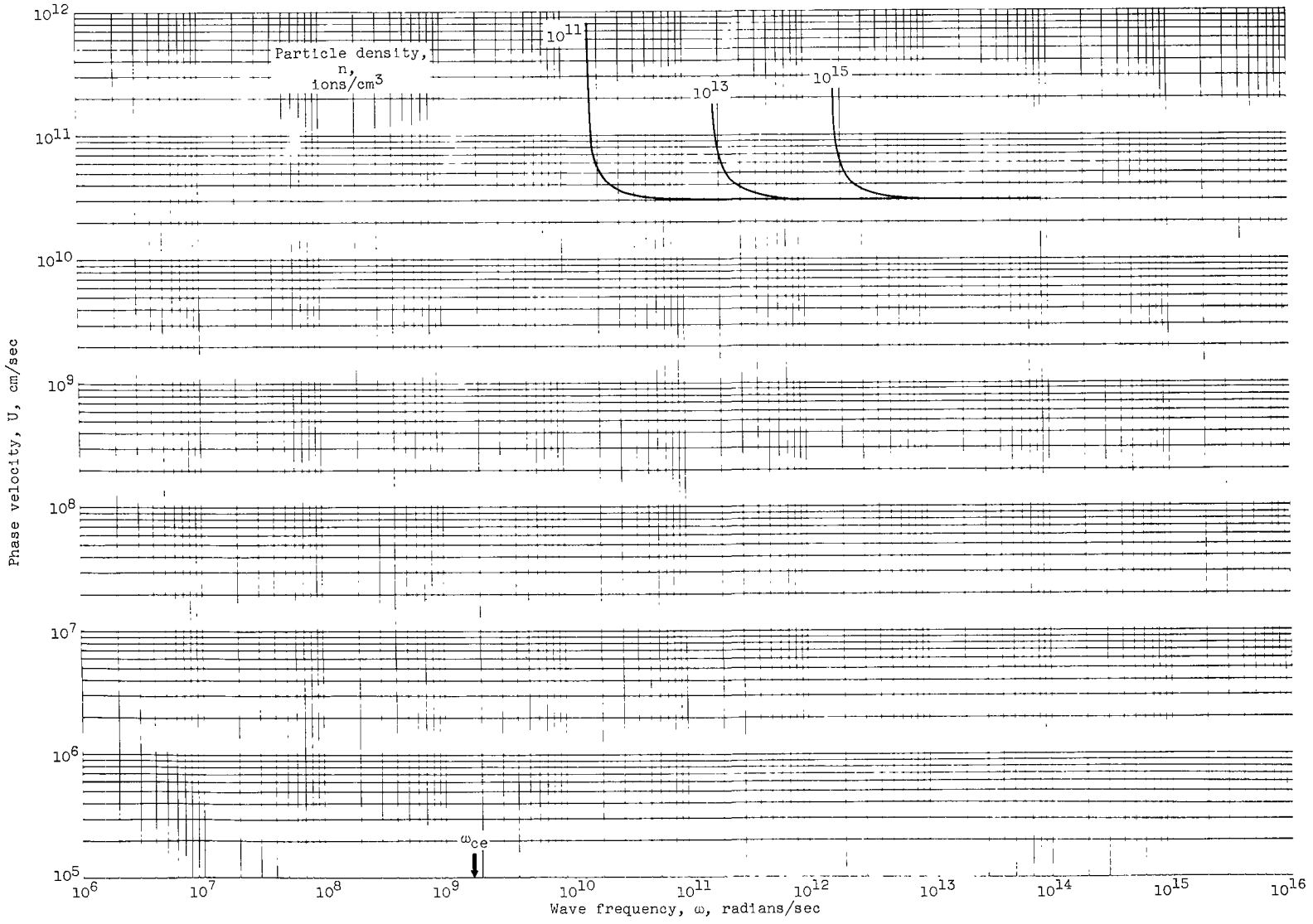

(b-1) Magnetic-field strength, 10^2 gauss.

(b) L mode; wave propagation angle, 0^o.

Figure 11. - Continued. Phase velocity as function of wave frequency. Astrom's model.

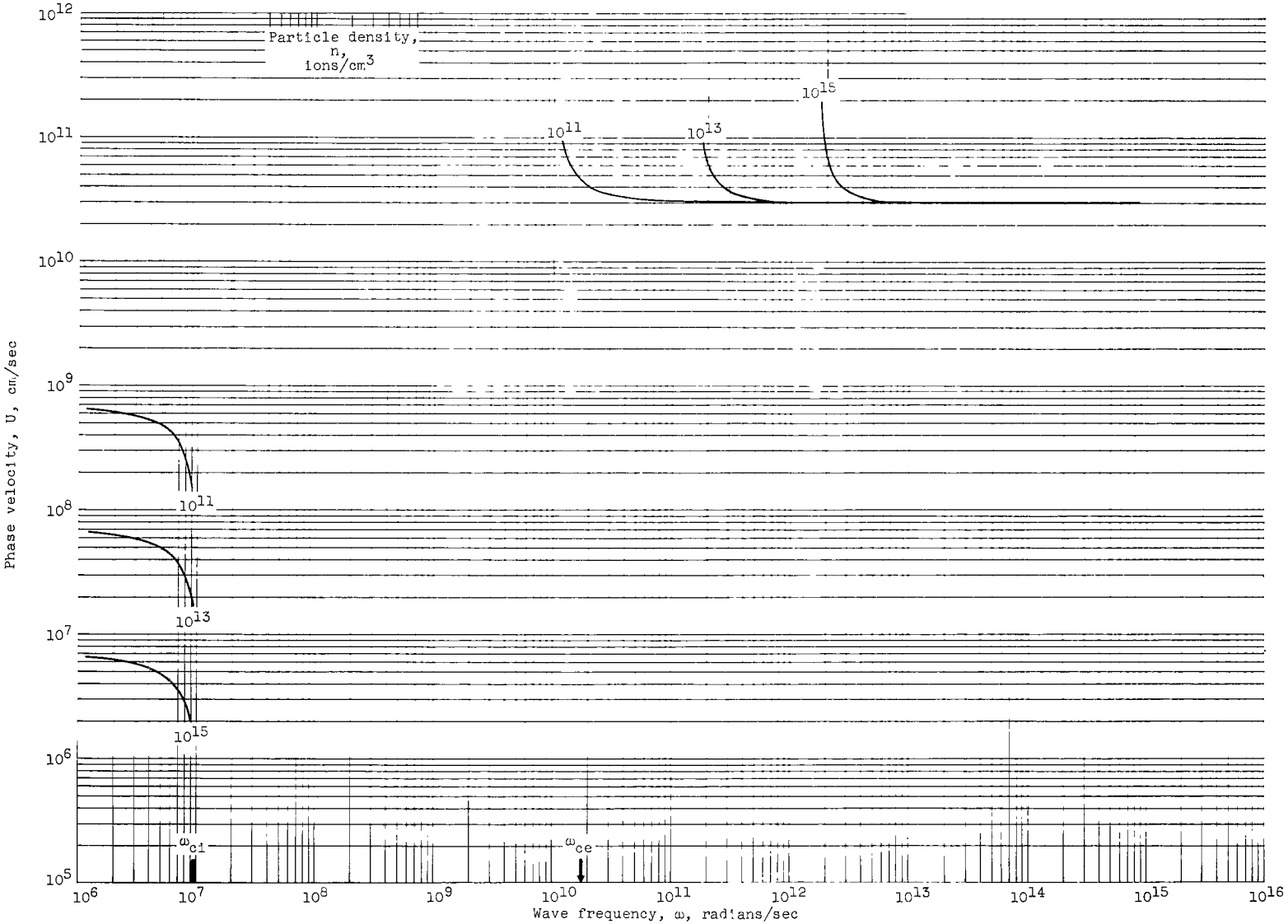

(b-2) Magnetic-field strength, 10^3 gauss.

(b) Continued. L mode; wave propagation angle, 0^o.

Figure 11. - Continued. Phase velocity as function of wave frequency. Astrom's model.

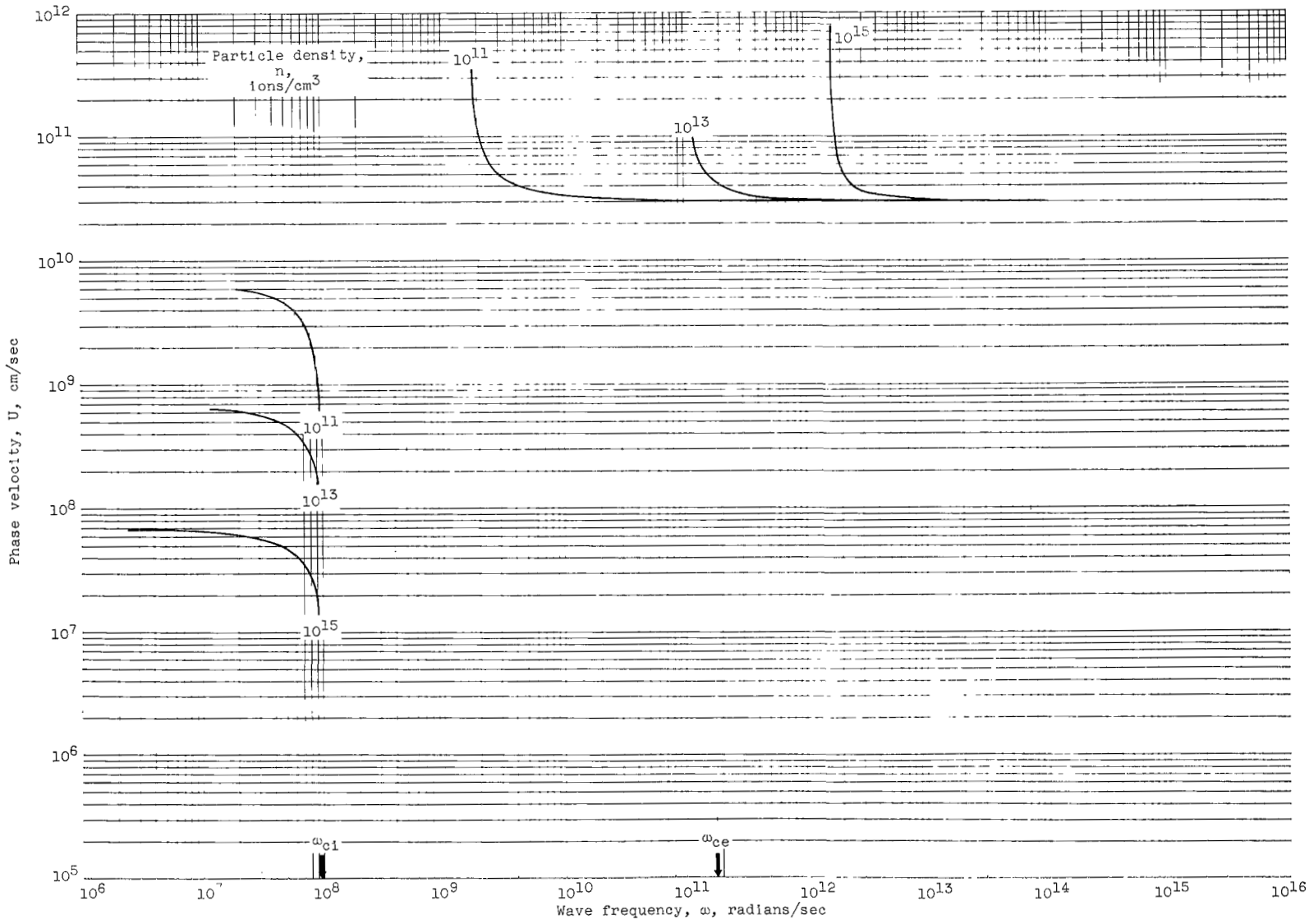

(b-3) Magnetic-field strength, 10^4 gauss.

(b) Continued. L mode; wave propagation angle, 0°.

Figure 11. - Continued. Phase velocity as function of wave frequency. Astrom's model.

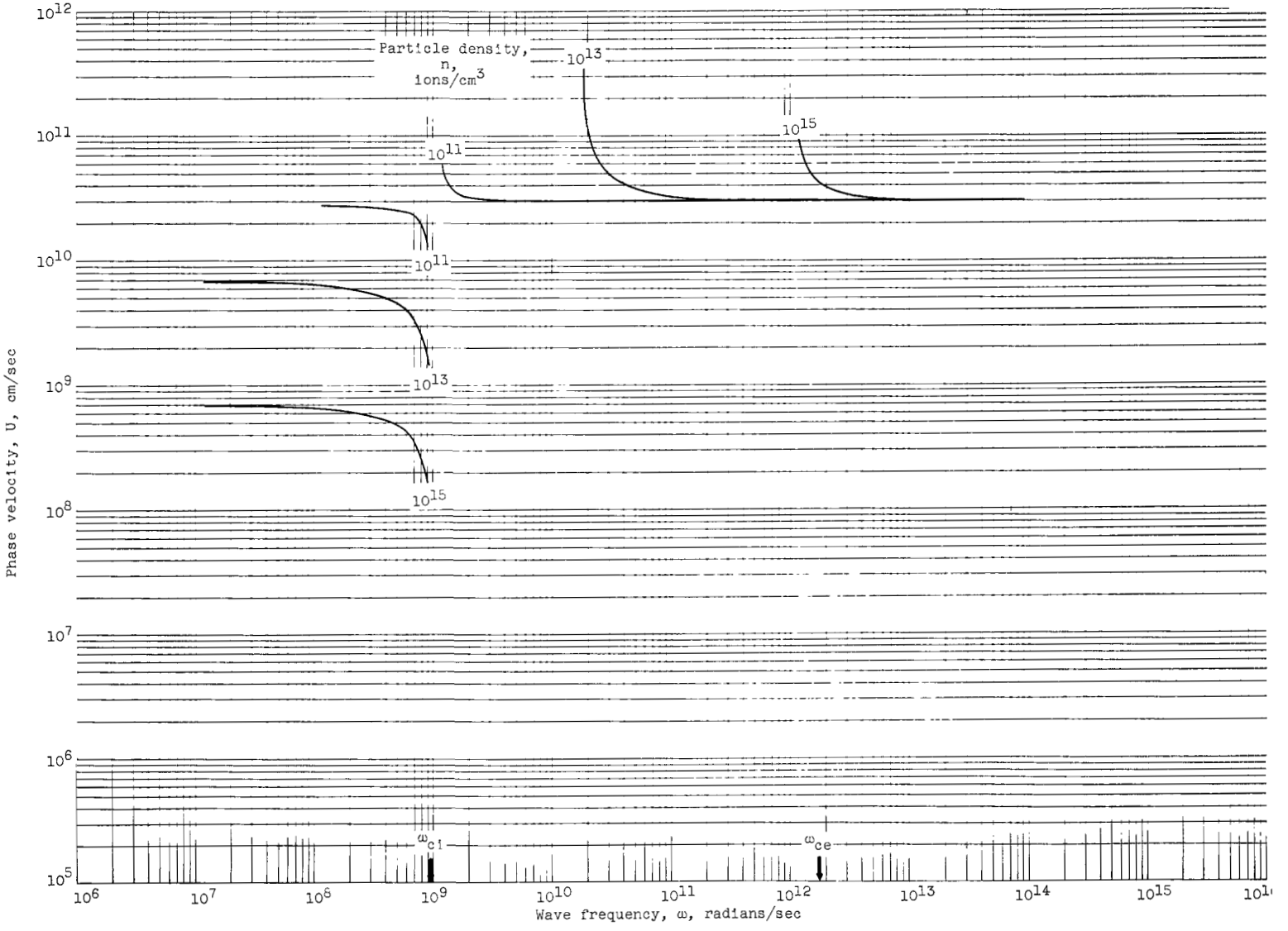

(b-4) Magnetic-field strength, 10^5 gauss.

(b) Concluded. L mode; wave propagation angle, 0^o.

Figure 11. - Continued. Phase velocity as function of wave frequency. Astrom's model.

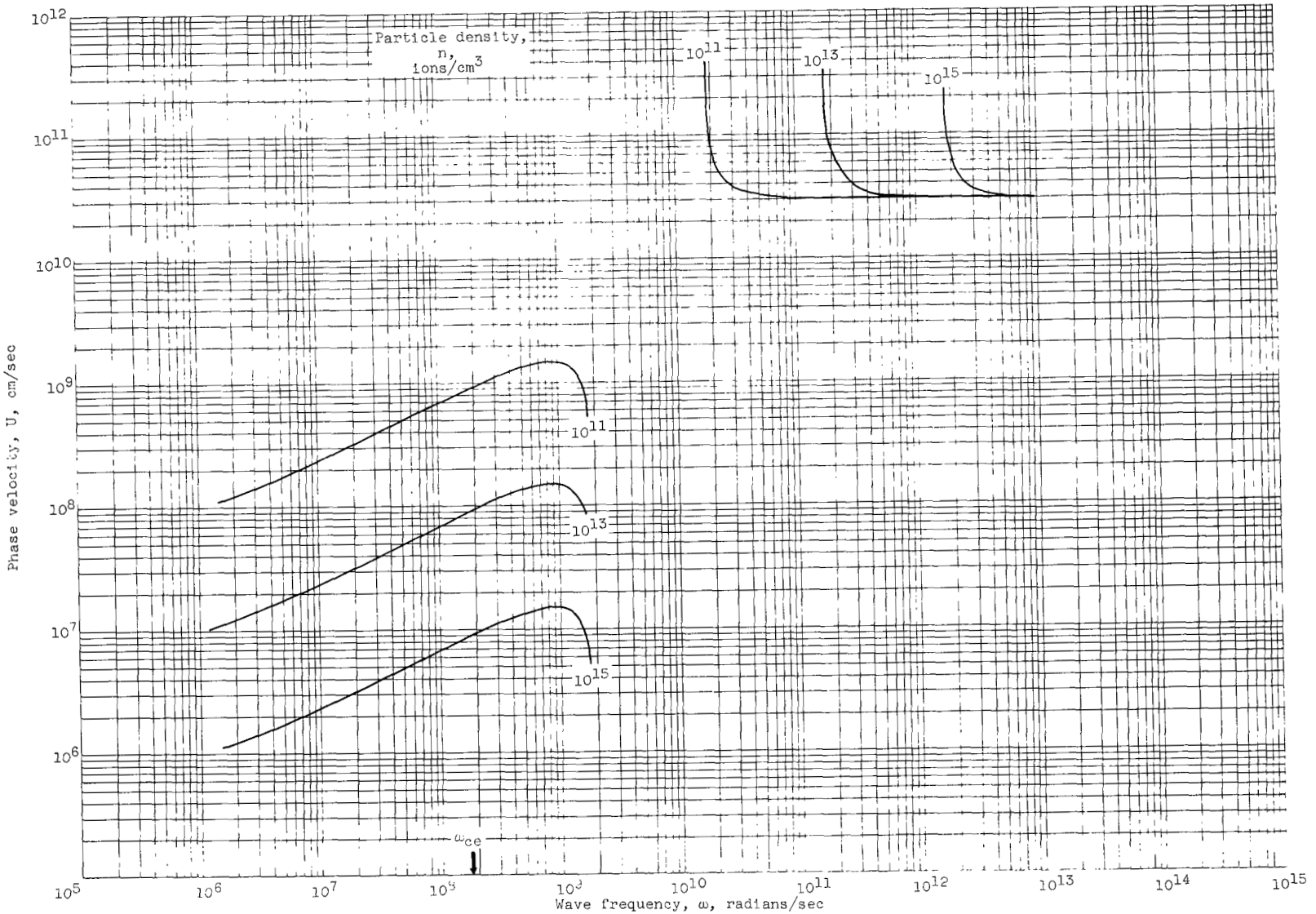

(c-1) Magnetic-field strength, 10^2 gauss.

(c) R mode; wave propagation angle, 0°.

Figure 11. - Continued. Phase velocity as function of wave frequency. Astrom's model.

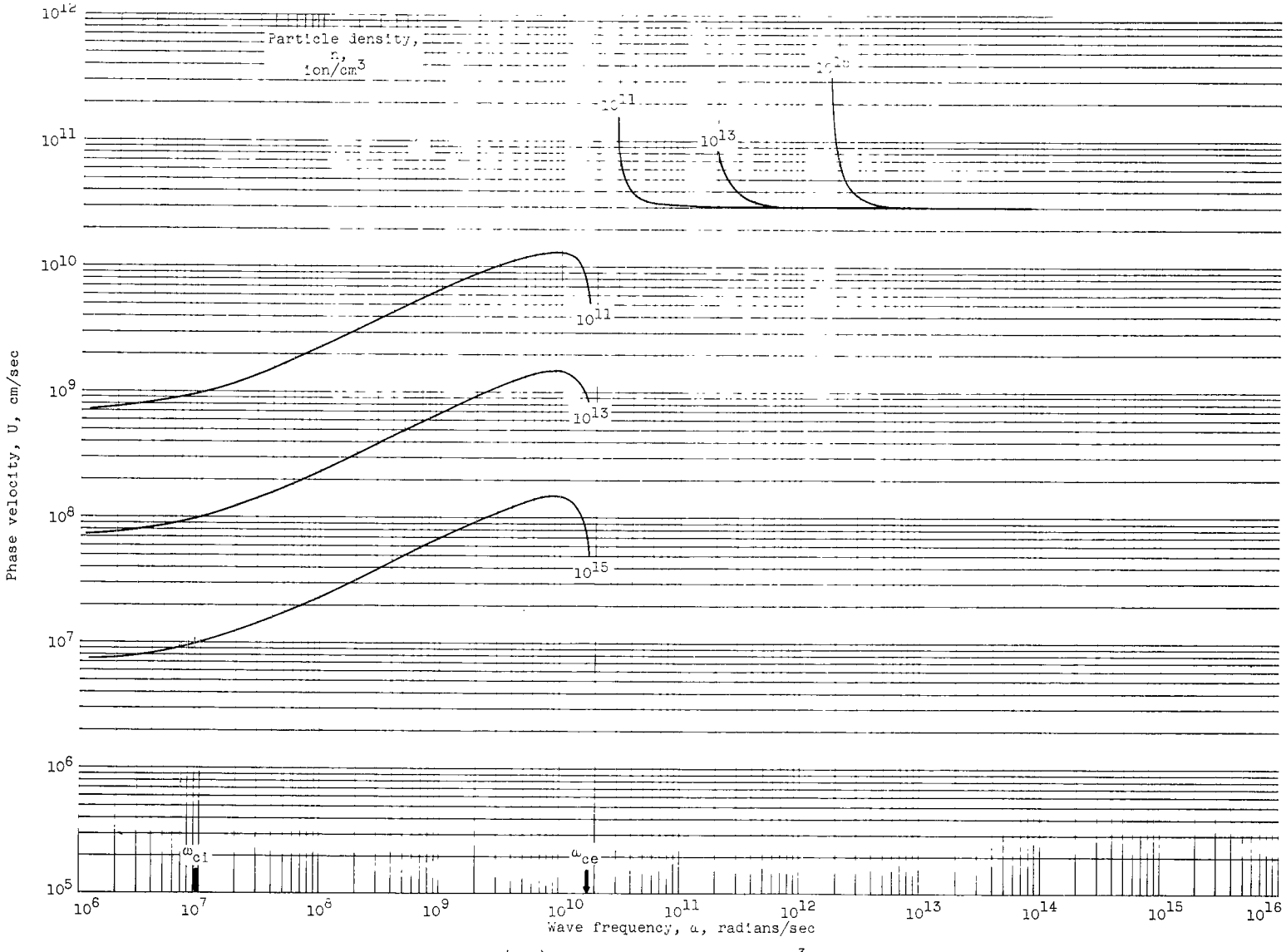

(c-2) Magnetic-field strength, 10^3 gauss.

(c) Continued. R mode; wave propagation angle, 0^o.

Figure 11. - Continued. Phase velocity as function of wave frequency. Astrom's model.

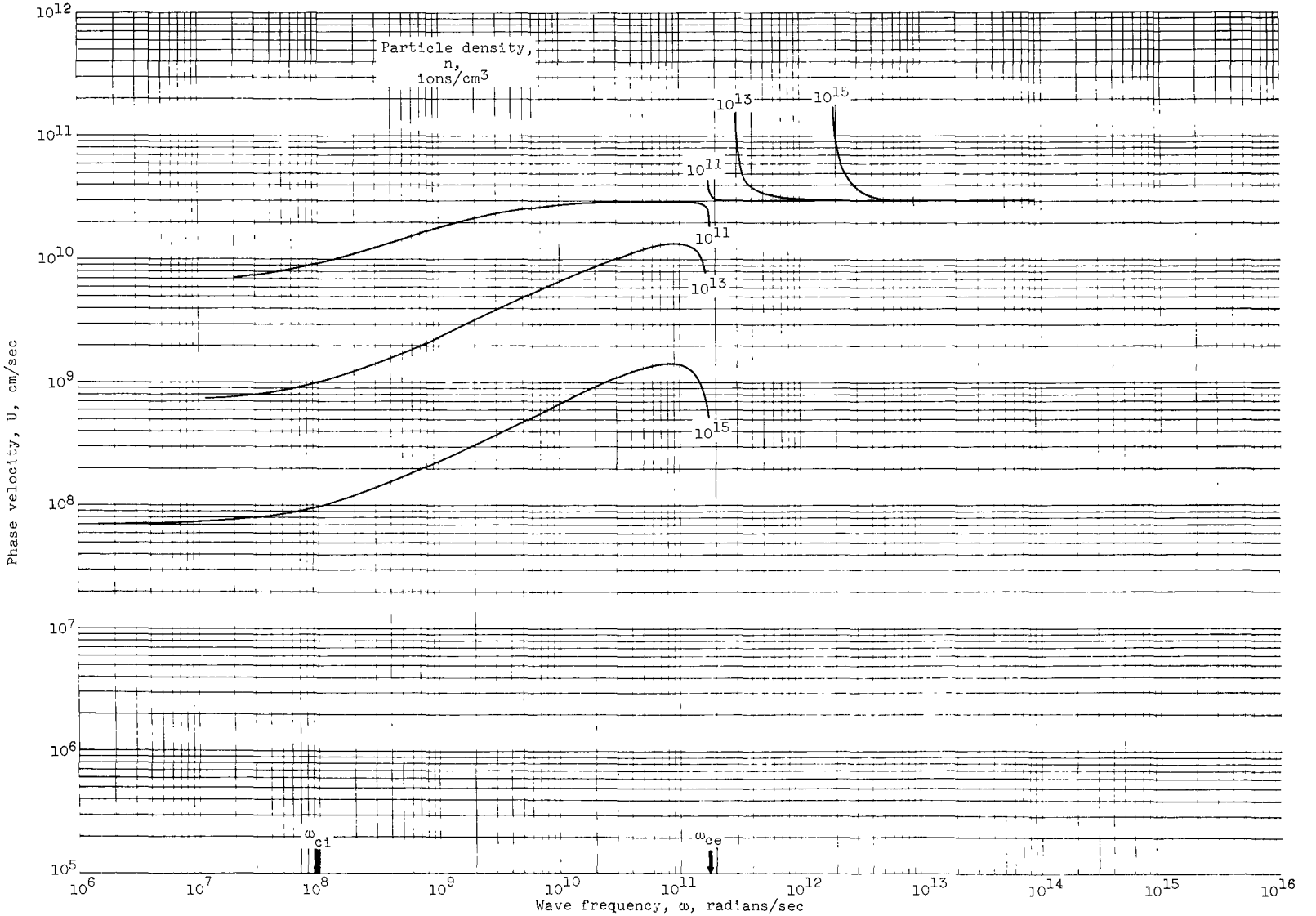

(c-3) Magnetic-field strength, 10^4 gauss.

(c) Continued. R mode; wave propagation angle, 0^o.

Figure 11. - Continued. Phase velocity as function of wave frequenc . Astrom's model.

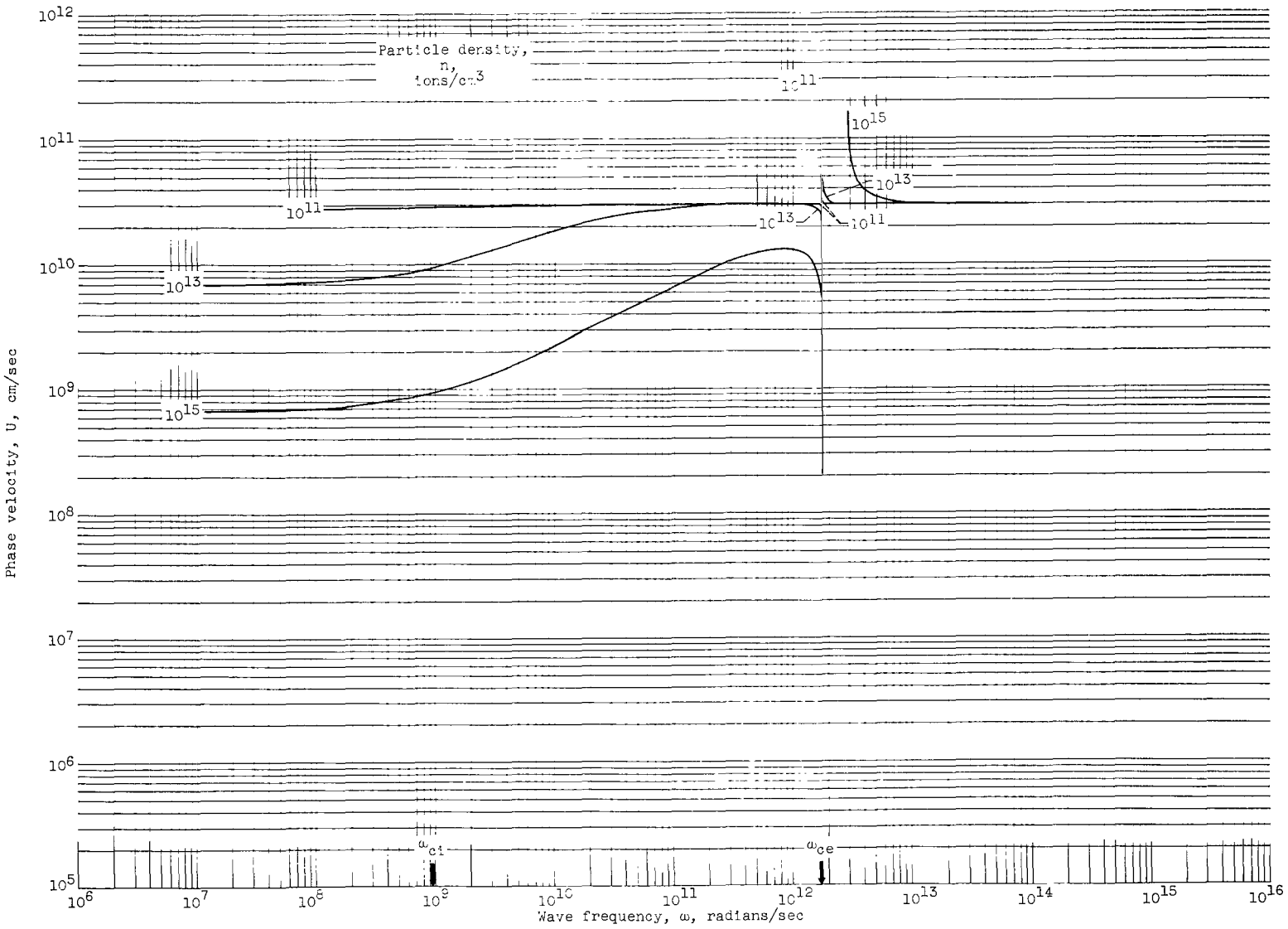

(c-4) Magnetic-field strength, 10^5 gauss.

(c) Concluded. R mode; wave propagation angle, 0^o.

Figure 11. - Continued. Phase velocity as function of wave frequency. Astrom's model.

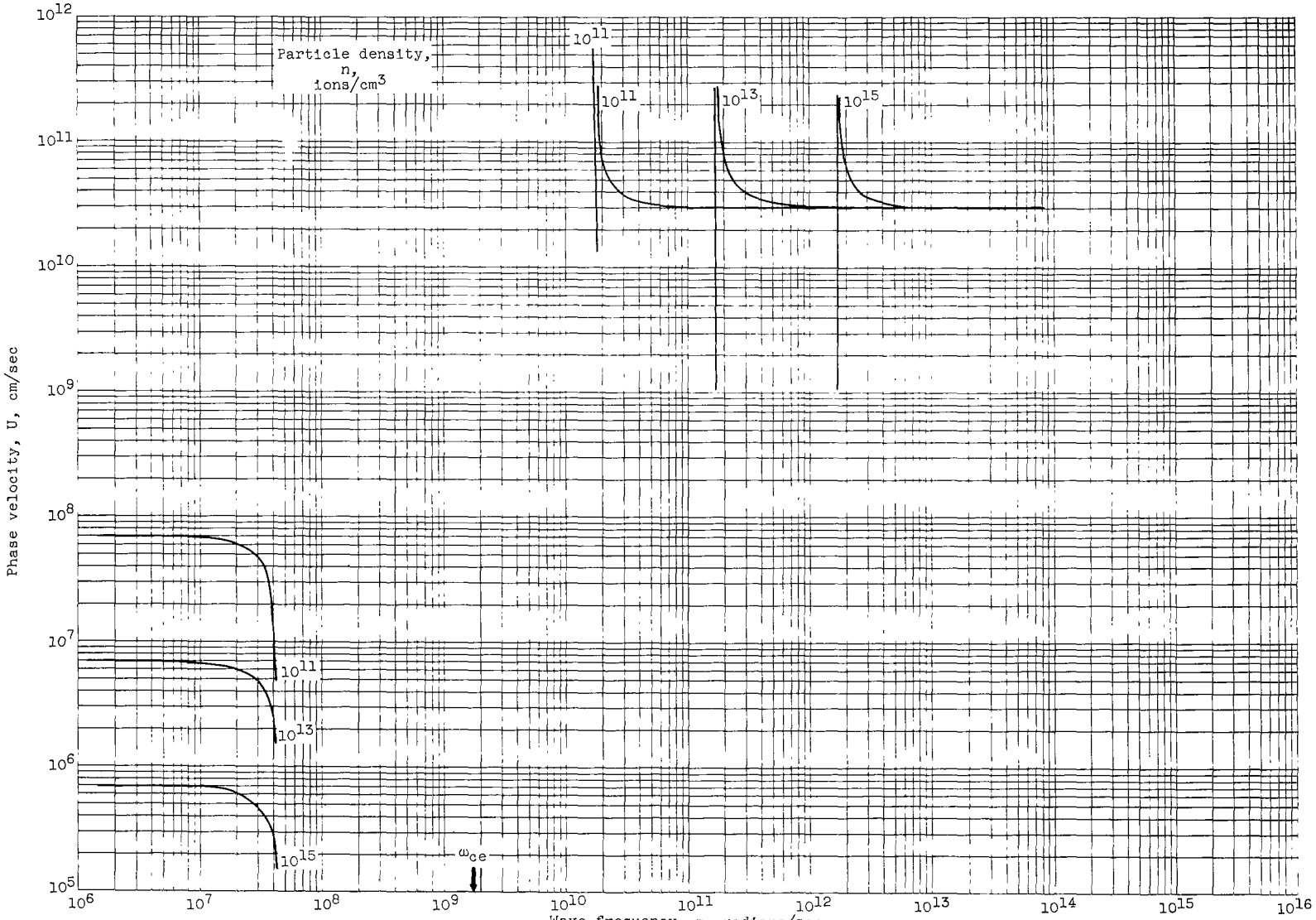

(d-1) Magnetic-field strength, 10^2 gauss.

(d) S mode; wave propagation angle, 90°.

Figure 11. - Continued. Phase velocity as function of wave frequency. Astrom's model.

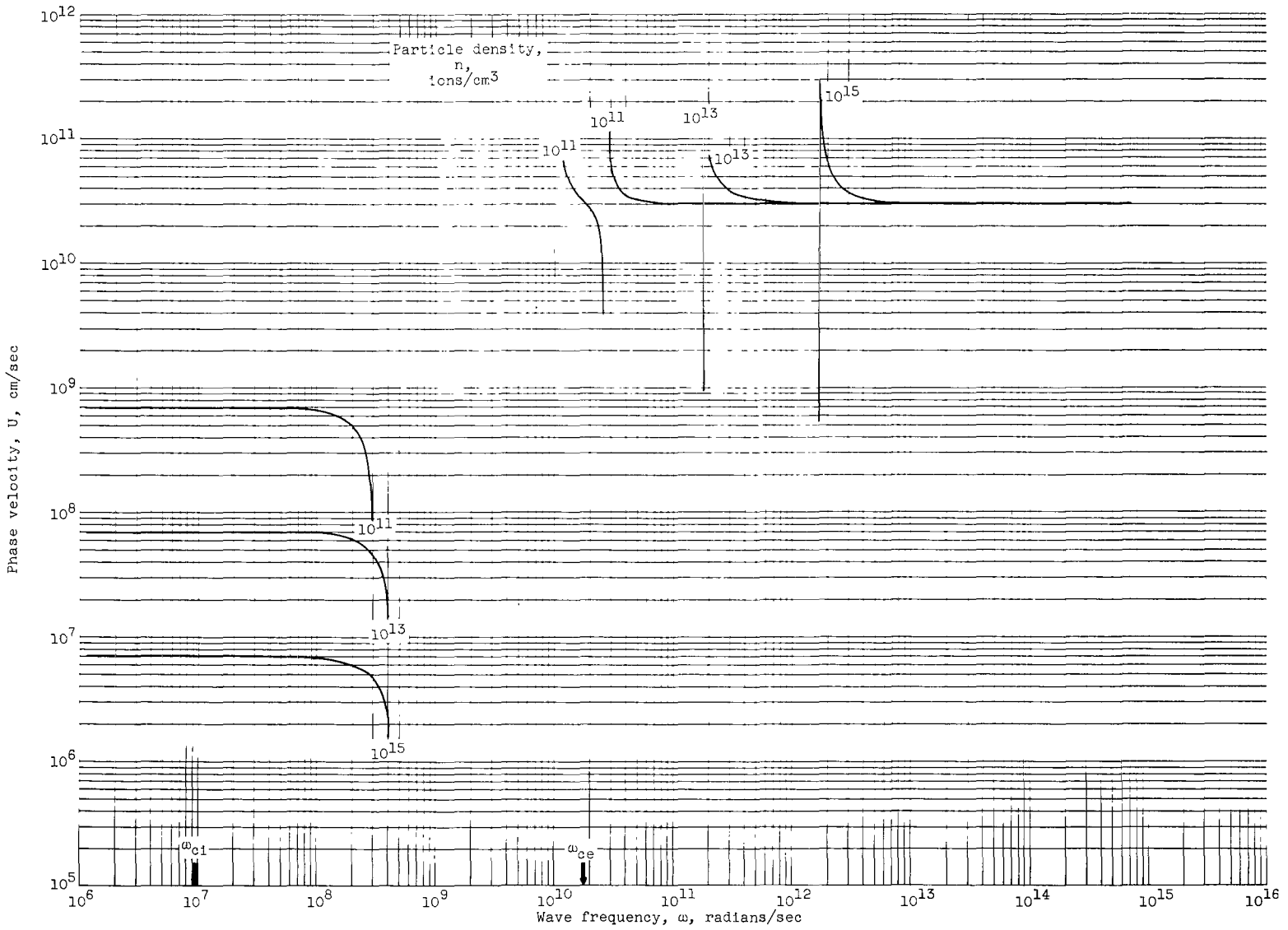

(d-2) Magnetic-field strength, 10^3 gauss.

(d) Continued. S mode; wave propagation angle, 90^o.

Figure 11. - Continued. Phase velocity as function of wave frequency. Astrom's model.

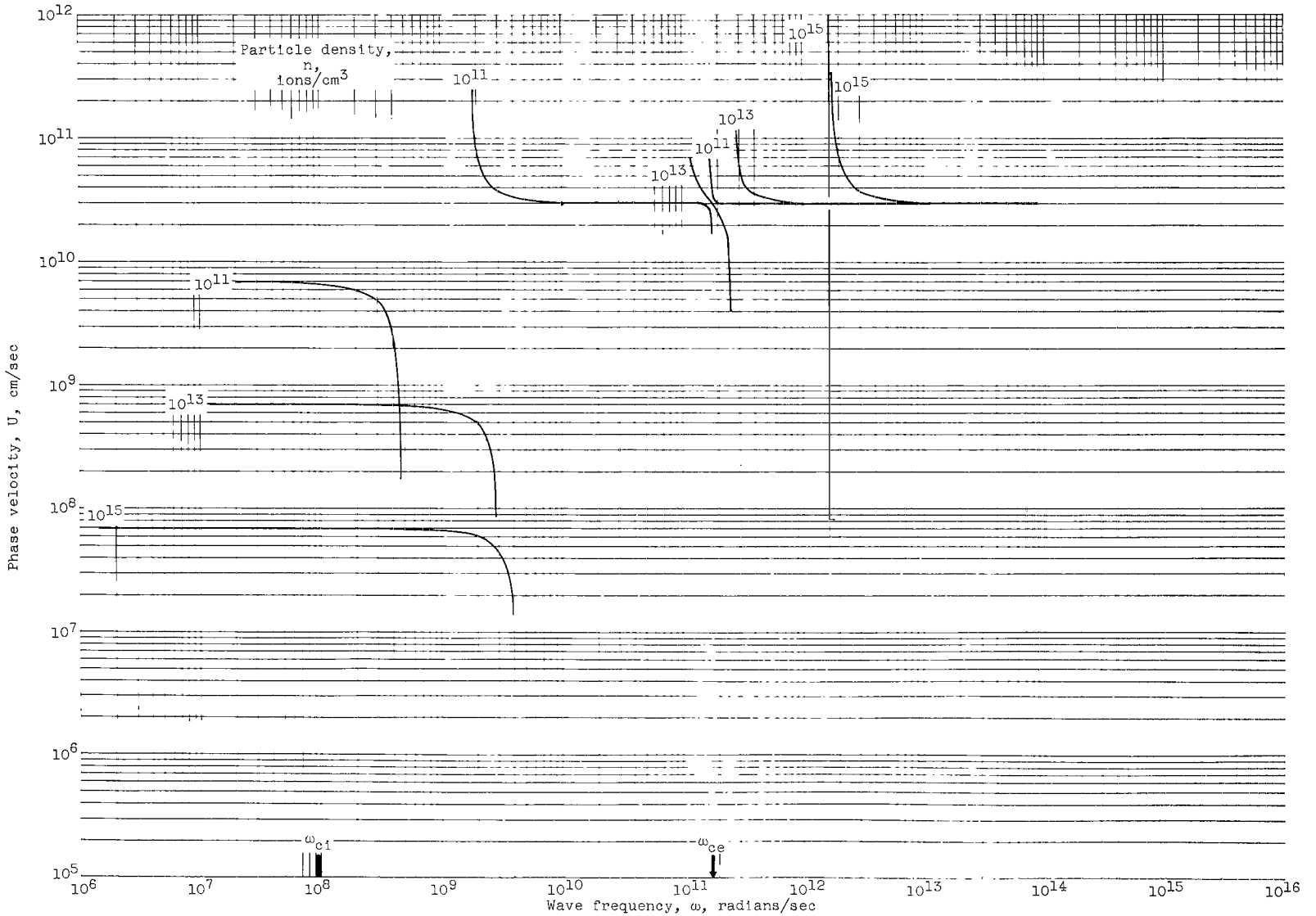

(d-3) Magnetic-field strength, 10^4 gauss.

(d) Continued. S mode; wave propagation angle, 90°.

Figure 11. - Continued. Phase velocity as function of wave frequency. Astrom's model.

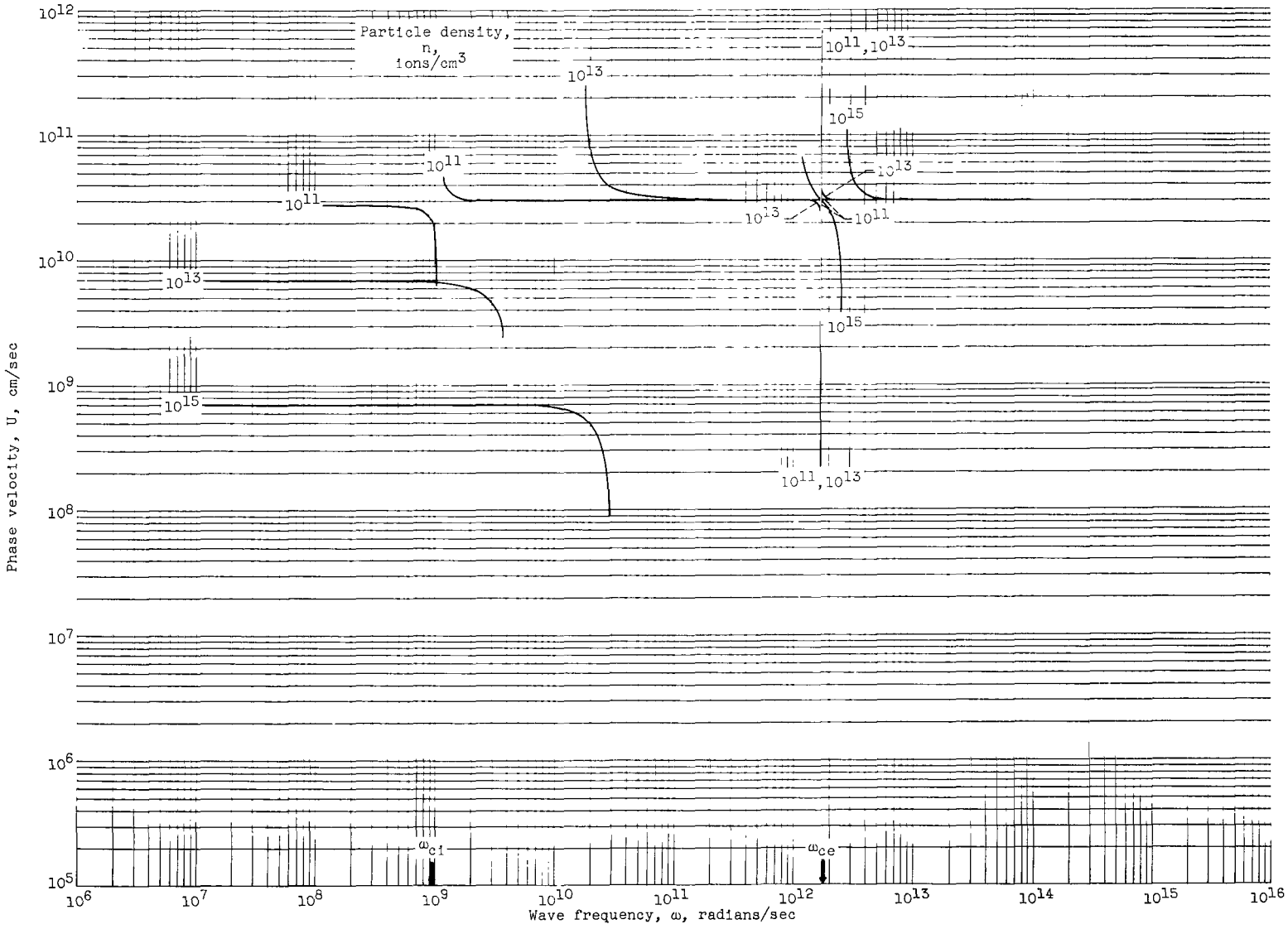

(d-4) Magnetic-field strength, 10^5 gauss.

(d) Concluded. S mode; wave propagation angle, 90°.

Figure 11. - Concluded. Phase velocity as function of wave frequency. Astrom's model.

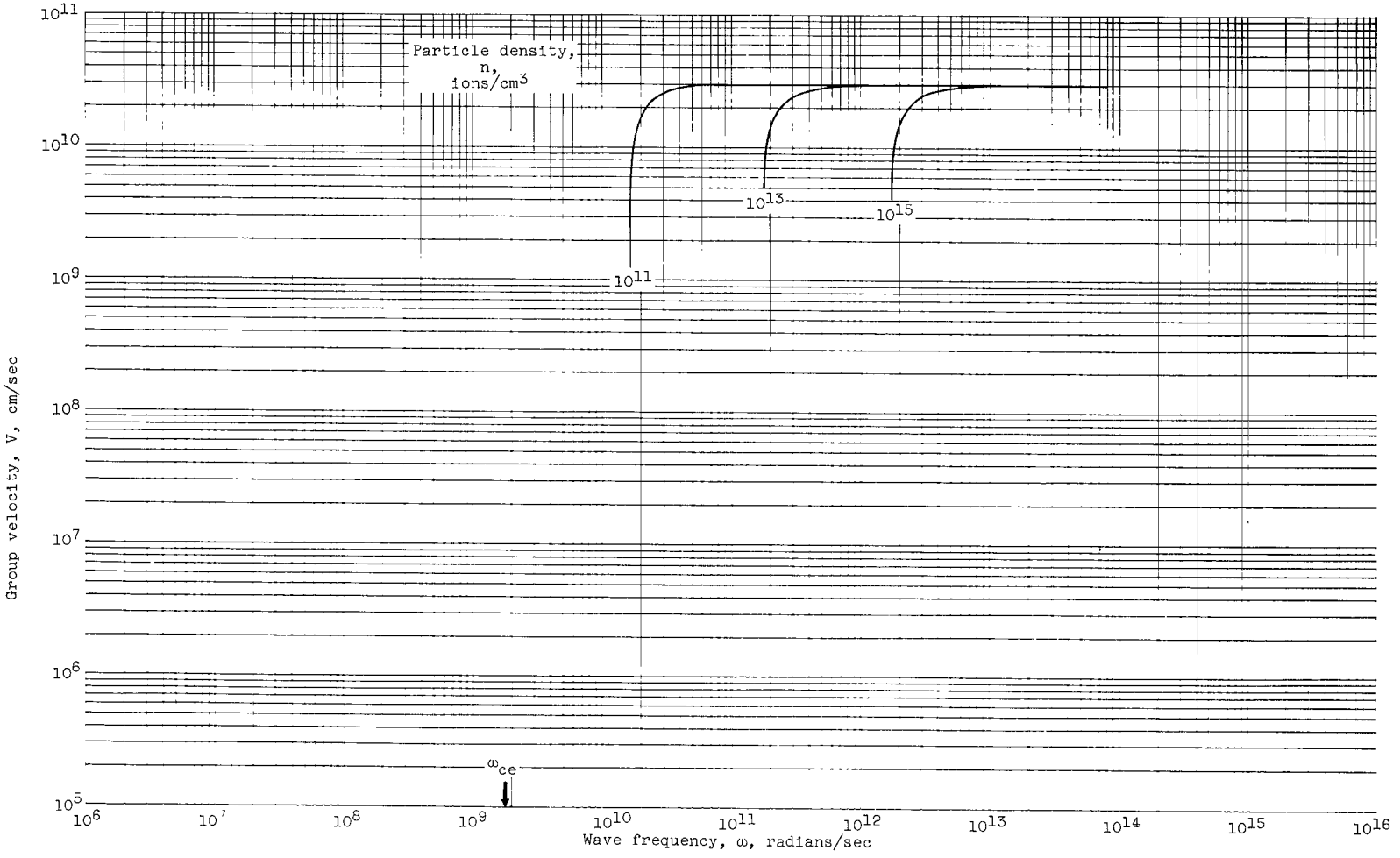

(a-1) Magnetic-field strength, 10^2 gauss.

(a) L mode; wave propagation angle, 0°.

Figure 12. - Group velocity as function of frequency. Astrom's model.

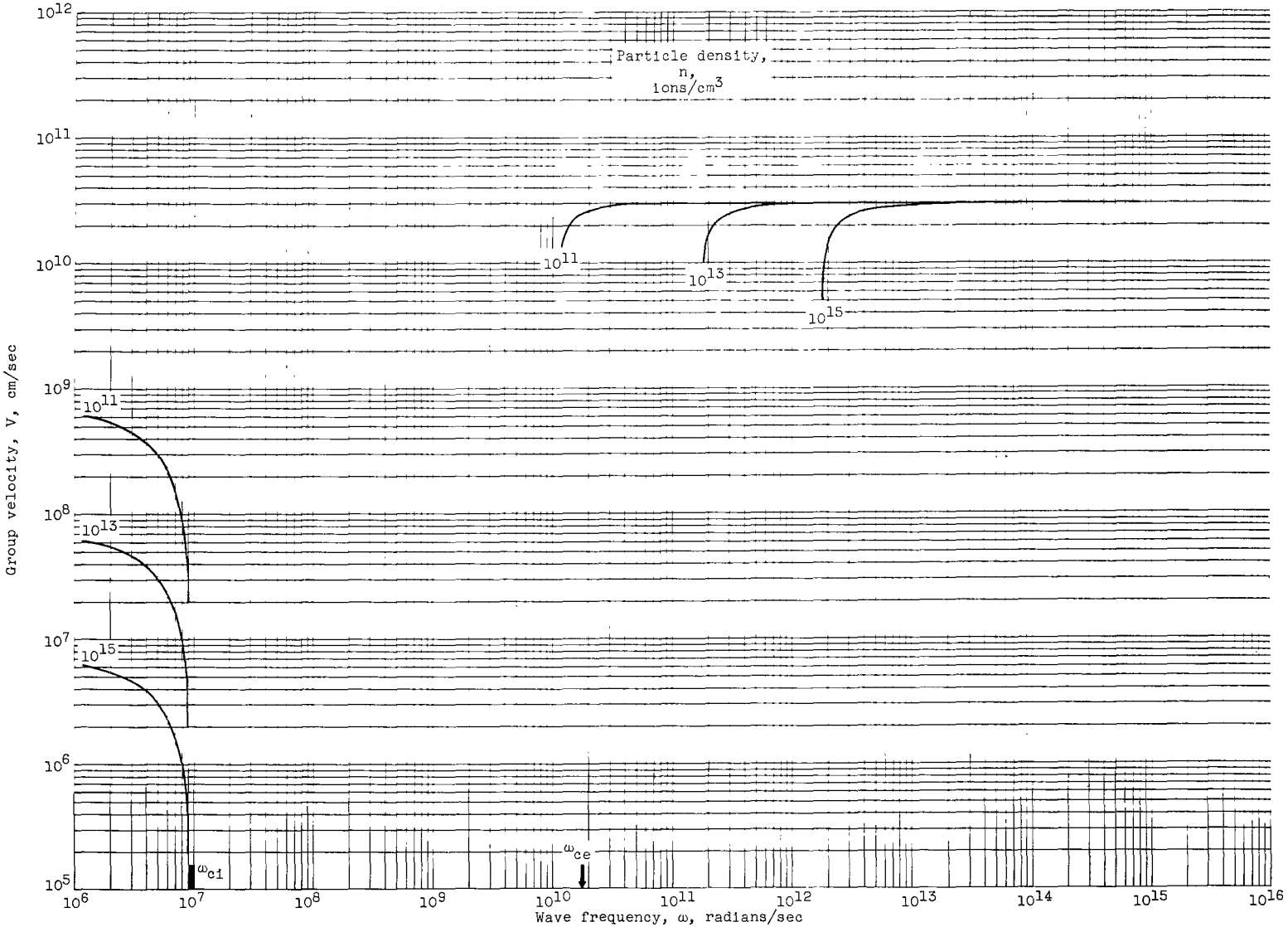

(a-2) Magnetic-field strength, 10^3 gauss.

(a) Continued. L mode; wave propagation angle, 0^o.

Figure 12. - Continued. Group velocity as function of frequency. Astrom's model.

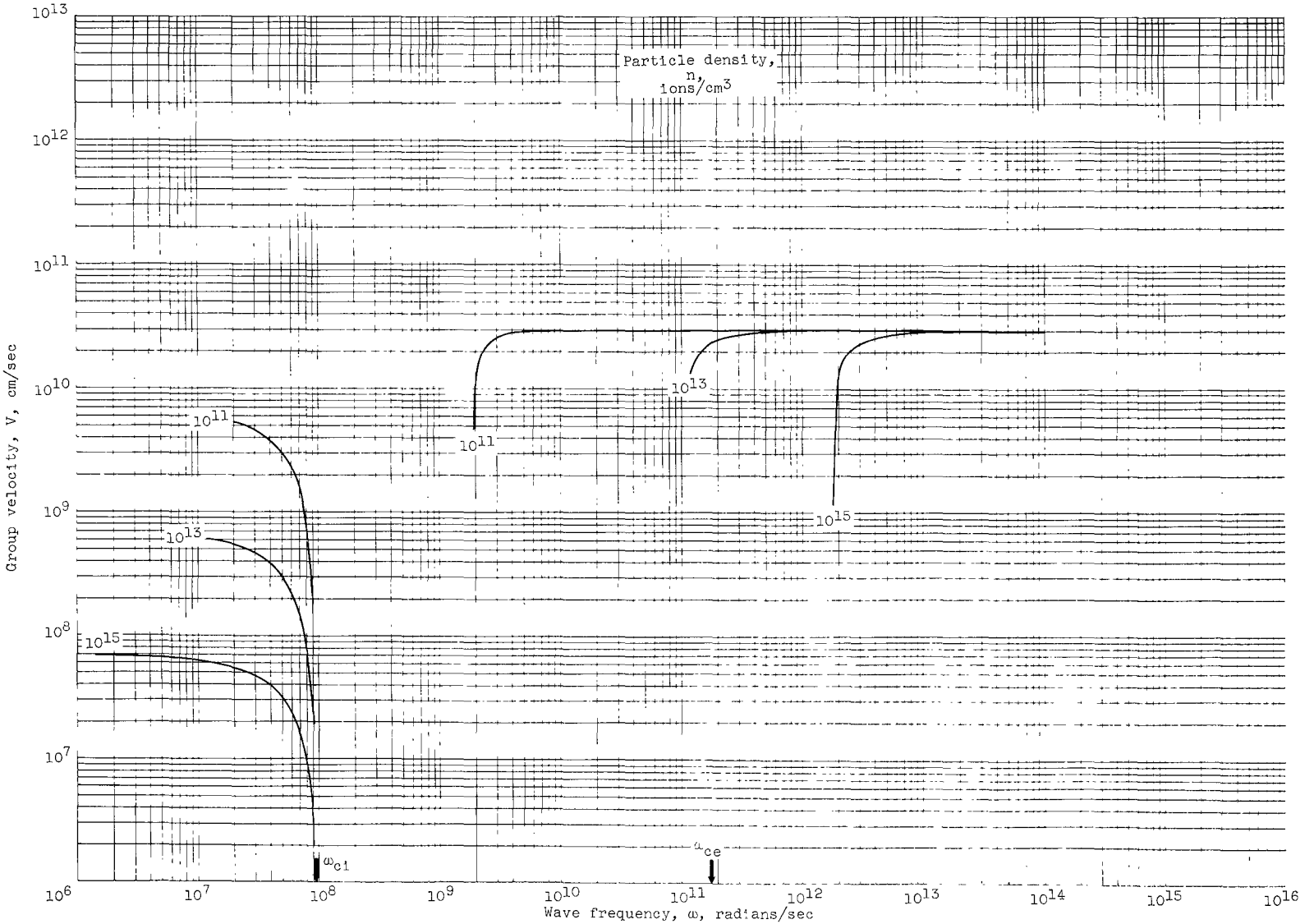

(a-3) Magnetic-field strength, 10^4 gauss.

(a) Continued. L mode; wave propagation angle, 0^o.

Figure 12. - Continued. Group velocity as function of frequency. Astrom's model.

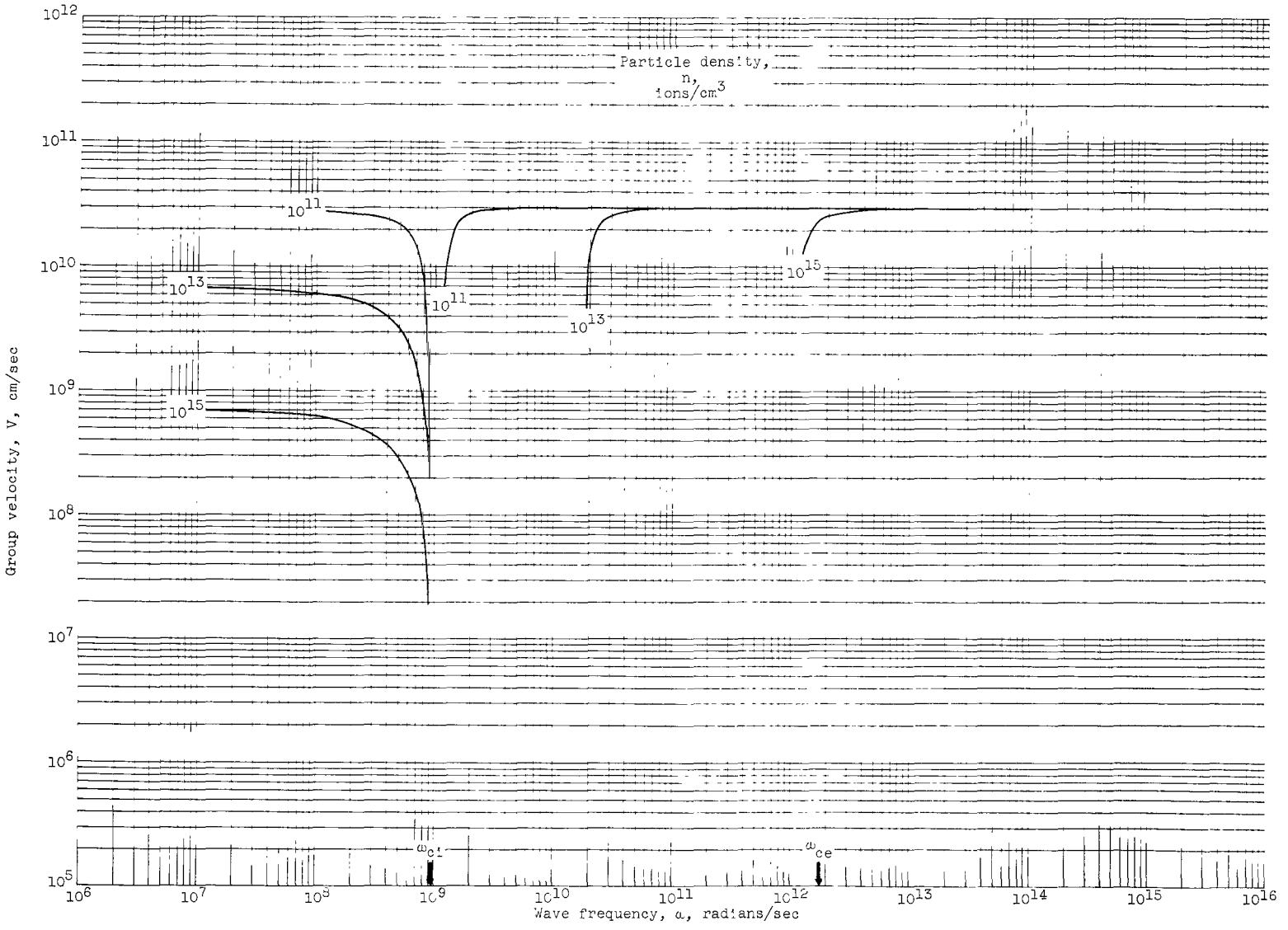

(a-4) Magnetic-field strength, 10^5 gauss.

(a) Concluded. L mode; wave propagation angle, 0^o.

Figure 12. - Continued. Group velocity as function of frequency. Astrom's model.

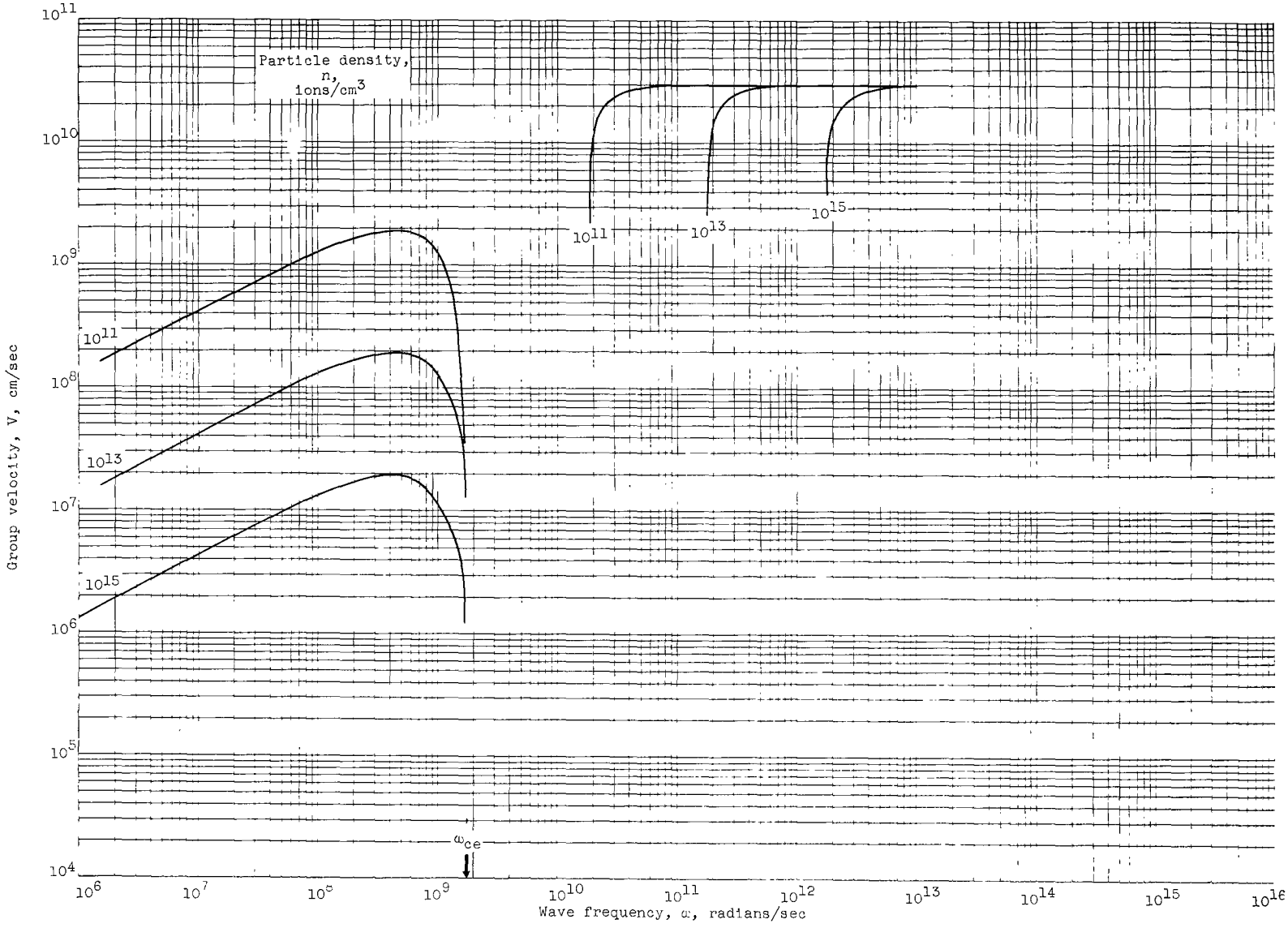

(b-1) Magnetic-field strength, 10^2 gauss.

(b) R mode; wave propagation angle, 0°.

Figure 12. - Continued. Group velocity as function of frequency. Astrom's model.

(b-2) Magnetic-field strength, 10^3 gauss.

(b) Continued. R mode; wave propagation angle, 0^o.

Figure 12. - Continued. Group velocity as function of frequency. Astrom's model.

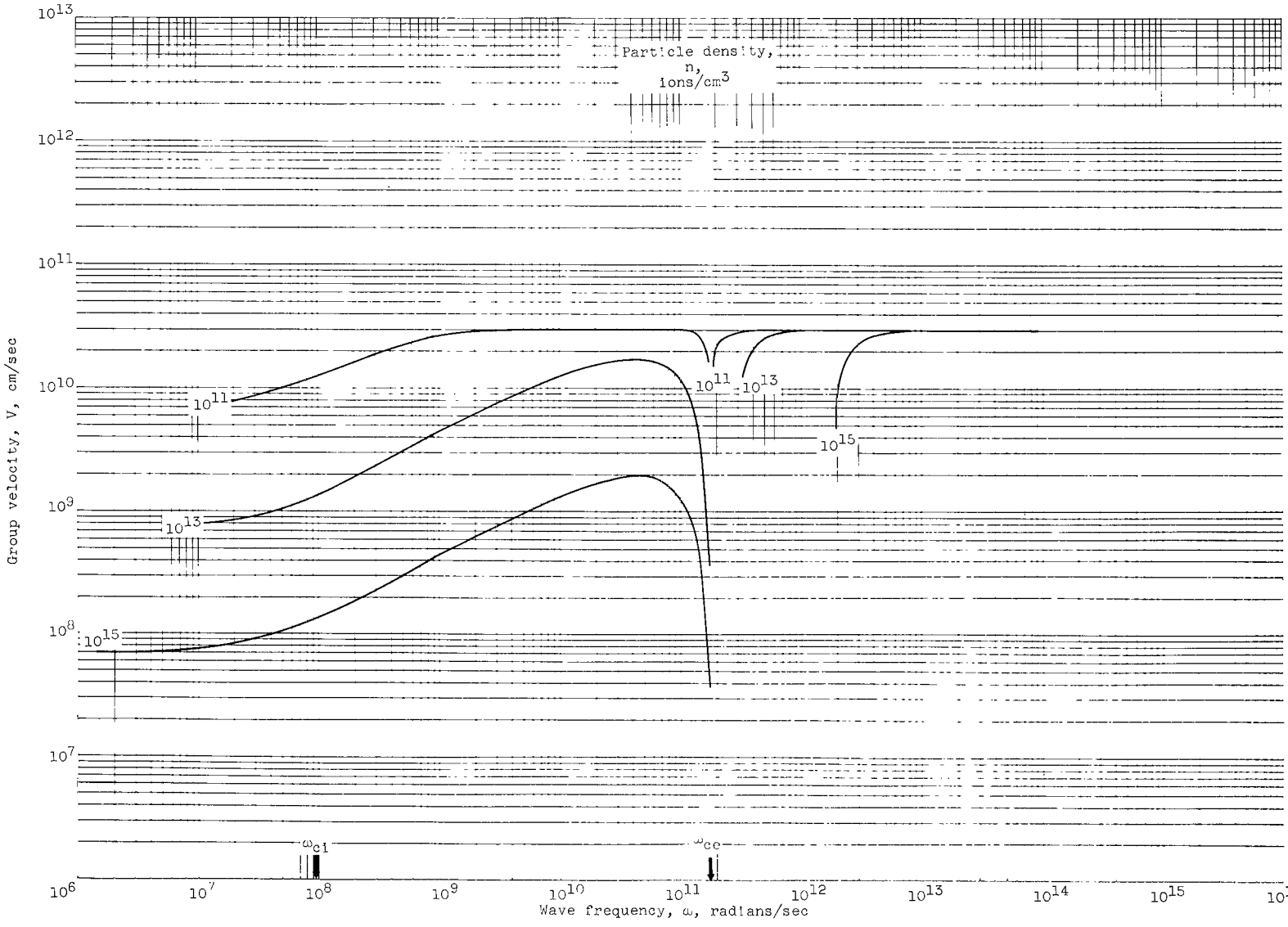

(b-3) Magnetic-field strength, 10^4 gauss.

(b) Continued. R mode; wave propagation angle, 0^o.

Figure 12. - Continued. Group velocity as function of frequency. Astrom's model.

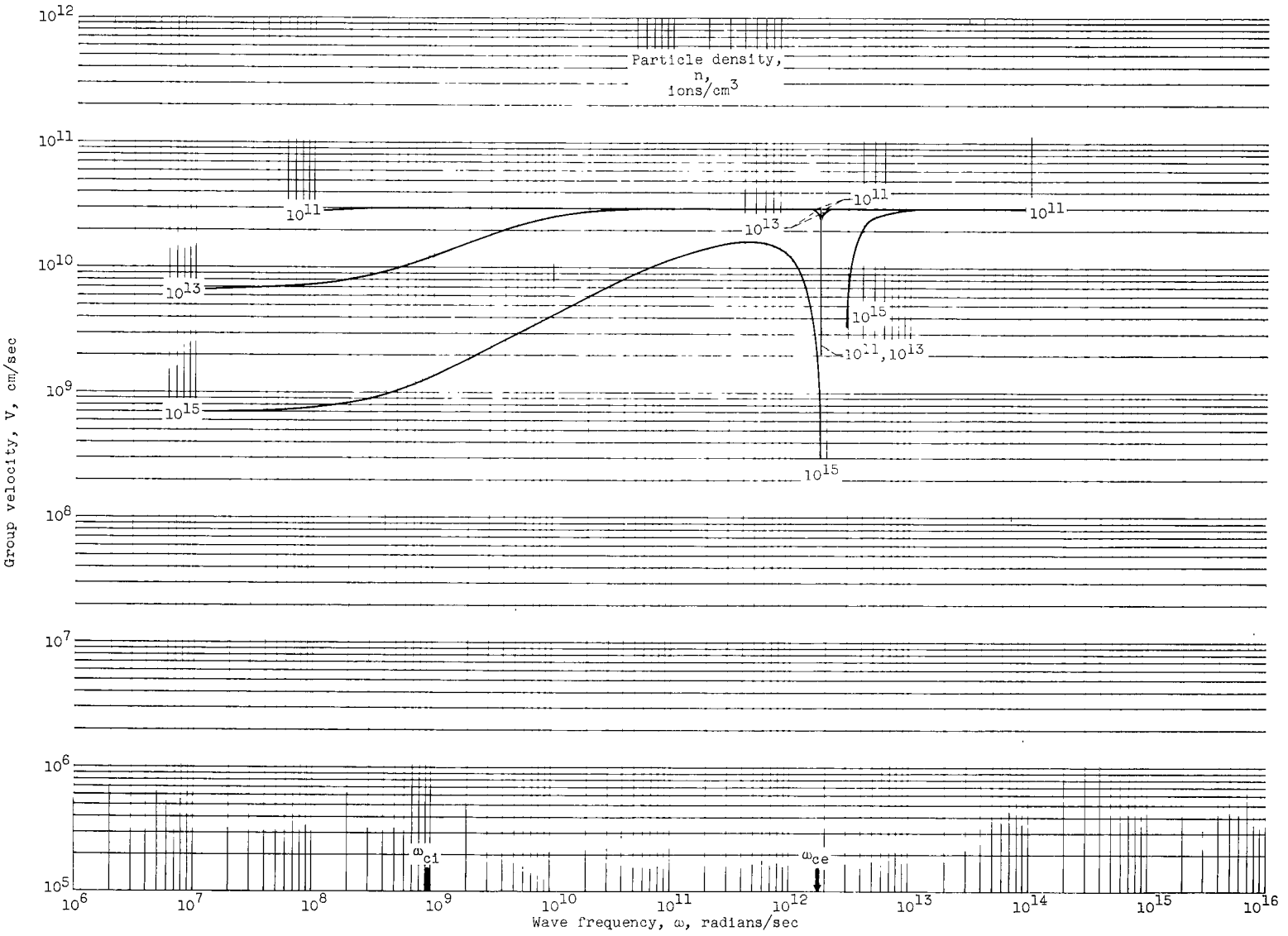

(b-4) Magnetic-field strength, 10^5 gauss.

(b) Concluded. R mode; wave propagation angle, 0°.

Figure 12. - Continued. Group velocity as function of frequency. Astrom's model.

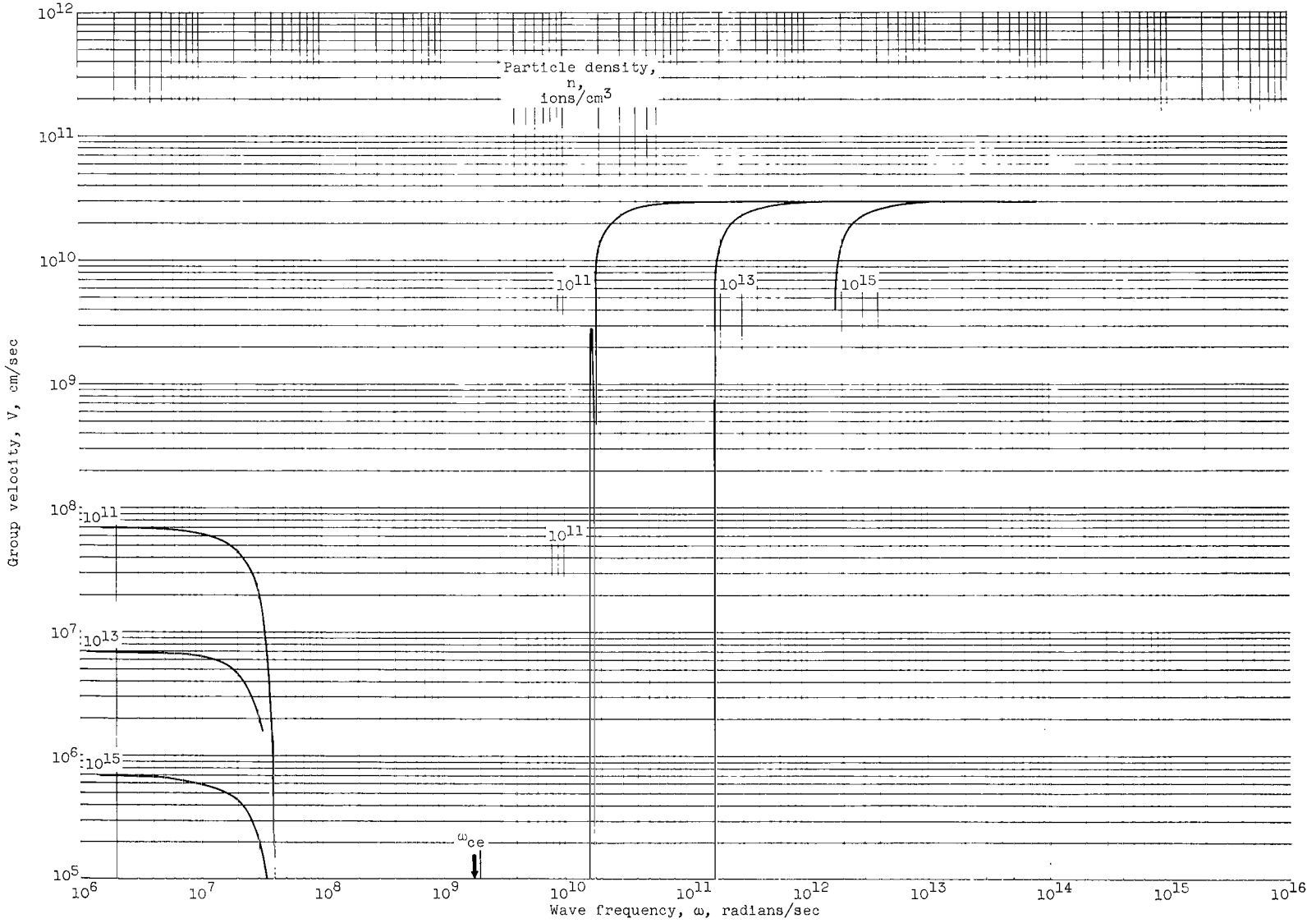

(c-1) Magnetic-field strength, 10^2 gauss.

(c) S mode; wave propagation angle, 90°.

Figure 12. - Continued. Group velocity as function of frequency. Astrom's model.

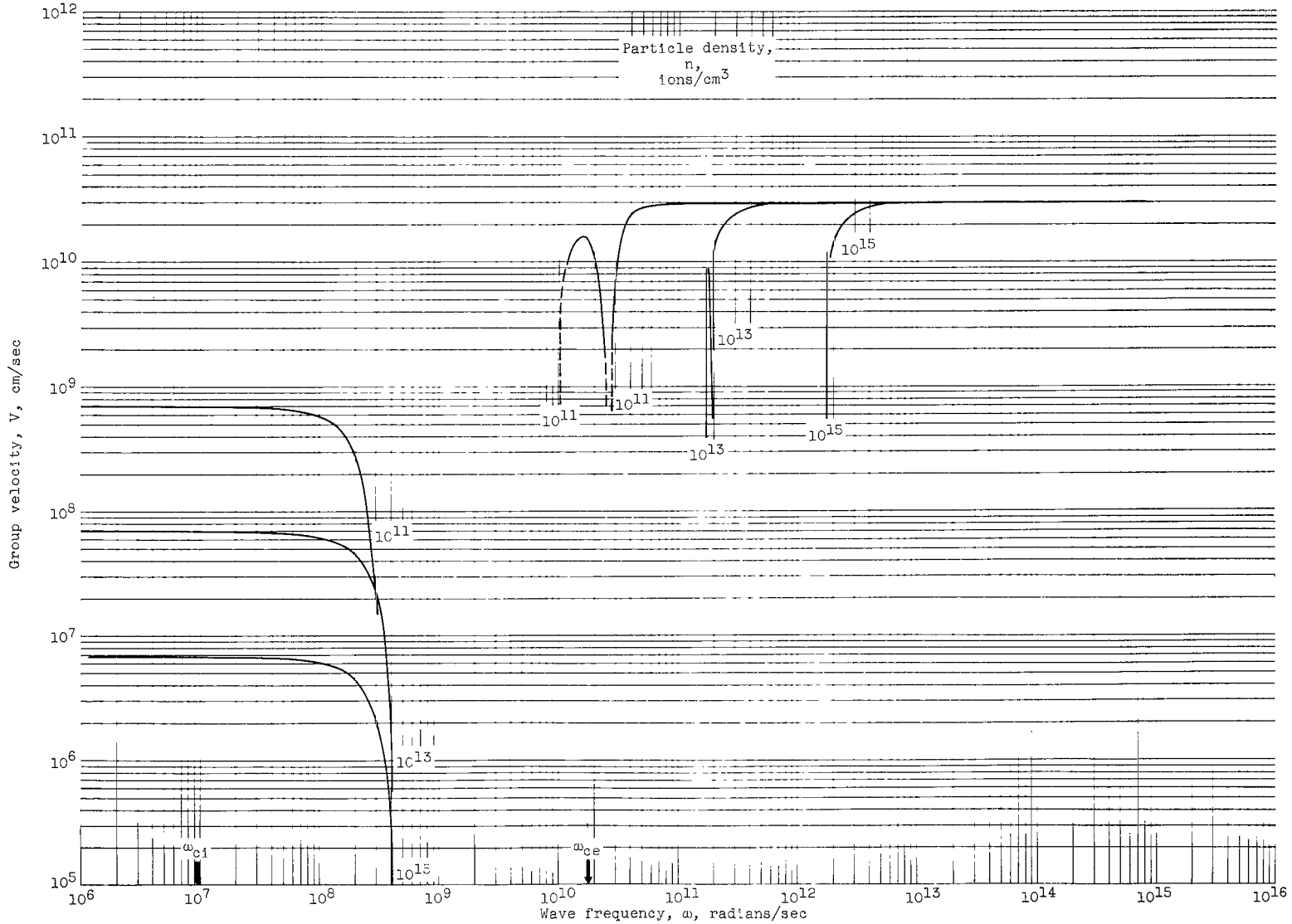

(c-2) Magnetic-field strength, 10^3 gauss.

(c) Continued. S mode; wave propagation angle, 90°.

Figure 12. - Continued. Group velocity as function of frequency. Astrom's model.

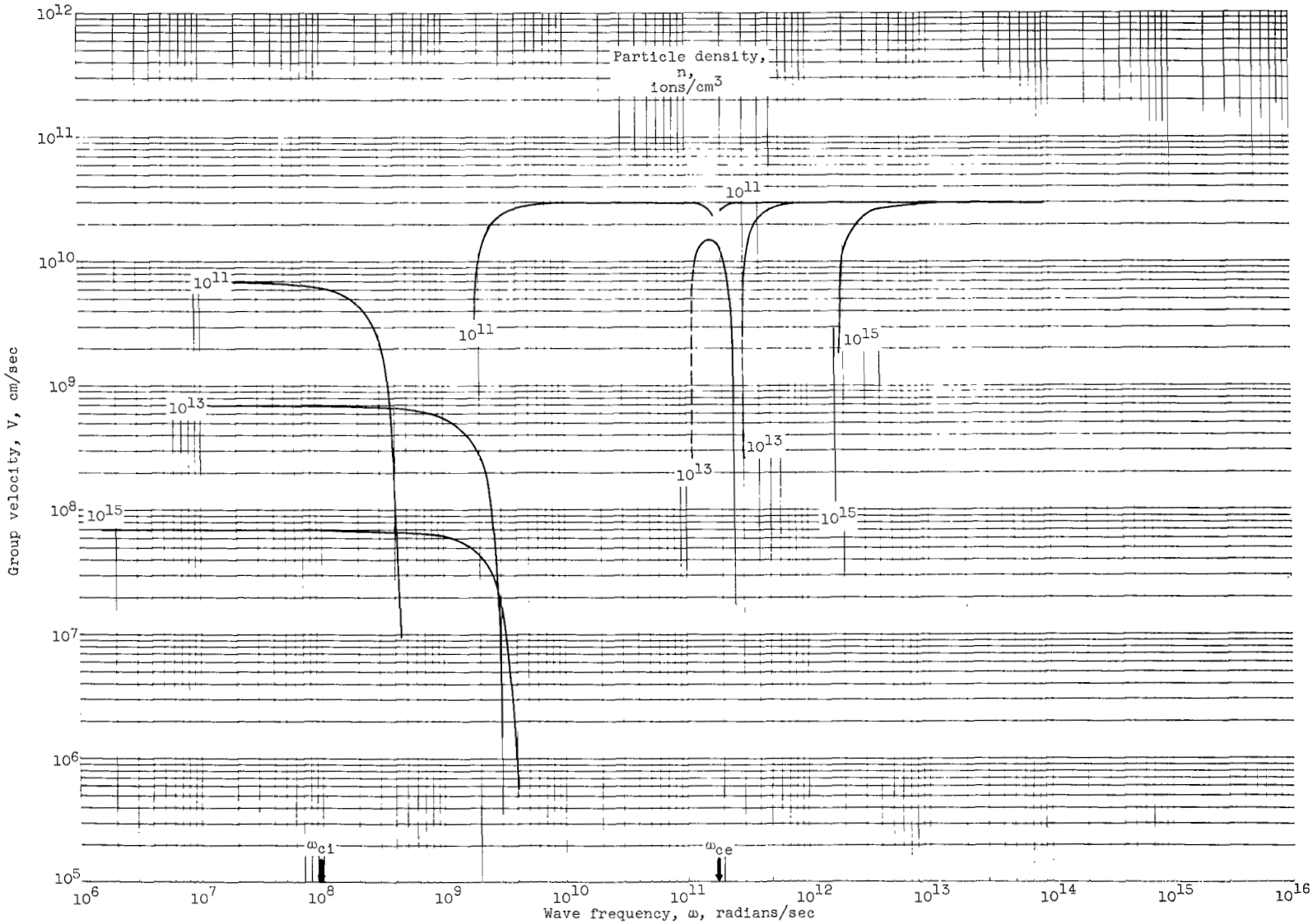

(c-3) Magnetic-field strength, 10^4 gauss.

(c) Continued. S mode; wave propagation angle, 90°.

Figure 12. - Continued. Group velocity as function of frequency. Astrom's model.

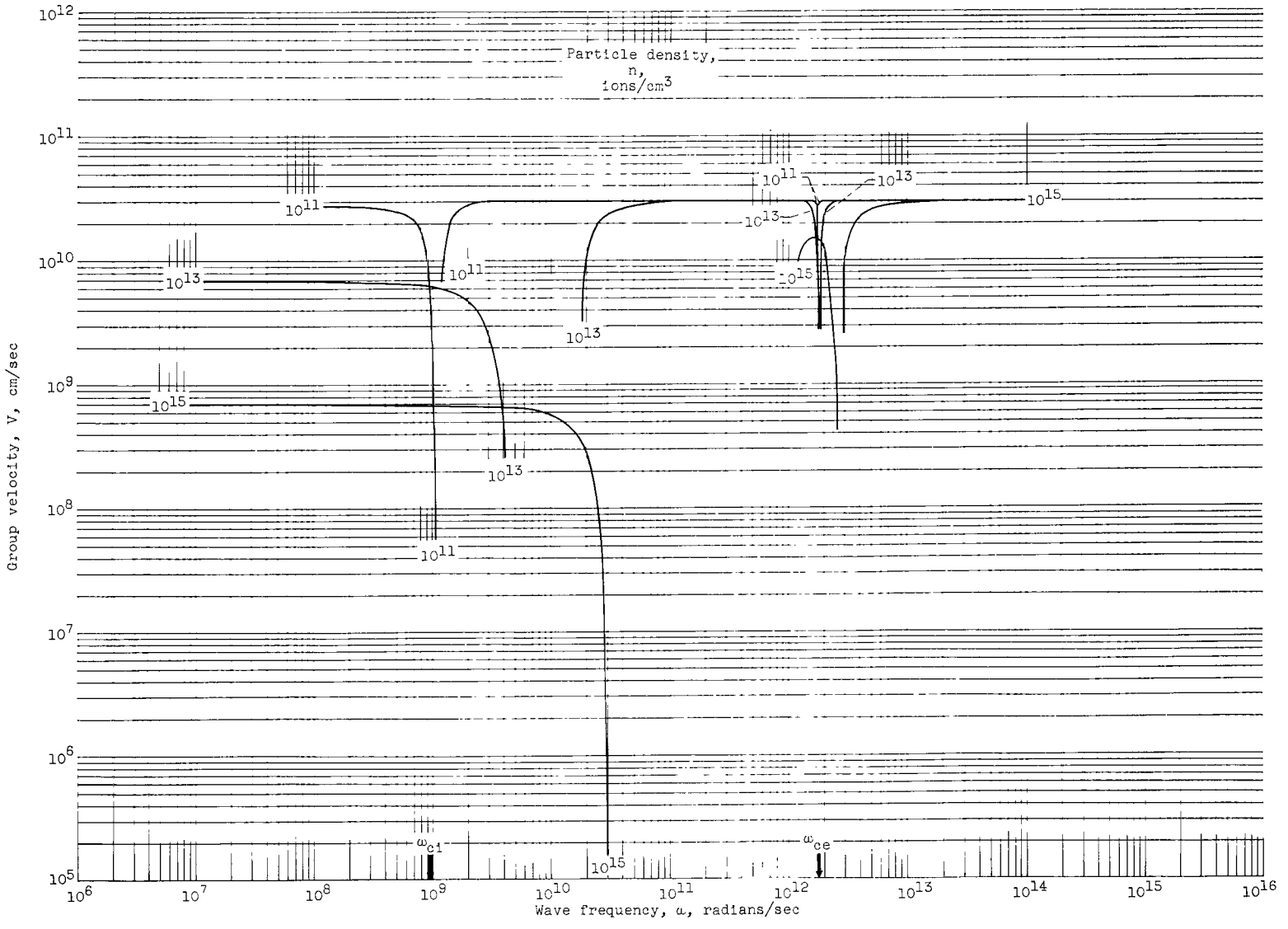

(c-4) Magnetic-field strength, 10^5 gauss.

(c) Concluded. S mode; wave propagation angle, 90°.

Figure 12. - Concluded. Group velocity as function of frequency. Astrom's model.

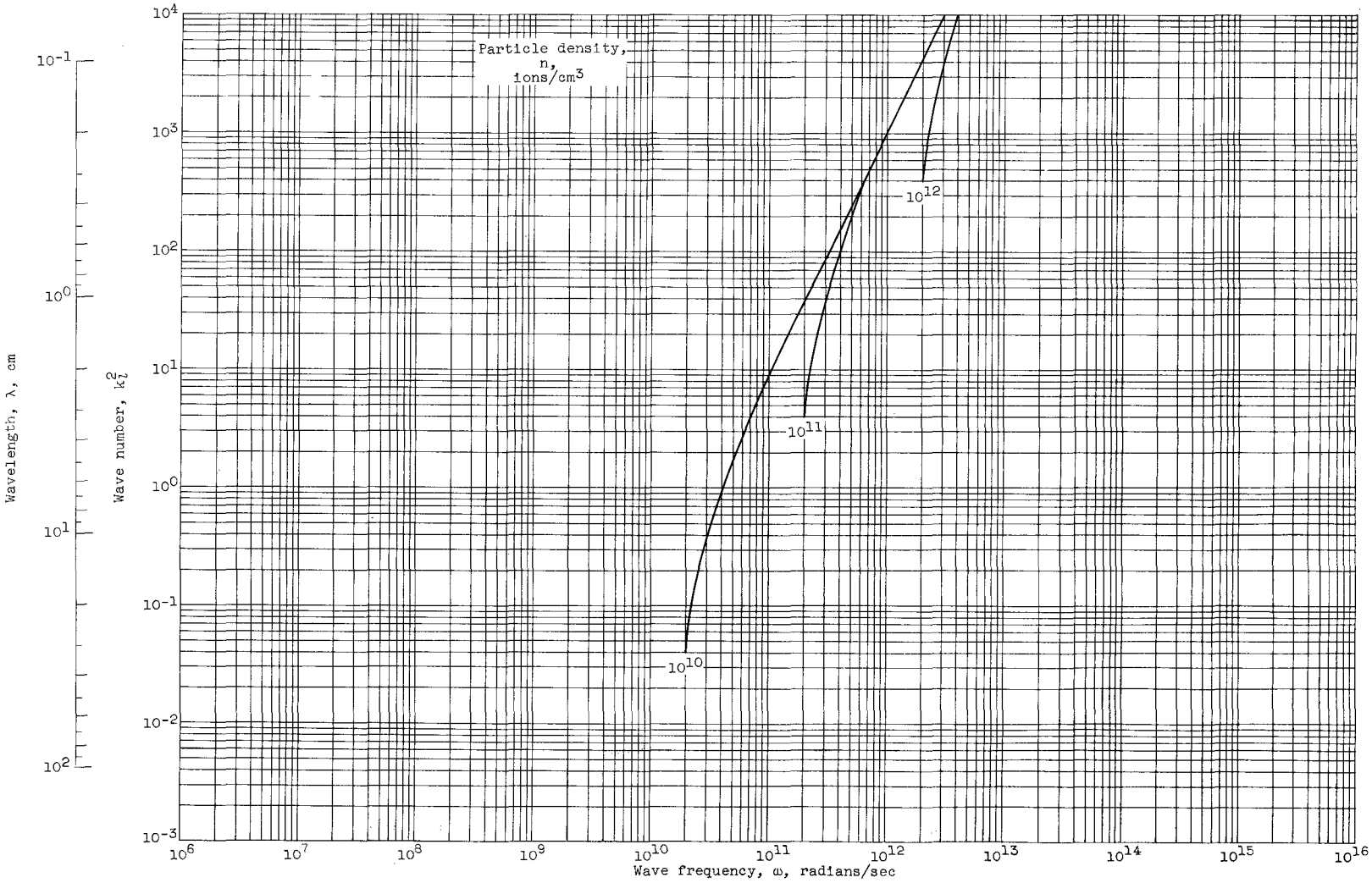

(a-1) Magnetic-field strength, 10^2 gauss.

(a) L mode; wave propagation angle, 0°.

Figure 13. - Wave number as function of frequency. Wave propagation angles, 0° and 90°; simplified Ohm's law approximation.

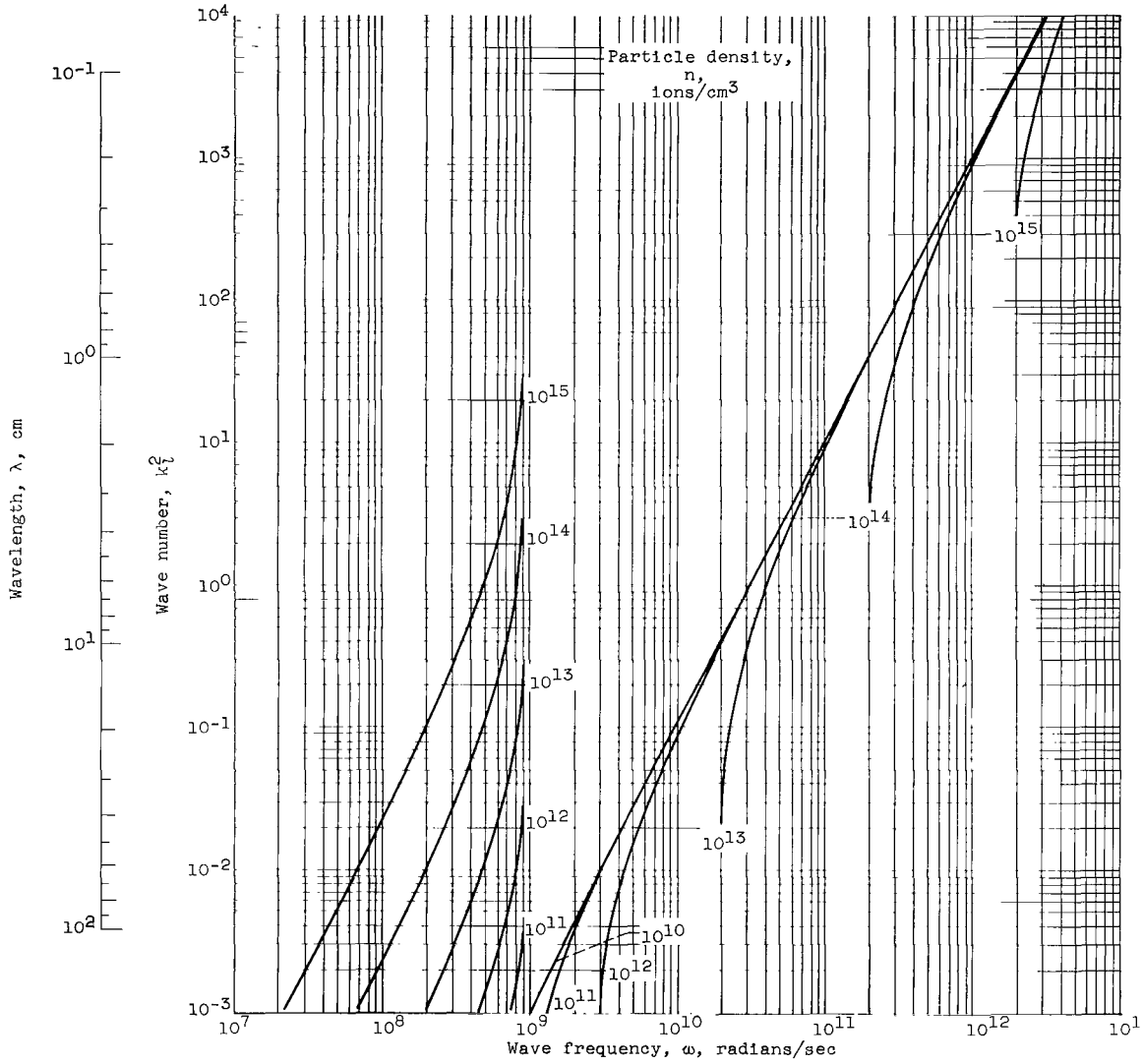

(a-2) Magnetic-field strength, 10^5 gauss.

(a) Concluded. L mode; wave propagation angle, 0°.

Figure 13. - Continued. Wave number as function of frequency. Wave propagation angles, 0° and 90°; simplified Ohm's law approximation.

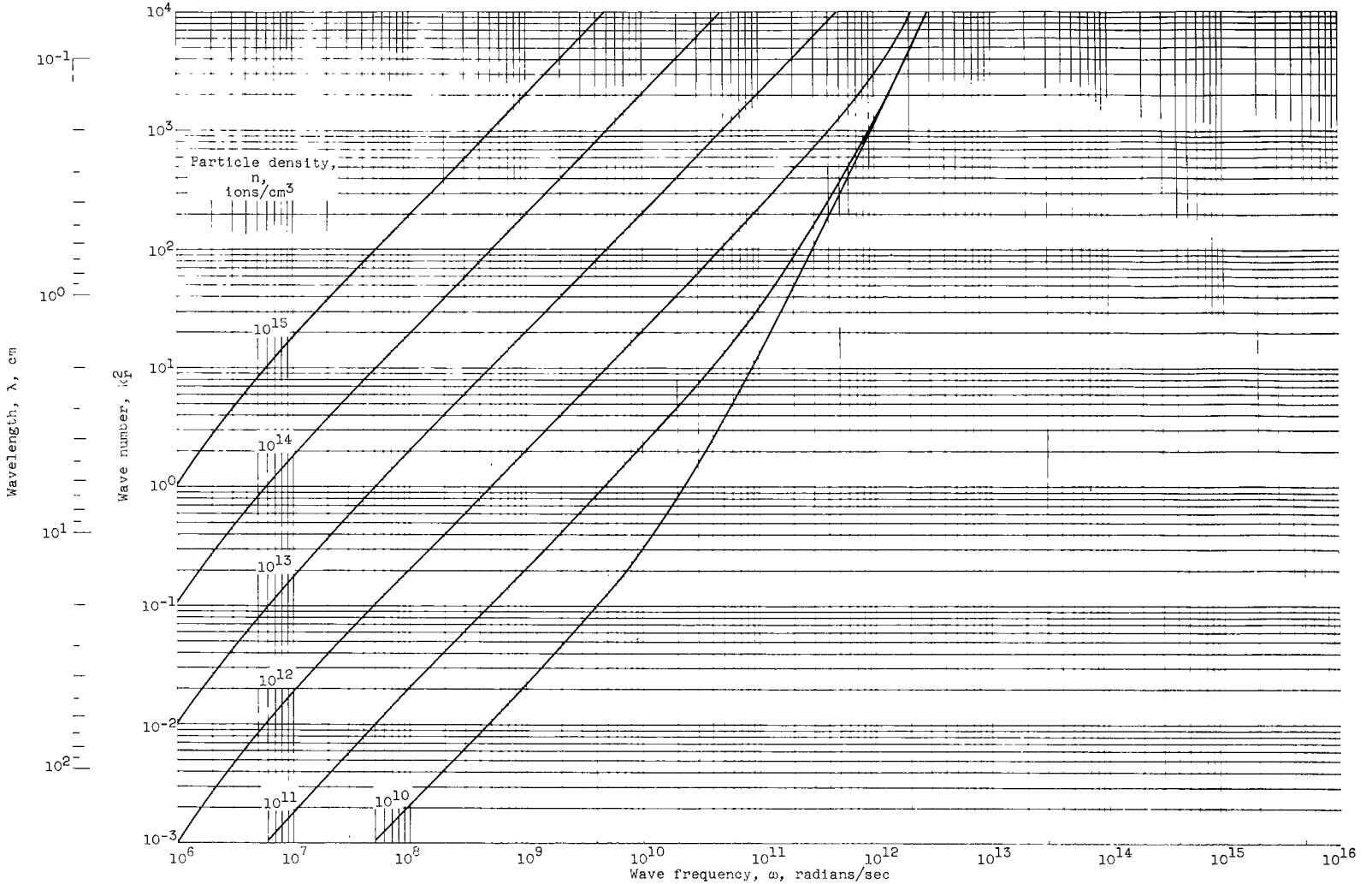

(b-1) Magnetic-field strength, 10^2 gauss.

(b) R mode; wave propagation angle, 0°.

Figure 13. - Continued. Wave number as function of frequency. Wave propagation angles, 0° and 90°; simplified Ohm's law approximation.

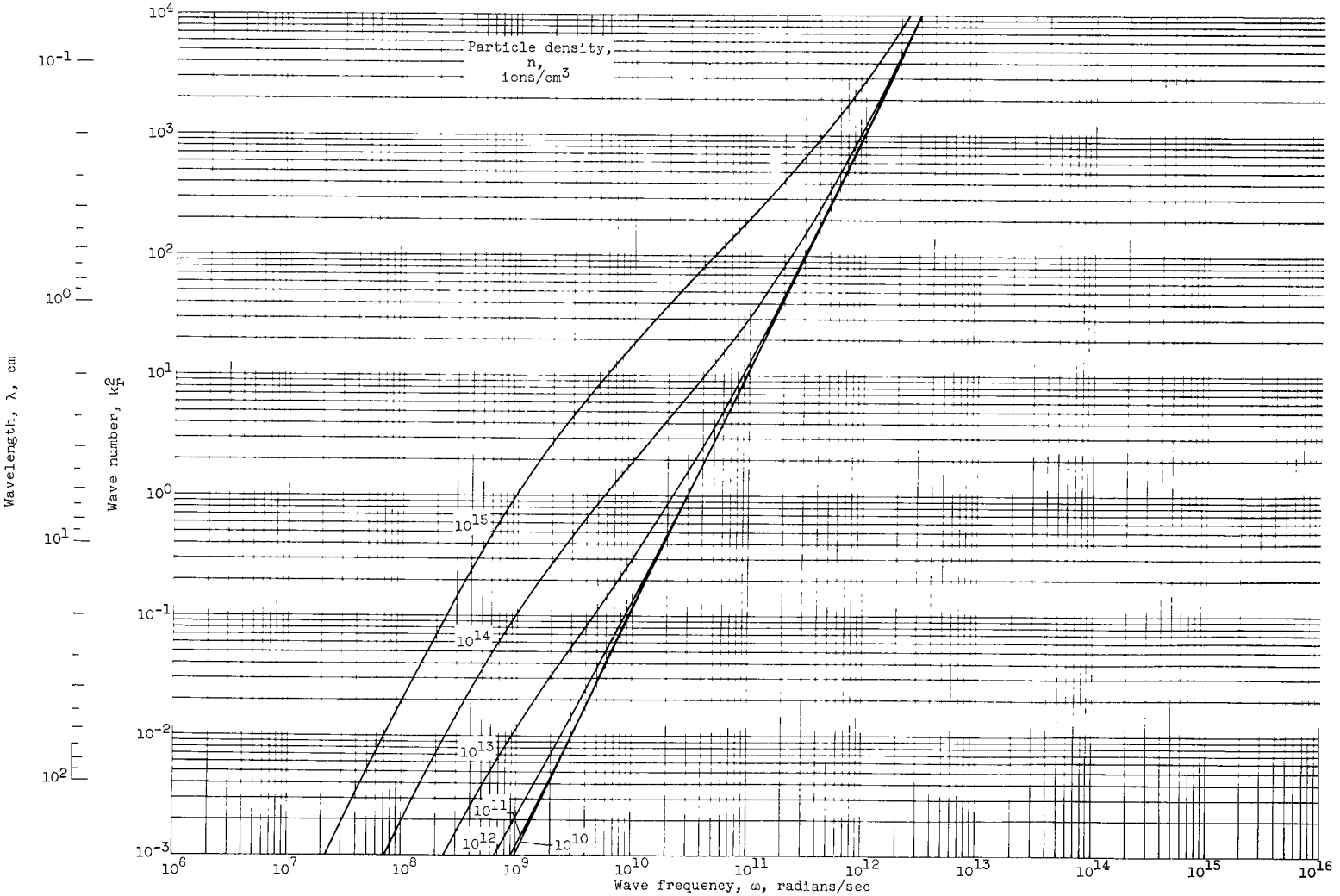

(b-2) Magnetic-field strength, 10^5 gauss.

(b) Concluded. R mode; wave propagation angle, 0°.

Figure 13. - Continued. Wave number as function of frequency. Wave propagation angles, 0° and 90°; simplified Ohm's law approximation.

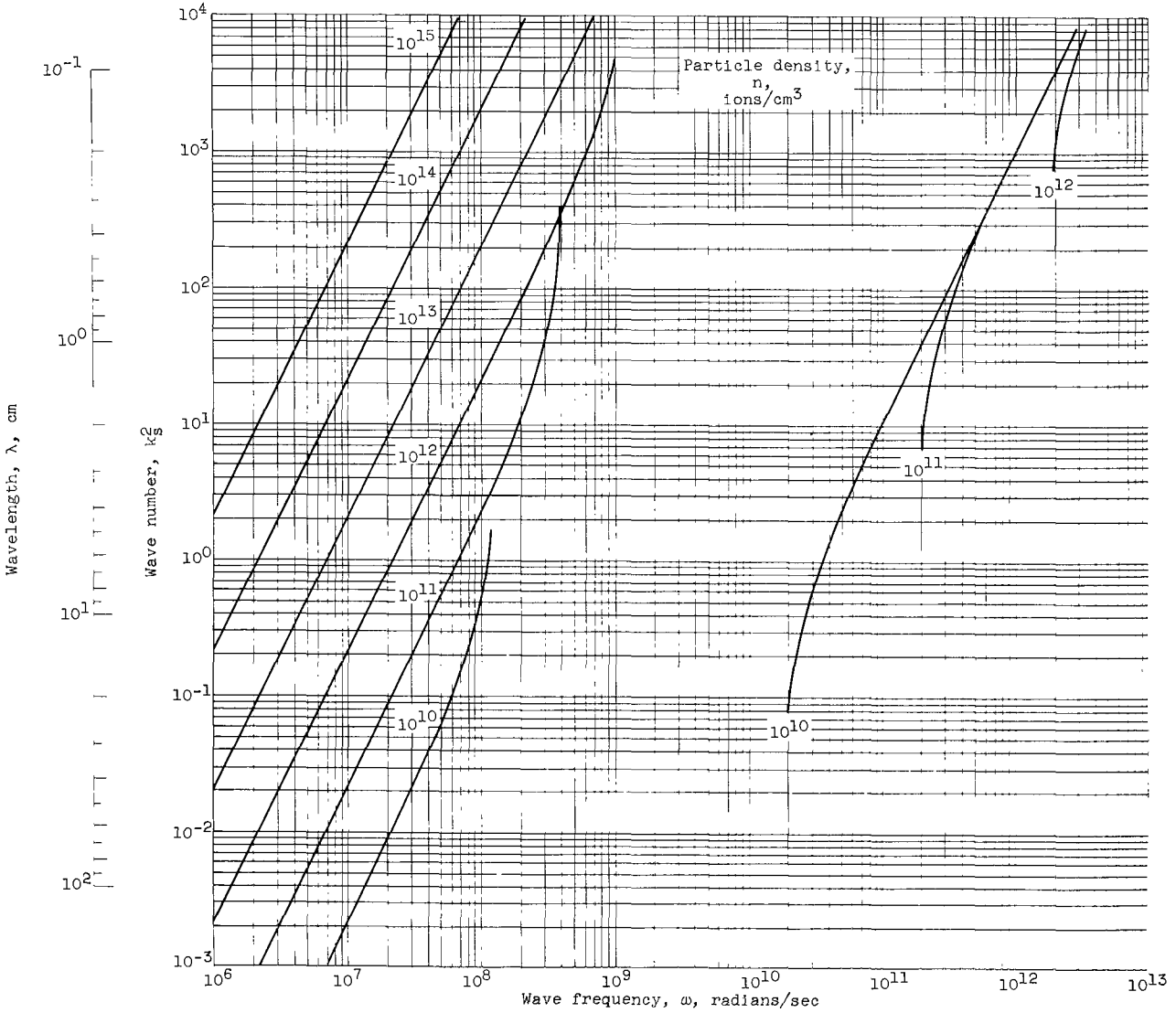

(c-1) Magnetic-field strength, 10^2 gauss.

(c) S mode; wave propagation angle, 90^o.

Figure 13. - Continued. Wave number as function of frequency. Wave propagation angles, 0^o and 90^o; simplified Ohm's law approximation.

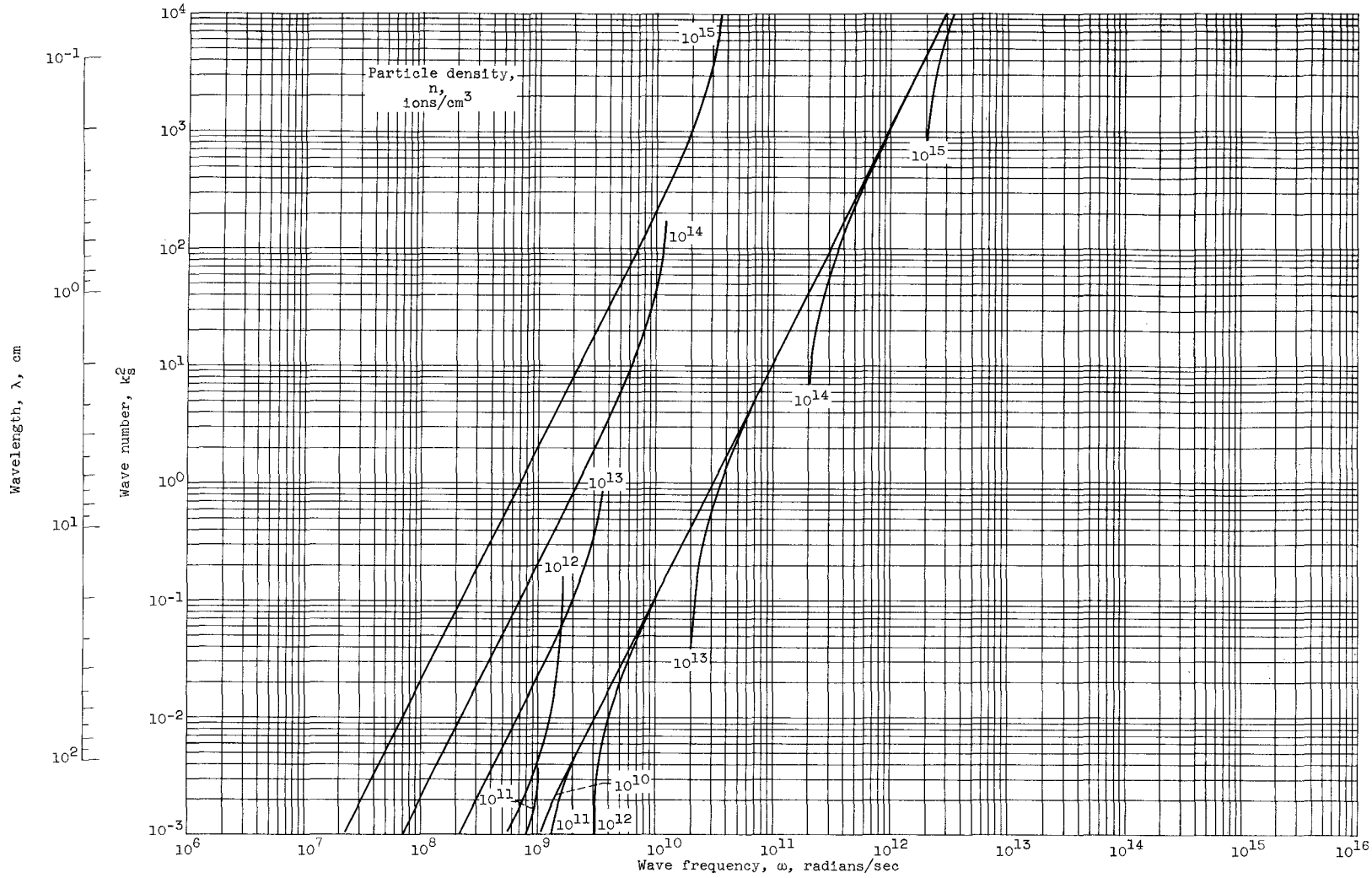

(c-2) Magnetic-field strength, 10^5 gauss.

(c) Concluded. S mode; wave propagation angle, 90°.

Figure 13. - Concluded. Wave number as function of frequency. Wave propagation angles, 0° and 90°; simplified Ohm's law approximation.

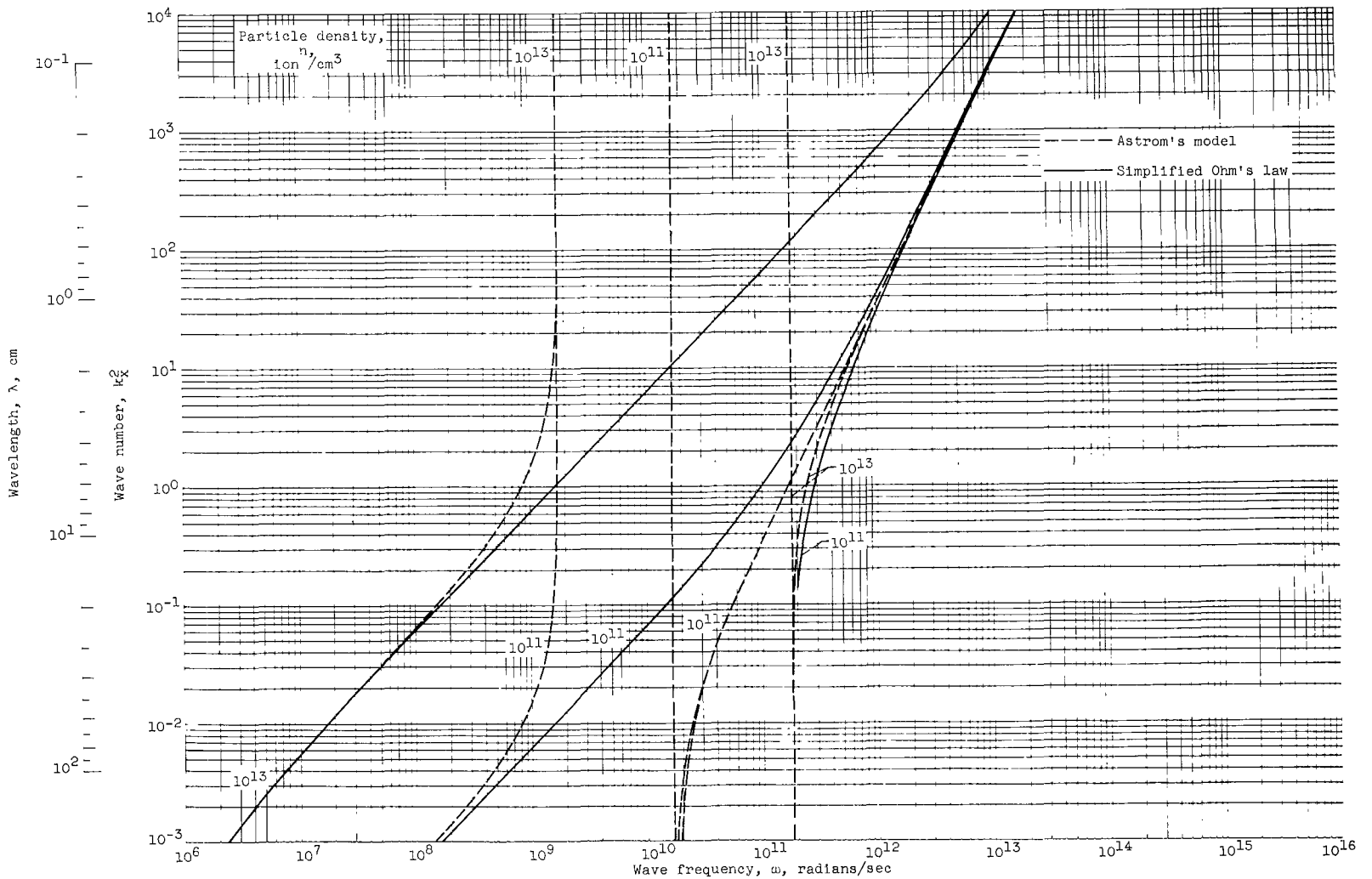

(a-1) x-component.

(a) Magnetic-field strength, 10^2 gauss.

Figure 14. - Wave number as function of frequency. Wave propagation angle, 10^0; simplified Ohm's law.

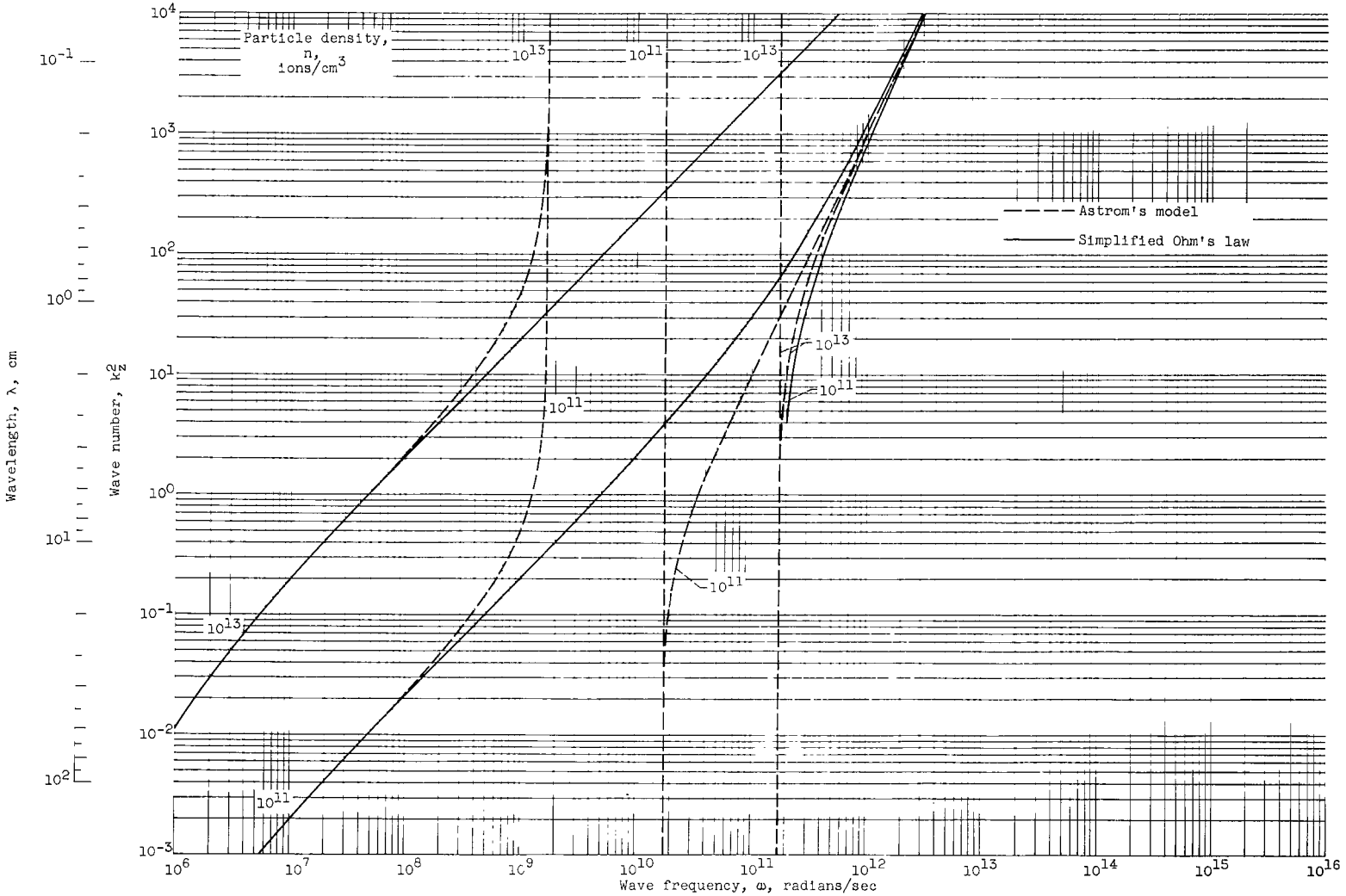

(a-2) z-component.

(a) Concluded. Magnetic-field strength, 10^2 gauss.

Figure 14. - Continued. Wave number as function of frequency. Wave propagation angle, 10^o; simplified Ohm's law.

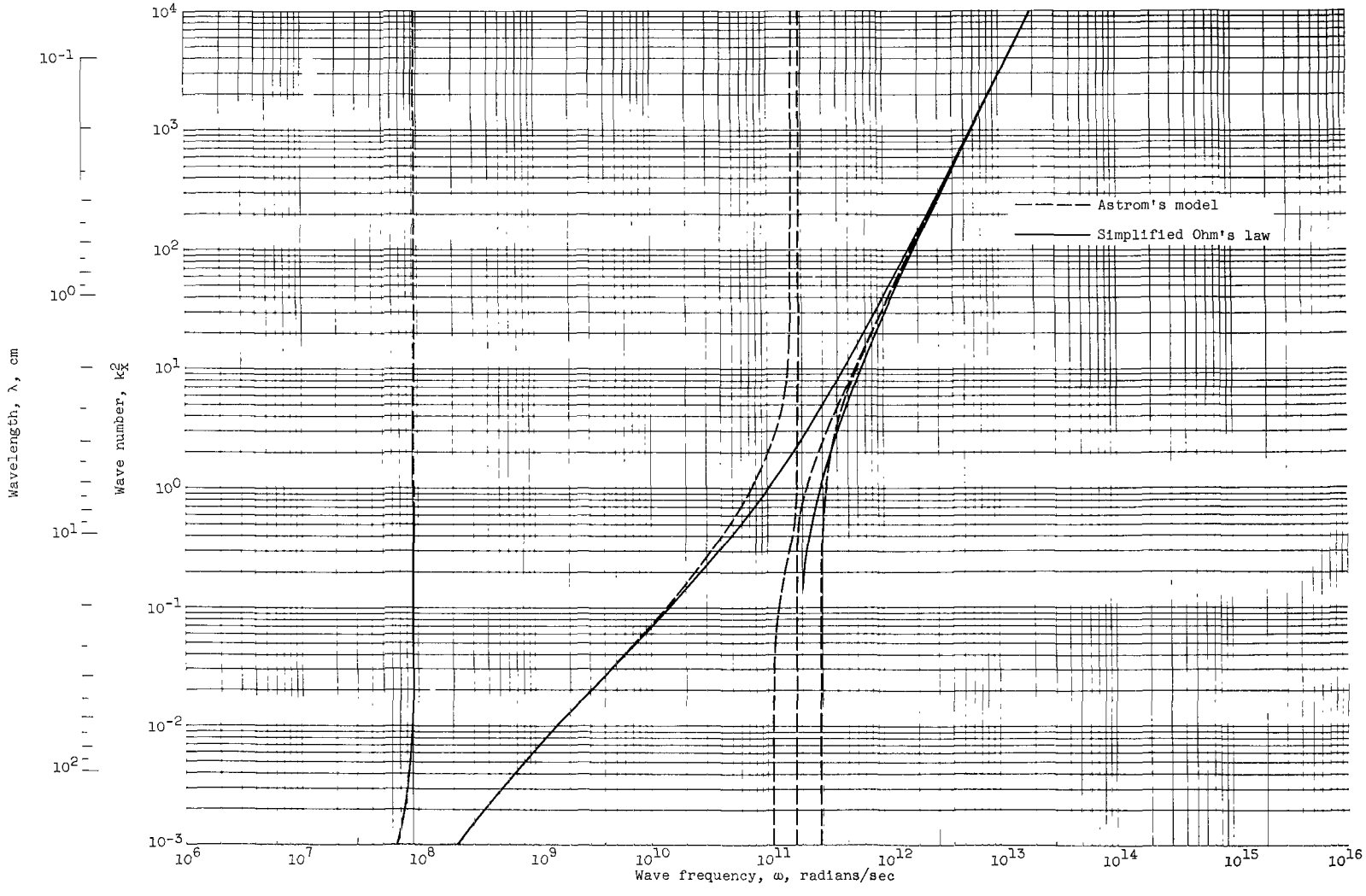

(b-1) x-component.

(b) Magnetic-field strength, 10^4 gauss; particle density, 10^{13} ions per cubic centimeter.

Figure 14. - Continued. Wave number as function of frequency. Wave propagation angle, 10^o; simplified Ohm's law.

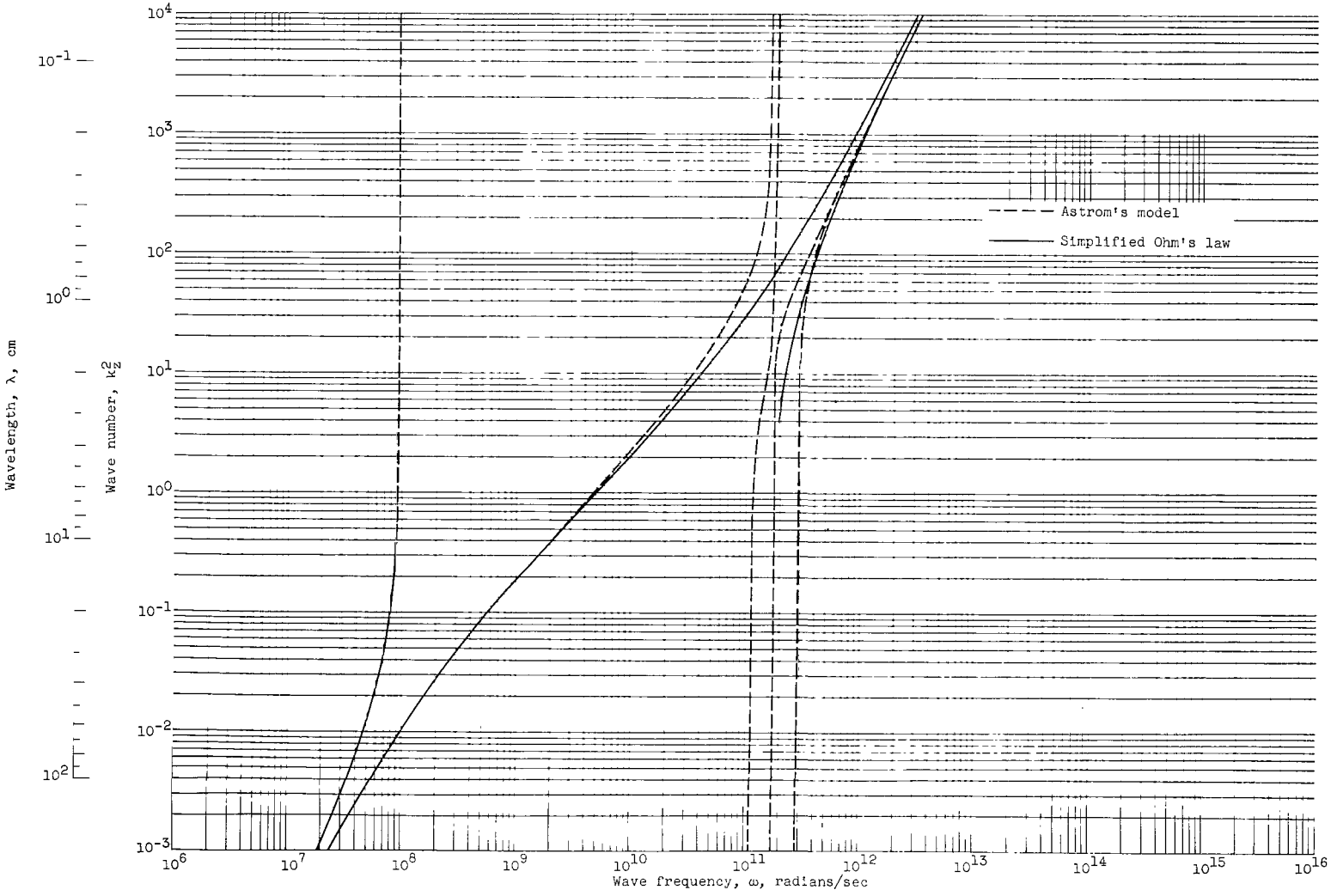

(b-2) z-component.

(b) Concluded. Magnetic-field strength, 10^4 gauss; particle density, 10^{13} ions per cubic centimeter.

Figure 14. - Concluded. Wave number as function of frequency. Wave propagation angle, 10^o; simplified Ohm's law.

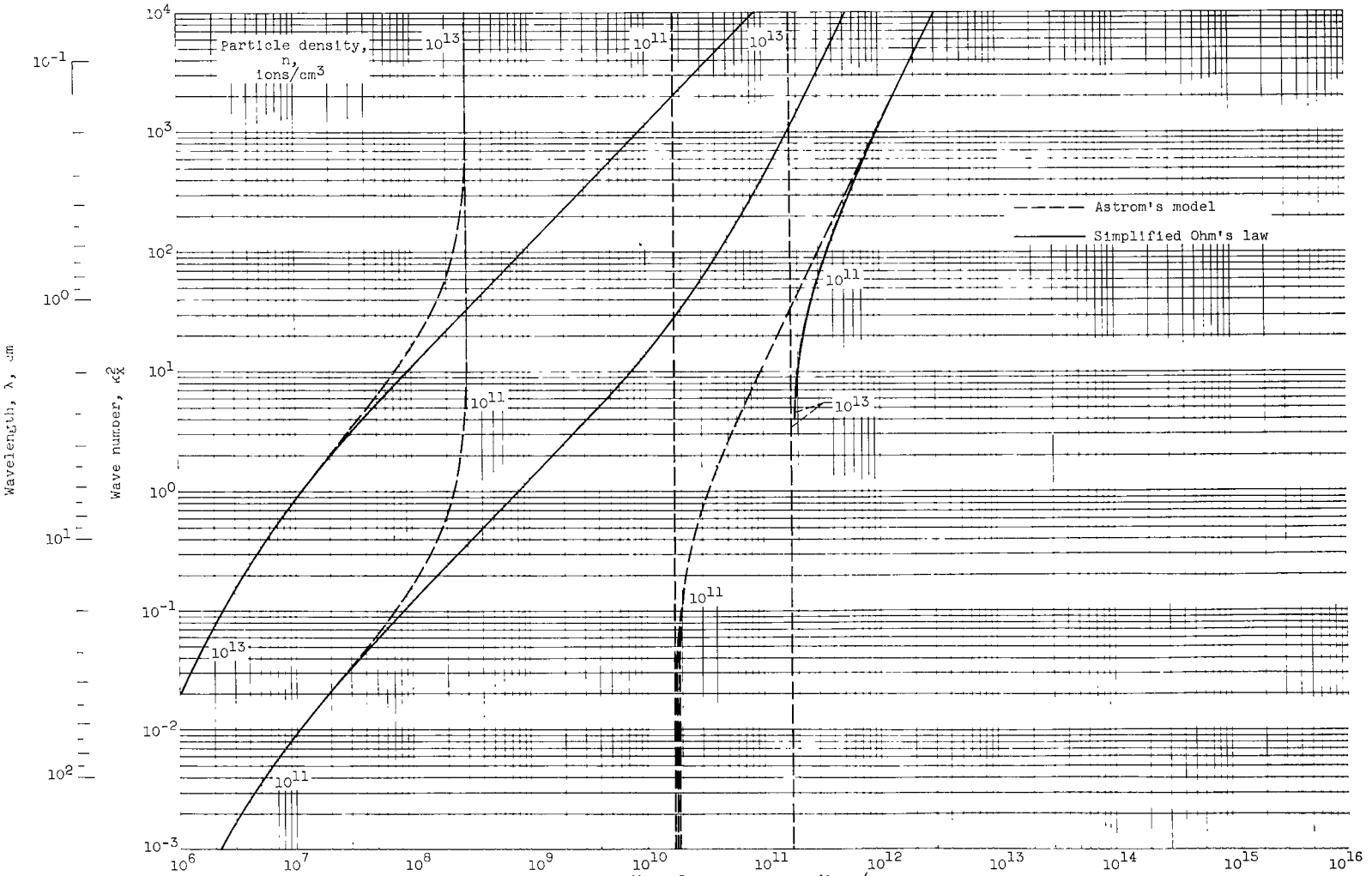

(a-1) x-component.

(a) Magnetic-field strength, 10^2 gauss.

Figure 15. - Wave number as function of frequency. Wave propagation angle, 80°; simplified Ohm's law.

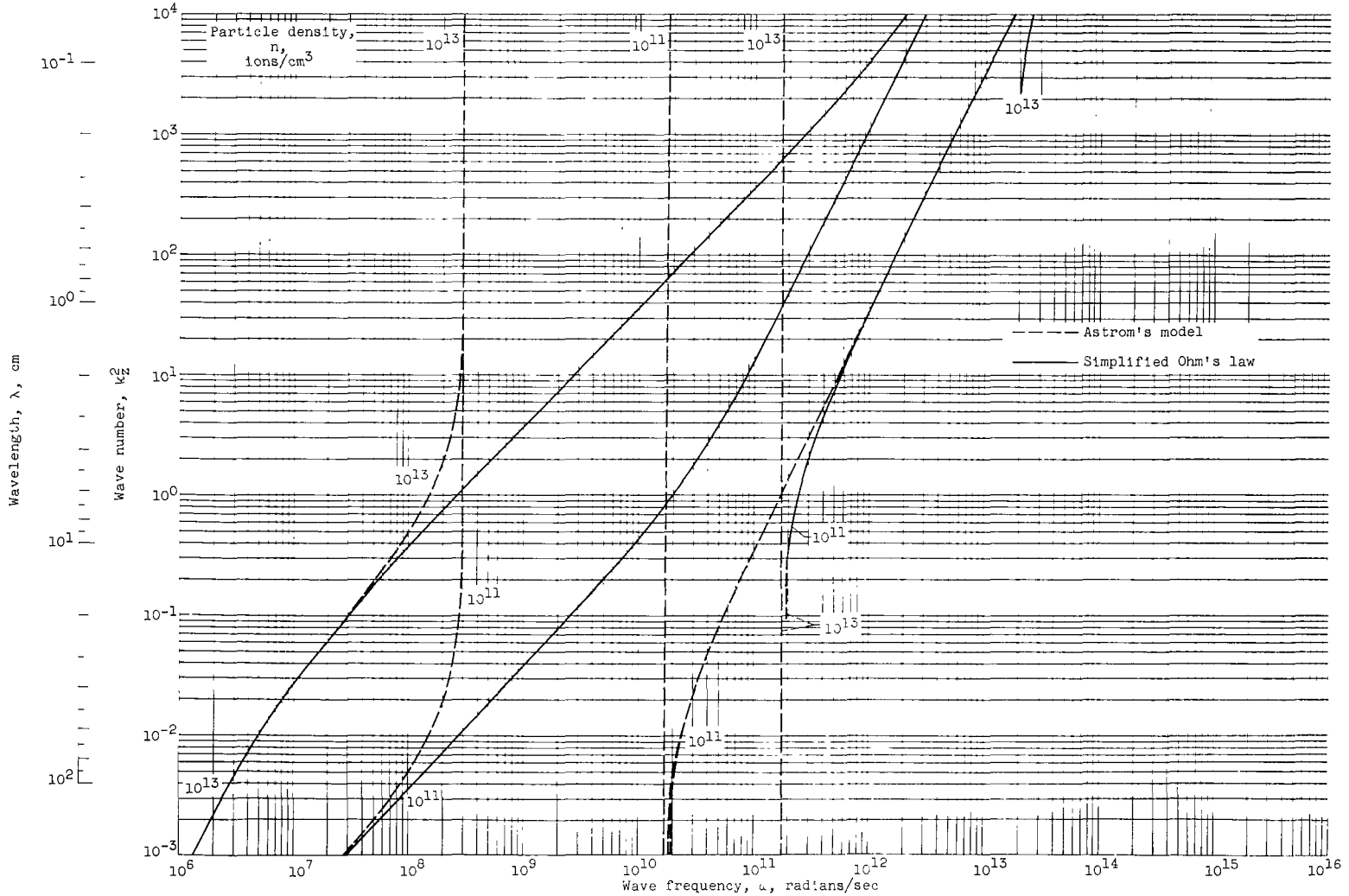

(a-2) z-component.

(a) Concluded. Magnetic-field strength, 10^2 gauss.

Figure 15. - Continued. Wave number as function of frequency. Wave propagation angle, 80°; simplified Ohm's law.

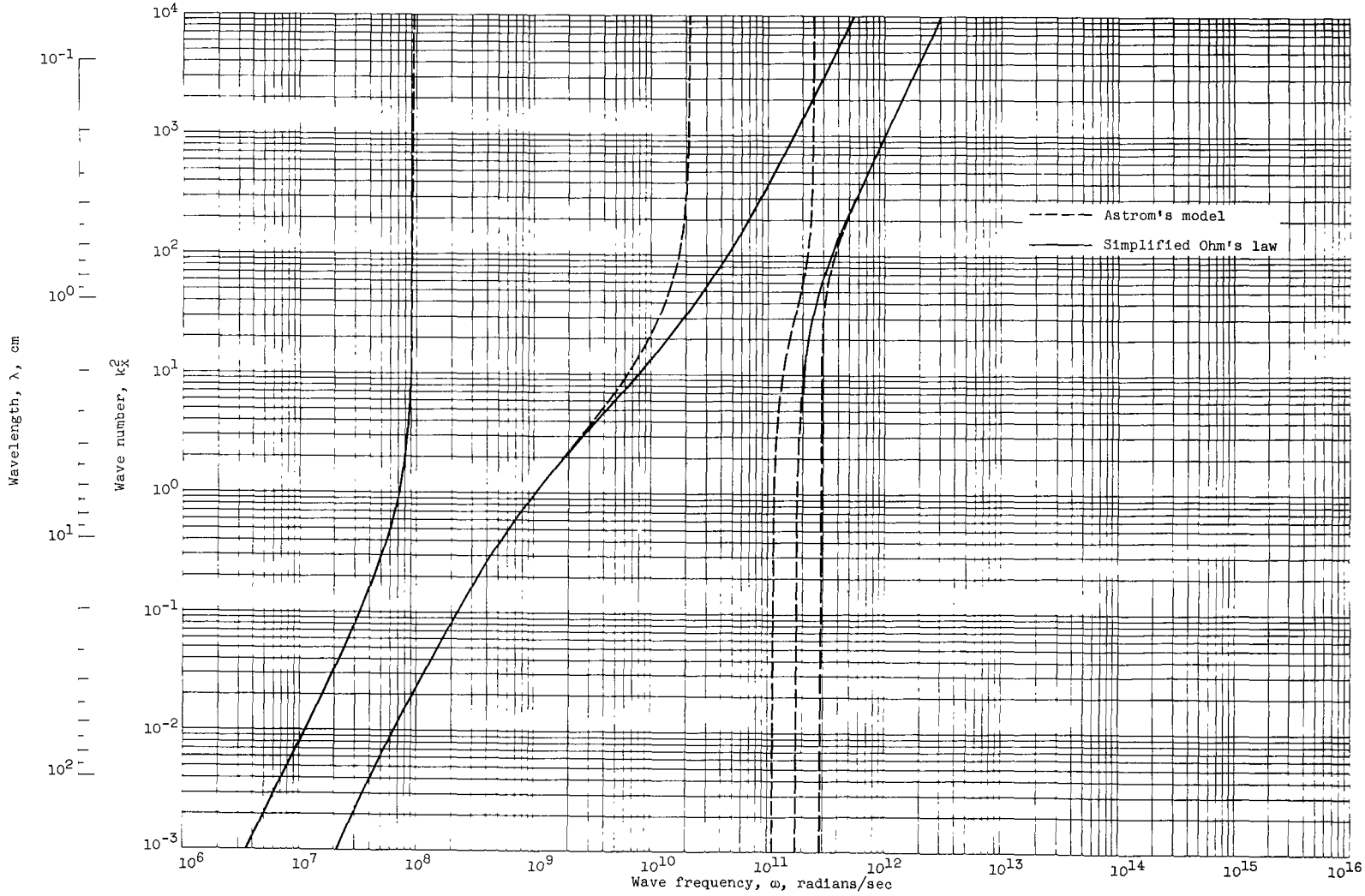

(b-1) x-component.

(b) Magnetic-field strength, 10^4 gauss; particle density, 10^{13} ions per cubic centimeter.

Figure 15. - Continued. Wave number as function of frequency. Wave propagation angle, 80°; simplified Ohm's law.

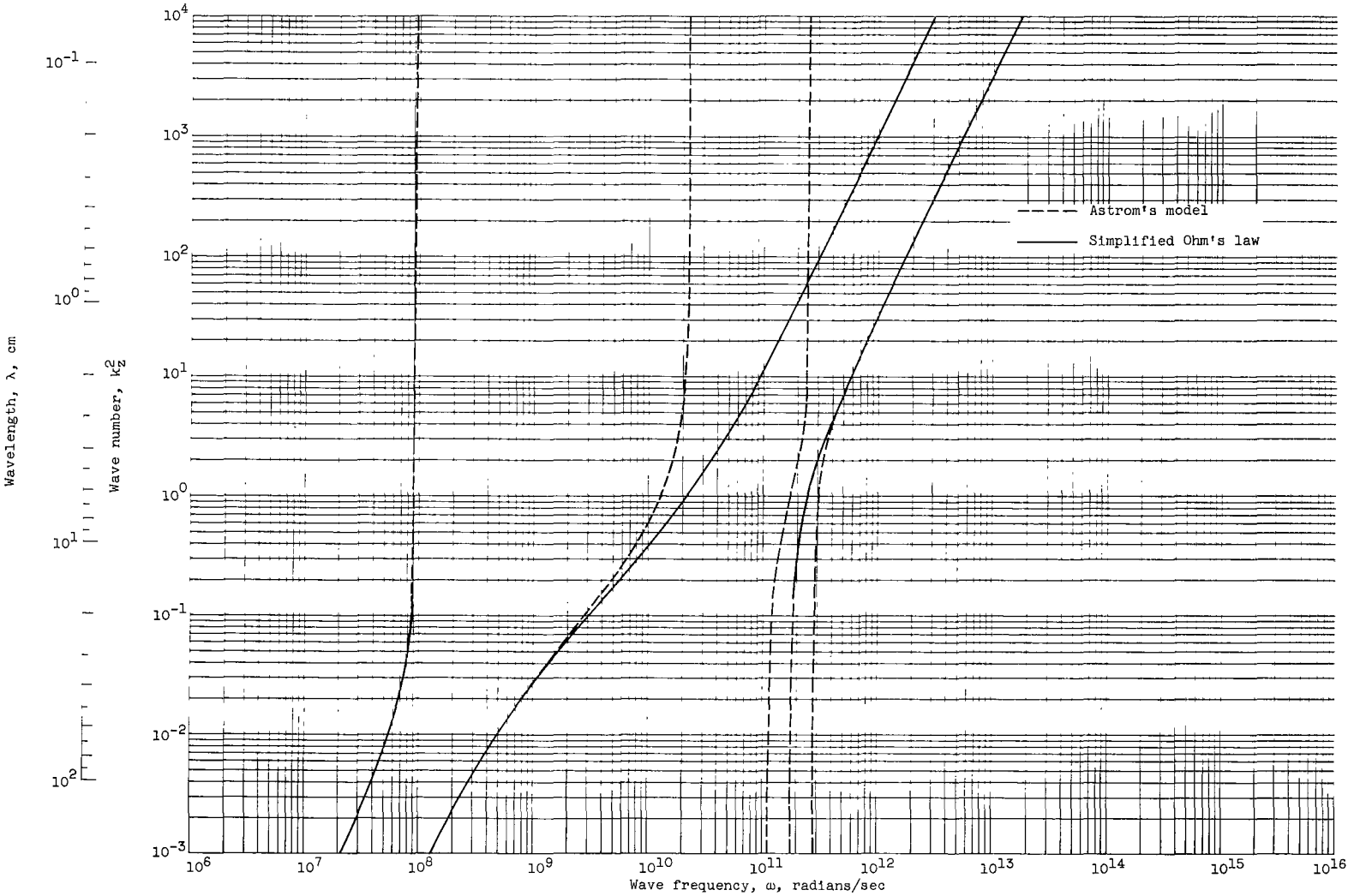

(b-2) z-component.

(b) Magnetic-field strength, 10^4 gauss; particle density, 10^{13} ions per cubic centimeter.

Figure 15. - Concluded. Wave number as function of frequency. Wave propagation angle, 80°; simplified Ohm's law.

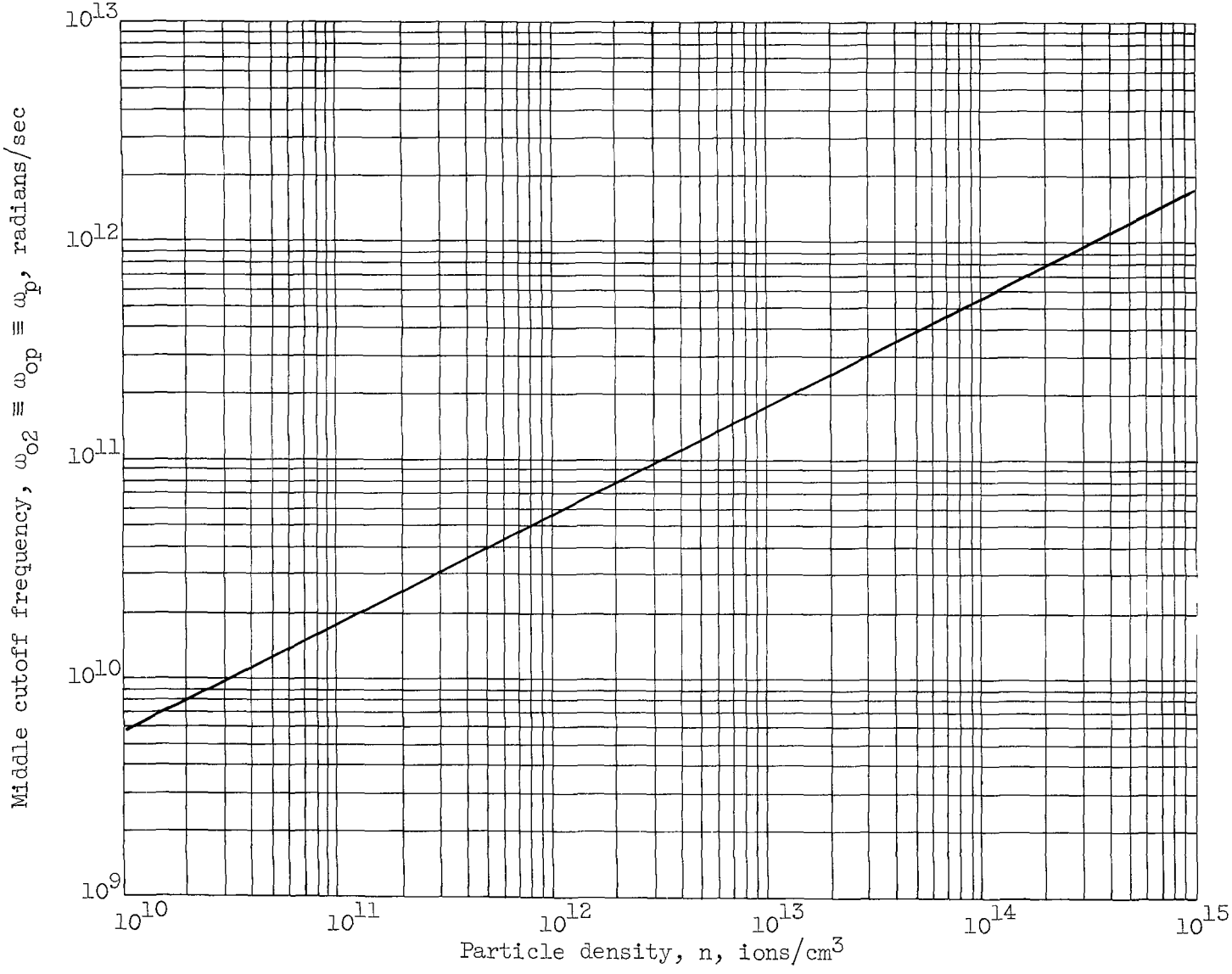

(a) $\omega_{os} \equiv \omega_{op} \equiv \omega_p$.

Figure 16. - Cutoff frequencies as functions of density.

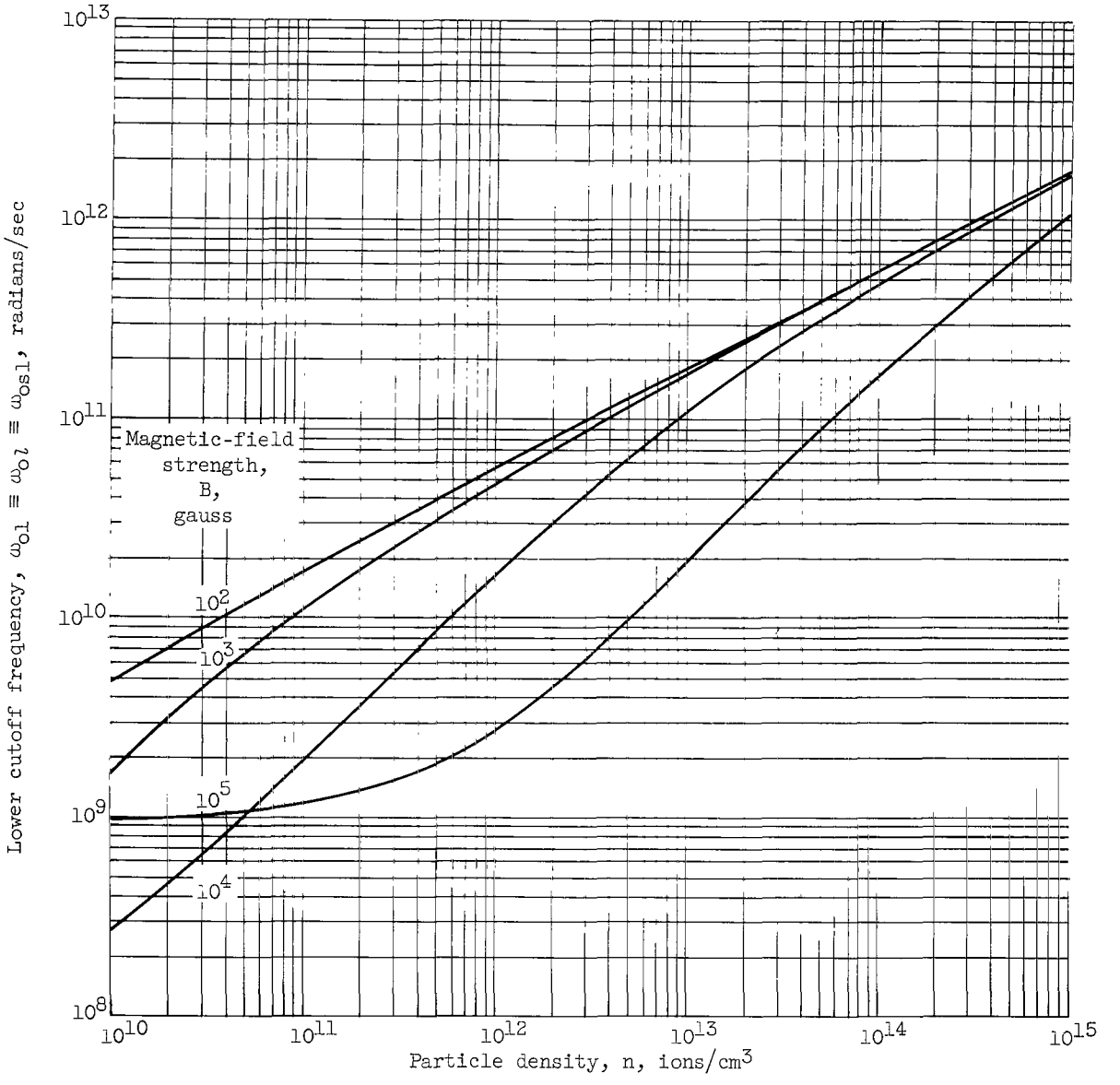

(b) $\omega_{0l} \equiv \omega_{0l} \equiv \omega_{0sl}$.

Figure 16. - Continued. Cutoff frequencies as functions of density.

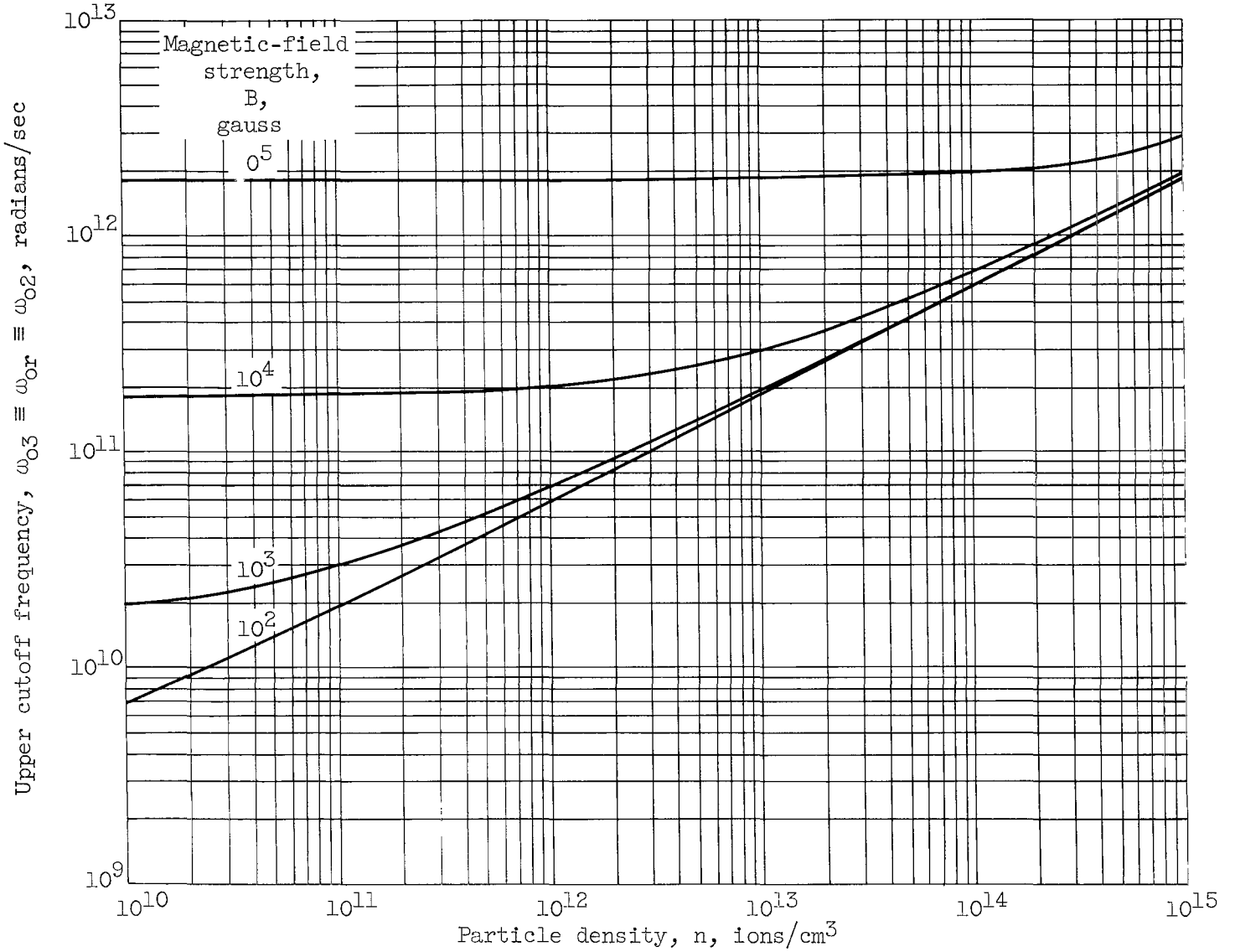

(c) $\omega_{o3} \equiv \omega_{or} \equiv \omega_{os2}$.

Figure 16. - Concluded. Cutoff frequencies as functions of density.

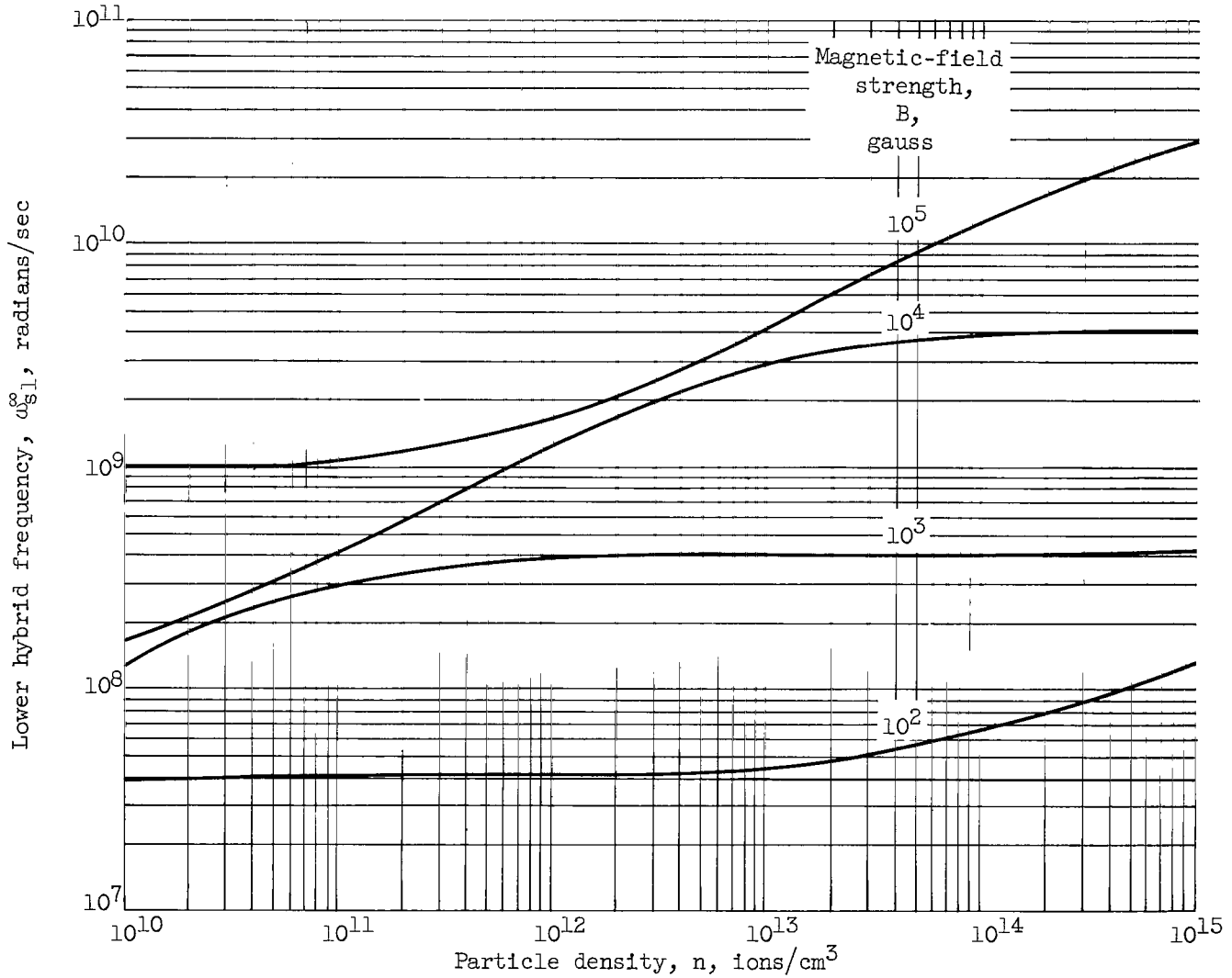

(a) Lower hybrid frequency.

Figure 17. - Resonance frequencies of principal modes as functions of particle density.

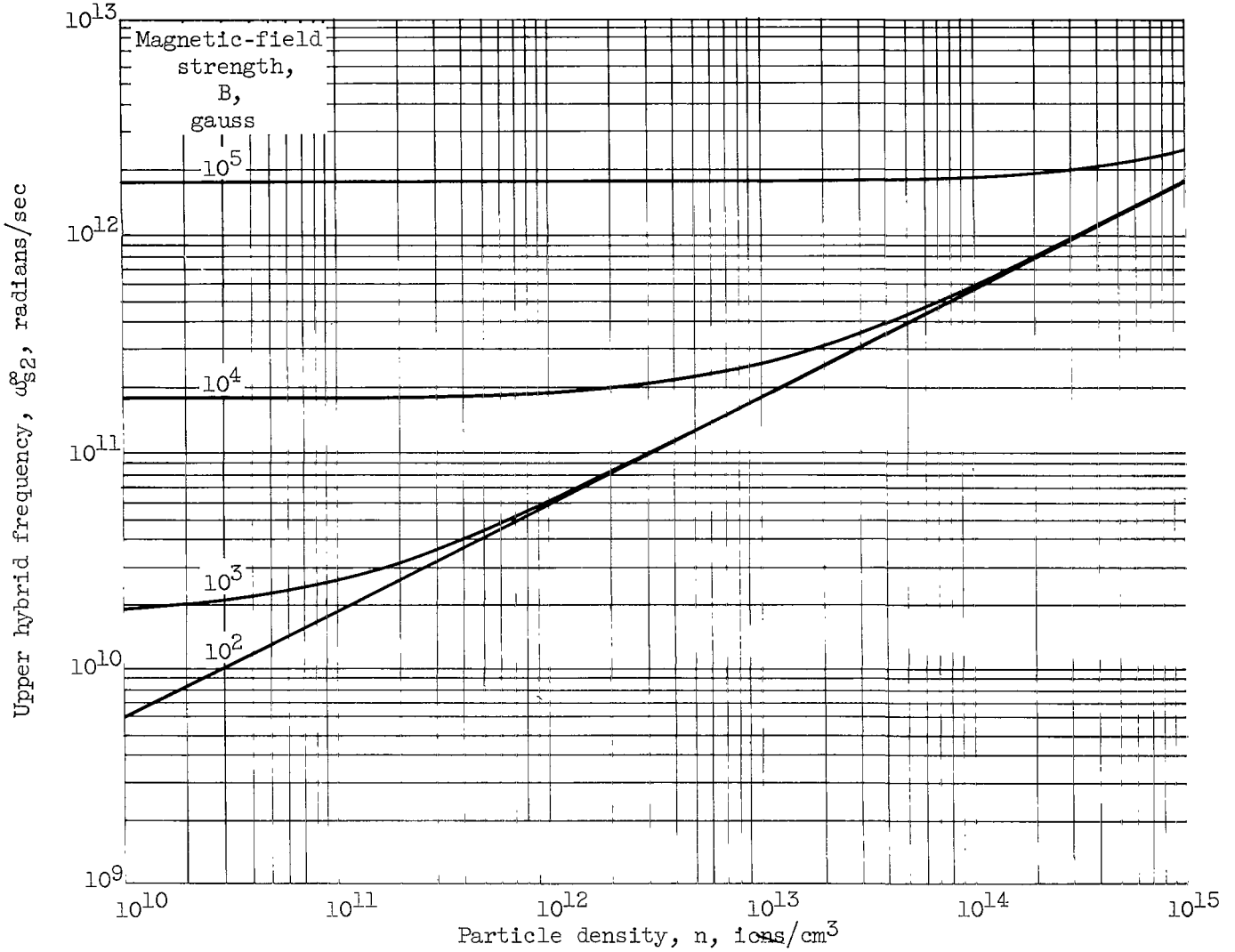

(b) Upper hybrid frequency.

Figure 17. - Concluded. Resonance frequencies of principal modes as functions of particle density.

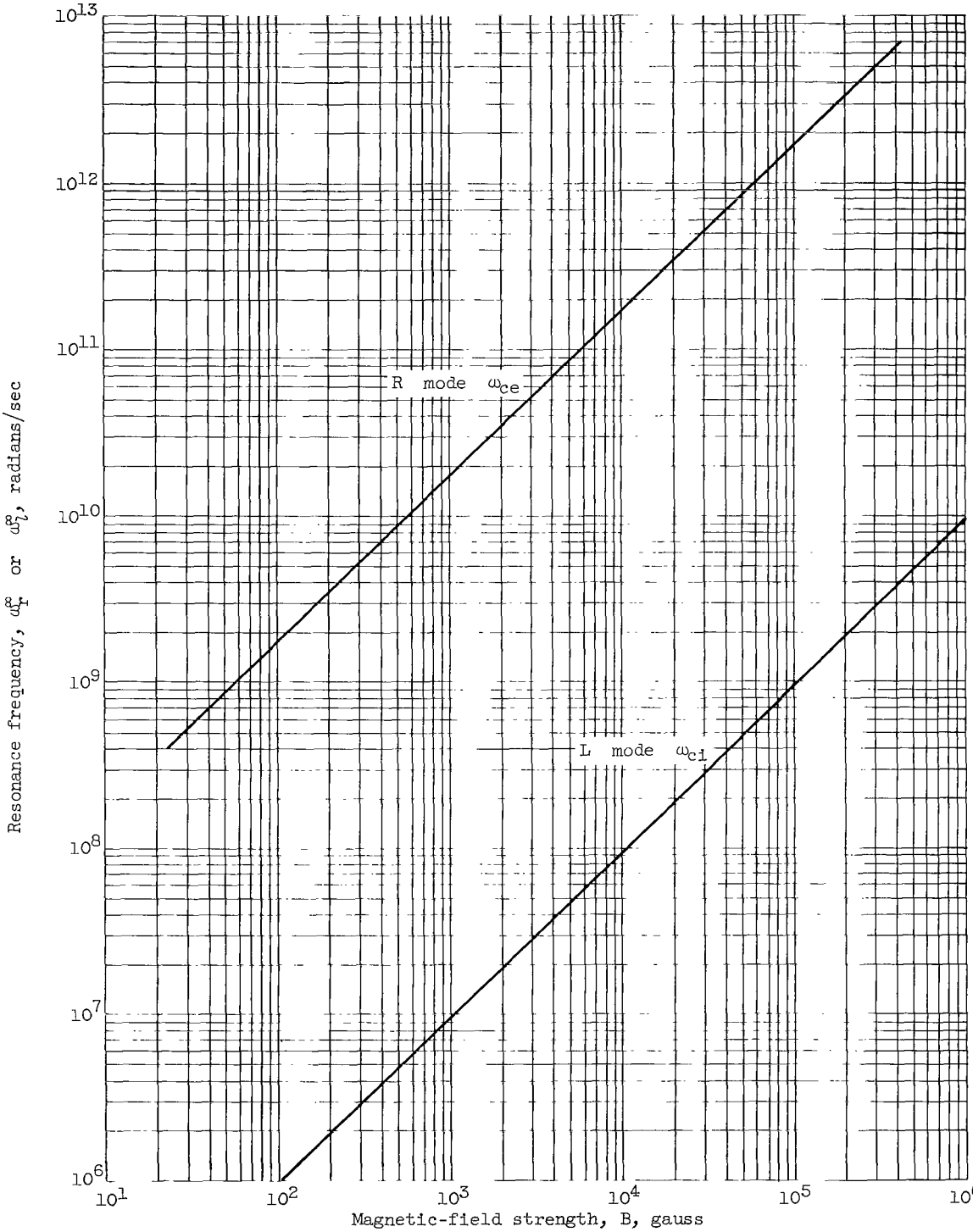

Figure 18. - Resonance frequencies of R and L modes as functions of magnetic-field strength.

NASA-Langley, 1964

"The National Aeronautics and Space Administration . . . shall . . . provide for the widest practical appropriate dissemination of information concerning its activities and the results thereof . . . objectives being the expansion of human knowledge of phenomena in the atmosphere and space."

—NATIONAL AERONAUTICS AND SPACE ACT OF 1958

NASA SCIENTIFIC AND TECHNICAL PUBLICATIONS

TECHNICAL REPORTS: Scientific and technical information considered important, complete, and a lasting contribution to existing knowledge.

TECHNICAL NOTES: Information less broad in scope but nevertheless of importance as a contribution to existing knowledge.

TECHNICAL MEMORANDUMS: Information receiving limited distribution because of preliminary data, security classification, or other reasons.

CONTRACTOR REPORTS: Technical information generated in connection with a NASA contract or grant and released under NASA auspices.

TECHNICAL TRANSLATIONS: Information published in a foreign language considered to merit NASA distribution in English.

TECHNICAL REPRINTS: Information derived from NASA activities and initially published in the form of journal articles or meeting papers.

SPECIAL PUBLICATIONS: Information derived from or of value to NASA activities but not necessarily reporting the results of individual NASA-programmed scientific efforts. Publications include conference proceedings, monographs, data compilations, handbooks, sourcebooks, and special bibliographies.

Details on the availability of these publications may be obtained from:

SCIENTIFIC AND TECHNICAL INFORMATION DIVISION

NATIONAL AERONAUTICS AND SPACE ADMINISTRATION

Washington, D.C. 20546